SATELLITE REMOTE SENSING OF MID-LEVEL CLOUDS

A Dissertation

by

HONGCHUN JIN

Submitted to the Office of Graduate Studies of
Texas A&M University
in partial fulfillment of the requirements for the degree of

DOCTOR OF PHILOSOPHY

Approved by:

Chair of Committee,	Shaima Nasiri
Committee Members,	Sarah Brooks
	Ping Yang
	Thomas Wilheit
	Robert Hetland
Department Head,	Ping Yang

December 2012

Major Subject: Atmospheric Sciences

ABSTRACT

This dissertation aims to study the mid-level clouds using satellite observations. It consists of two major parts: characteristics (including cloud top/base heights, cloud top pressure and temperature, and cloud thickness) and thermodynamic phase of mid-level clouds. Each part devotes to a particular issue of significant importance for satellite-based remote sensing of mid-level clouds.

The first part of this dissertation focuses on the impacts of three definitions of the mid-level clouds based on cloud top pressure, cloud top height, and cloud base height on mid-level cloud characteristics. The impacts of multi-layer clouds on satellite-based global statistics of clouds at different levels, particularly for mid-level clouds, are demonstrated. Mid-level clouds are found to occur more frequently underlying upper-level clouds. Comparisons of cloud amounts between a merged CALIPSO, CloudSat, CERES, and MODIS (CCCM) dataset and International Satellite Cloud Climatology Project (ISCCP) climatology are made between July 2006 and December 2009. Midlevel cloud characteristics are shown to be sensitive to perturbations in midlevel boundary pressures and heights.

The second part focuses on the thermodynamic phase of mid-level clouds. A new algorithm to detect cloud phase using Atmospheric Infrared Sounder (AIRS) high spectral measurements is introduced. The AIRS phase algorithm is based on the newly developed High-spectral-resolution cloudy-sky Radiative Transfer Model (HRTM).The AIRS phase algorithm is evaluated using the CALIPSO cloud phase products for single-layer, heterogeneous, and multi-layer scenes. The AIRS phase algorithm has excellent performance (>90%) in detecting ice clouds compared to the CALIPSO ice clouds. It is capable of detecting optically thin ice clouds in tropics and

clouds in the mid-temperature range. Thermodynamic phase of mid-level clouds are investigated using the spatially collocated AIRS phase and CALIPSO phase products between December 2007 and Novermber 2008. Overall, the statistics show that ice, liquid water, and mixed-phase of the mid-level clouds are approximately 20%, 40%, and 40%, globally.

DEDICATION

This dissertation is dedicated to my family who always supported me through my life.

ACKNOWLEDGEMENTS

I would like to acknowledge many people who have contributed to this dissertation.

First of all, I would like to thank my advisor, Dr. Shaima Nasiri, for her wise guidance and tremendous support for the past four years. I would also like to thank my committee members, Drs. Sarah Brooks, Ping Yang, Thomas Wilheit, and Robert Hetland, for their constructive suggestions to improve this dissertation.

Thanks also goes to my group members, colleagues, the department faculty and staffs, and friends for making my time at Texas A&M University memorable and enjoyable.

I would like to thank my parents for their unconditional love and support throughout my life. Last, but not least I would like to thank my wife Xia and daughter Alice, for the loving support and patience they have given me all these years.

This research was supported by the NASA grant NNX10AP06G.

TABLE OF CONTENTS

LIST OF FIGURES

LIST OF TABLES

1. INTRODUCTION

1.1 Mid-level clouds and climate

Mid-level clouds (approximately between 2 and 6 km) cover a substantial portion (about 10∼30%) of the globe (Hahn and Warren 1999; Hahn and Warren 2003; Stubenrauch et al. 2006). They interact strongly with both solar and terrestrial radiation fields, and therefore play an important role in the planetary radiative energy budget (Hartmann et al. 1992; Poetzsch-Heffter et al. 1995; Sun and Shine 1995; Chen et al. 2000; Mace et al. 2006). Yet mid-level clouds have been studied less than their low and high counterparts due to the lack of observations, even though they occur frequently in the tropics, the mid-latitudes, and the high-latitudes (Curry et al. 1996; Fleishauer et al. 2002; Mace et al. 2006; Shupe et al. 2008; Riihimaki et al. 2012).

Mid-level clouds impact both energy budget and vertical profile of heating in the atmosphere, however, the radiative effects and latent heating impacts are not well interpreted because they depend on the knowledge of frequency of occurrence, characteristics, and thermodynamic phase of these clouds. Many characteristics, and even the definition of a mid-level cloud, are not well understood and are in need of clarification. The defining characteristics of mid-level clouds depend on the region and/or observational techniques. For example, the International Satellite Cloud Climatology Project (ISCCP, Rossow and Schiffer 1999) and TIROS-N Observational Vertical Sounders Path-B (TOVS-B, Stubenrauch et al. 2006) are both long-term global climatologies that define mid-level clouds as having cloud top pressure between 680 and 440 hPa (Figure 1.1). Human observers from the surface, on the other hand, typically focus on cloud base height, and consider the sum of nimbostra-

tus, altostratus, and altocumulus as mid-level clouds. Surface-based remote sensing typically define mid-level clouds as having cloud top and/or base height between 3 to 8 km (Mace et al. 2006; Riihimaki et al. 2012). However, observational assessment of mid-level clouds is difficult because these clouds are often obscured or blocked by higher or lower clouds when observed remotely from the top of atmosphere (TOA) or surface, respectively.

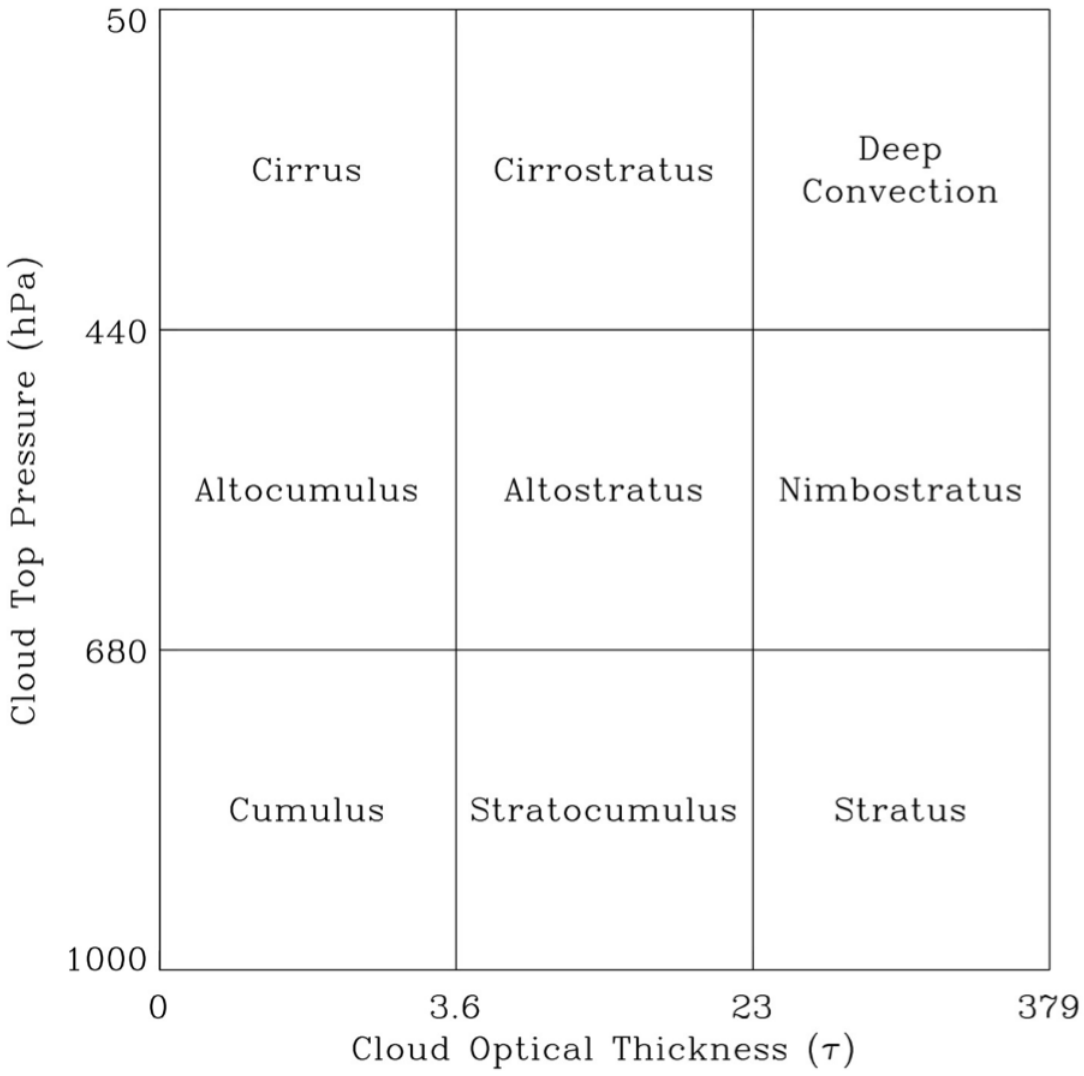

Figure 1.1 The ISCCP cloud classification scheme.

Previous studies indicate that mid-level cloud frequency varies from tropics to high-latitudes. By combining the statistics of cloud layer occurrence from ISCCP and an analysis of radiosonde humidity profiles, Rossow and Zhang (2010) developed a statistical model that associates each cloud type (Figure 1.1) with a particular cloud vertical structure. They found that mid-level cloud amounts increase from lower to higher latitudes. They additionally reported that mid-level cloud amounts are generally less than both low- and high-level cloud amounts, except in the polar regions. Zhang et al. (2010) using Cloud-Aerosol Lidar and Infrared Pathfinder Satellite Observations (CALIPSO) showed that higher frequencies of thin mid-level clouds were found during night overpasses than daytime overpasses. This difference was substantially higher in the tropics than in mid-latitudes and polar regions.

Thermodynamic phase of mid-level clouds plays an important role in the determination of radiation budget (Sun et al. 1994; Sun et al. 1995). Mid-level clouds often extend through or are completely above the melting layer (Fleishauer et al. 2002). These clouds often contain water droplets, ice crystals, or a combination of both phases of hydrometeors, in other words, they can be mixed-phase (Heymsfiled et al. 1991; Field 1999; Fleishauer et al. 2002; Shupe et al. 2008; Riihimaki et al. 2012). The potential for complex microphysics makes the remote sensing and dynamical modeling of mid-level clouds challenging (Yang et al. 2003; Platnick et al. 2003; Sun et al. 1995). While much knowledge has been learned from liquid water clouds and ice clouds, mixed-phase clouds introduce substantial uncertainties in satellite remote sensing and radiative transfer modeling. Simulations of General Circulation Models (GCMs) are very sensitive to the phase of cloud particles (Gregory and Morris 1996; Rotstayn et al. 2000; Morrison et al. 2005; Liu et al. 2007; Fridlind et al. 2007; Luo et al. 2008). Treut et al. (1995) developed a couple of cloud parameterization schemes using different combinations of effective radius and absorption coefficient

for mid-level mixed-phase clouds. Their results showed that shortwave (SW) and longwave (LW) radiative forcings are substantially different for the two schemes. Additionally, mid-level mixed-phase clouds have implications for aviation safety. A review by Riley (1998) had suggested that aircraft may be traveling through mixed-phase clouds at least 20% of the time, which can lead to aircraft icing because of these conditions.

Mid-level clouds are not well represented in GCMs (Korolev et al. 2003; Zhang et al. 2005; Wyant et al. 2006) and Numerical Weather Prediction (NWP) models (Bodas-Salcedo et al. 2008). GCMs often underestimate mid-level cloud frequency (Zhang et al. 2005), and usually have difficulty in accurately characterizing the phase of hydrometeors in the mixed-phase regimes (Gregory and Morris 1996; Rotstayn et al. 2000; Klein et al. 2009). Improving climate model predictions requires accurate observational constraints. Comparisons between CALIPSO cloud observations, GCM output, and GCM output combined with a CALIPSO simulator showed that mid-level cloud frequencies from the GCM were much lower than those from CALIPSO, and even vanished when GCM output was coupled to the CALIPSO simulator (Chepfer et al. 2008). This indicates that the representation of mid-level clouds in the GCM needs to be improved, including the formation processes and their physical and microphysical properties. Vertical resolution may be a reason for the under-representation of mid-level clouds in numerical models. Some mid-level clouds are geometrically thin (Smith et al. 2009; Riihimaki et al. 2012), and are difficult to fit in a model level (Smith et al. 2009). Observations of cloud geometric thickness may help to determine how much of an issue model vertical resolution plays in under-representation of mid-level clouds.

The feedback of mid-level clouds has important impacts on the climate system (Zelinka et al. 2012). A perturbation of the climate system can lead to changes in

global cloudiness, which in turn may either amplify or dampen the original perturbation. Therefore, it is important to understand how cloud radiative effects will change as the planet warms due to long-lived greenhouse gases. Any systematic changes in cloudiness that originate from "global warming" will lead to radiation anomalies that feedback on the climate system. Current GCMs suggest positive cloud feedbacks (Soden and Held 2006). Zelinka et al. (2012) proposed a novel technique using cloud radiative kernels to investigate cloud feedbacks using histograms of cloud fraction as a joint function of cloud top pressure and optical depth. They found that changes in mid-level cloud lead to positive SW cloud feedbacks.

Though a number of investigations had looked at mid-level clouds in tropics (Riihimaki et al. 2012), mid-latitudes (Heymsfiled et al. 1991; Field, 1999; Fleishauer et al. 2002; Mace et al. 2006), and high-latitudes (Shupe et al. 2008; Shupe, 2011), the studies either used either in-situ measurements or ground-based remote sensing and focused on mid-level cloud microphysical structures and cloud properties or climatologies. These observations are expensive and limited by their small spatial or temporal sample scales. Additionally, the sensitivities between existing cloud climatologies and cloud vertical structure need further investigation. Accurate global observations of mid-level clouds at high spatial and temporal resolution are necessary to improve our current understanding of these clouds, which includes their characteristics and bulk nature, as well as their thermodynamic phase. The synergistic use of National Aeronautics and Space Administration (NASA) spaceborne "A-Train" observations (Stephens et al. 2002) is a significant step in expanding our knowledge of mid-level clouds.

1.2 Current climatology of mid-level clouds

Despite the substantial efforts and significant progress made over the past few decades, reliable cloud climatology and retrieval of cloud properties from satellite observations still remain a challenge. These studies require good understanding of the characteristics and capabilities of the retrieval instruments, and also require good understanding of several different aspects of mid-level clouds. First, remote sensing of mid-level clouds needs clear characteristics, including definitions, frequency of occurrence, and sensitivities. Secondly, liquid water droplets and ice crystals behave radiatively different in the absorption of solar and infrared (IR) radiation, and therefore identification of the cloud particle phase is an important step in the retrieval of cloud particle size, optical thickness, and water path.

Considerable efforts have been devoted to establishing global cloud climatologies, however, working definitions or the classification of mid-level clouds vary with observational technique, region, and purpose (Poore et al. 1995; Hahn and Warren 1999; Rossow and Schiffer 1999; Hahn and Warren 2003; Stubenrauch et al. 2006, Mace et al. 2006; Riihimaki et al. 2012). The sensitivity of mid-level cloud frequency to the definition of "mid-level" is not well known and needs to be further studied.

Cloud climatologies observed from the surface typically focus on cloud base height. The Hahn and Warren (1999, 2003) climatologies were made from human perspective in which the sum of observations of nimbostratus, altostratus, and altocumulus, based on the World Meteorological Organization (WMO, 1988) synoptic cloud code, are mid-level clouds. The surface-based climatologies are further complicated by whether a cloud belongs to the low- or mid-level classification depending on the cloud type. For instance, a cloud base for nimbostratus can be between 0 and 3 km, while altostratus and altocumulus bases can be from 2 to 6 km.

Active ground-based vertically pointing Micropulse Lidar (MPL) and Millimeter Wavelength Cloud Radar (MMCR) enable us to measure cloud base and cloud top height simultaneously, which can help to facilitate the understanding of cloud climatologies. For example, Mace et al. (2006) considered mid-level clouds as having cloud base and cloud top between 3 km and 6.5 km at Department of Energy's (DOE) Atmospheric Radiation Measurement (ARM) program Southern Great Plains (SGP) site. Riihimaki et al. (2012) used MPL and MMCR observations at the ARM Tropical Western Pacific (TWP) site in Darwin, Australia and treated mid-level clouds with cloud top height between 4 km and 8 km.

Poore et al. (1995) combined 14 years (1975-1988) of rawinsonde and surface observations from 63 sites in the Northern Hemisphere (NH) and created a climatic dataset to investigate cloud layer thicknesses. They collected the statistics of layer thicknesses using two altitude classifications. First, the cloud base height (Z_b) of each cloud layer was used to define low-, mid- and high-level clouds as $Z_b \leq 2$ km, 2 km $< Z_b \leq 5$ km, and $Z_b > 5$ km, respectively. Second, low, middle, and high clouds were also defined using cloud top height (Z_t) as $Z_t \leq 3$ km, 3 km $< Z_t \leq 7.6$ km, and $Z_t > 7.6$ km (up to about 10.7 km), respectively.

Satellite-based cloud climatologies have traditionally classified clouds with respect to cloud top pressure. For example, both the ISCCP (Rossow and Schiffer 1999) and TOVS-B (Stubenrauch et al. 2006) long-term cloud climatologies define mid-level clouds as having cloud top pressure between 680 and 440 hPa (Figure 1.1), and define clouds above and below this layer as high- and low-level clouds, respectively. The High-Resolution Infrared Radiation Sounder (HIRS) multi-spectral IR data from National Oceanic and Atmospheric Administration (NOAA) operational polar orbiting satellites have been used for cloud detection for more than a decade (Wylie et al. 1994; Wylie and Menzel, 1999; Wylie et al. 2005). Wylie et al. (1994)

studied four years of global statistics using HIRS and defined mid-level clouds between 400 and 700 hPa. Wylie et al. (2005) showed trends in global cloud cover in two decades of HIRS observations, and they considered clouds between 440 and 700 hPa as mid-level clouds.

Cloud geometric thickness is important in determining LW cloud radiative impacts and in satellite-based retrievals of cloud properties (Garrett et al. 2009). Poore et al. (1995) studied cloud layer thickness from a combination of surface and upper-air observations and found small latitudinal and seasonal variations in cloud layer thickness of mid-level clouds defined using cloud base height. Wang et al. (2000) investigated the cloud vertical structure using a 20-year global radiosonde dataset and found that the average cloud layer thickness was approximately 1.6 km. However, recent studies showed that mid-level clouds tend to be thin in the tropical region (Zhang et al. 2010; Yasunaga et al. 2006; Ansmann et al. 2009; Riihimaki et al. 2012). Seifert et al. (2010) reported that mid-level clouds in the tropics are likely to be shorter-lived altocumulus layers rather than the thicker and more stable stratiform layer clouds of the mid-latitudes.

Mid-level cloud observations are made even more difficult by their potential for complex microphysics. In-situ measurements and lidar-based observations indicate that mid-level clouds can be composed of ice crystals, liquid water droplets, or a mixture of the two phases (Heymsfiled et al. 1991; Field 1999; Fleishauer et al. 2002; Shupe et al. 2008; Riihimaki et al. 2012). There is much uncertainty regarding the composition of clouds that resides at the temperature range between -40°C (the homogeneous nucleation) and 0°C. Early observations in the Arctic reported that predominately supercooled liquid water existed at temperatures as low as -32°C (Curry et al. 1996). Curry et al. (1996) also found complete crystalline clouds at temperatures as high as -14°C. Furthermore, there have been cases where ice

hydrometeors were observed as warm as -4°C (Curry et al. 2000). Garrett et al. (2009) suggested that cloud temperature is critical in determining LW cloud radiative impacts as well as the retrieval of cloud properties.

A number of studies have shown that the thermodynamic structure of mid-level clouds varies with latitudinal regions. Most in-situ observations of mid-level cloud have been made in mid-latitudes (Heymsfiled et al. 1991; Field 1999; Fleishauer et al. 2002), and the thermodynamic phase of these clouds can be mixed-phase (Fleishauer et al. 2002), entirely liquid phase (Field 1999; Fleishauer et al. 2002), or entirely ice phase (Heymsfiled et al. 1991). Typical mixed-phase clouds in the Arctic have two layers: liquid water droplets on the top and precipitating ice crystals at the bottom, and this pattern can exist for periods of time, even though the coexistence of liquid water and ice crystals is inherently unstable below freezing (Heymsfield et al. 1991; Rauber and Tokay 1991; Hobbs et al.1998; Pinto 1998; Girard and Blanchet 2001; Gayet et al. 2002). Shupe (2011), using ground-based measurements, found that few liquid-only clouds occur above 3 km although supercooled liquid water in mixed-phase clouds occurs at height up to about 7 km in the Arctic region. Riihimaki et al. (2012) found that mid-level clouds in the tropics have a high probability of containing supercooled liquid water at low temperatures: ∼20% of clouds at -30°C, ∼50% of clouds at -20°C, and ∼65% of clouds at -10°C contain supercooled liquid water. Satellite studies show that a larger amount of mid-level clouds contain only supercooled liquid water rather than mixed-phase in the tropics than in mid- or high-latitude (Zhang et al. 2010; Hu et al. 2010).

1.3 Issues, opportunities, and challenges

As described in the previous section, a good understanding of mid-level cloud climatologies and their uncertainties requires clear definitions and characteristics,

as well as a better identification of the thermodynamic phase of these clouds. Unfortunately, there are a few controversies issues that hamper the interpretation of mid-level cloud climatologies and obscure our understanding of the role of mid-level clouds in the climate system.

One of the biggest uncertainties in characterizing mid-level clouds is brought on by differences between climatologies. This is likely due to a combination of each study's different mid-level cloud definition and observational sensitivities and biases. For climate studies, it is important to understand how different instruments and/or observational approaches perceive cloud properties. In the case of surface climatologies (Hahn and Warren 1999), surface observers typically have more difficulties identifying altostratus/altocumulus and cirrus clouds reliably, in particular at night or when low-level clouds are present. Surface observations do not provide any information on cloud top height. Additionally, the surface information is not globally complete, coverage being particularly poor over the Southern Hemisphere (SH) oceans (Poore et al. 1995; Wang et al. 2000).

The traditional passive satellite observations (Rossow and Schiffer 1999; Wylie et al. 1994; Wylie and Menzel, 1999; Jin et al. 1996; Stubenrauch et al. 2006), on the other hand, are globally complete and can resolve mesoscale and synoptic-scale cloud variations, providing information from "top down" viewpoint about the vertical distribution of cloud-top locations. However, the satellite imagers and sounders can only see the uppermost cloud top in each vertical column, and the statistics only provide direct information about the cloud top pressure or height. Large discrepancies exist between the surface- and satellite-based cloud observations (Hahn and Warren 1999; Stubenrauch et al. 2006), and the differences are likely due to the different definitions and sensitivities. Cumulus congestus, which frequently occurs in the tropics (Johnson et al. 1999), is an example of a cloud that maybe classified as

mid-level by a satellite approach, but low-level by a ground-based observer. A more promising approach uses active sensors, such as lidars (Sassen 1991), cloud radars (Shupe et al. 2008), or both (Uttal et al. 1995; Wang et al. 1999; Mace et al. 2006; Riihimaki et al. 2012) to profile cloud layers from the surface. However, these instruments cannot provide coverage of whole synoptic systems or complete global coverage until they are implemented on satellites (Stephens et al. 2002).

Inconsistency in defining mid-level clouds makes comparisons between the available climatologies and/or model simulations even more difficult than such comparisons usually are. For instance, even though the ISCCP and TOVS-B climatologies have the same definition of mid-level clouds, global coverage between 1987 and 1995 was 12.1% in the TOVS-B dataset, but 18.5% in the ISCCP dataset (Stubenrauch et al. 2006). There are also large zonal differences between these datasets, as well as NASA Aqua and Terra satellite instrument datasets (Wu et al. 2009). Global statistics using HIRS reported that 27% of the observations were mid-clouds (Wylie et al. 1994). Wylie et al. (2005) found that mid-level clouds are approximately 18% of the observations; however, if a random overlap assumption is considered in the statistical procedure, the mid-level clouds can be as high as 26%. Additionally, mid-level cloud amounts reported by surface observers were 26.2% over land (1971-1996) and 28.8% over ocean (1954-1996) (Hahn and Warren 1999; Hahn and Warren 2003).

Another large uncertainty in the study of mid-level clouds is the cloud layering (i.e. multi-layer clouds) impacts on the general circulations and climatological statistics. Changes of cloud vertical structure affect the atmospheric circulations in the GCMs through their modification of the radiative heating profile within the atmosphere (Slingo and Slingo, 1988; Randall et al. 1989; Slingo and Slingo, 1991; Wang and Rossow, 1998). An accurate characterization of the vertical distributions of cloud in the atmosphere is critical for calculating the radiative flux within and at

the top of atmosphere. Barker et al. (2003) showed that, for a given distribution of liquid water content, changing the cloud overlap conditions can lead to the changes of zonal mean TOA cloud radiative effect by up to 50 Wm^{-2}.

Multi-layer clouds can be defined as clouds that do not behave physically and radiatively as single-layer clouds. Inferences from global radiosonde data indicated that multi-layer clouds occur over 40% of the time and are predominately two-layered (Poore et al. 1995; Wang et al. 2000). Using spatially collocated CloudSat and CALIPSO data within Clouds and the Earth's Radiant Energy System (CERES) footprint, Li et al. (2011) reported that the global mean multi-layer cloud fraction (the ratio between the occurrence of multi-layer clouds and all pixels) is about 26%. Figure 1.2 shows the global distributions of mid-level clouds in the multi-layer cloud regimes in terms of ISCCP classification scheme. Mid-level clouds over low clouds occur mainly in the mid- and high-latitudes over ocean, whereas high-level clouds over mid-level clouds occur more frequently globally, particularly in the tropics and high-latitudes. Additionally, the high over mid-level clouds are more populated over land than over ocean.

Recent advances in remote sensing technologies, such as NASA's "A-Train" satellite constellation, have provided unprecedented opportunities to improve our understanding of mid-level clouds. The near simultaneous data from these satellites are providing comprehensive information about aerosols, clouds, radiative fields, and other important atmospheric components, and therefore a unique opportunity to gain better understanding of climate change (Stephens 2005). Some key instruments for cloud studies on board of "A-Train" include the Cloud-Aerosol Lidar with Orthogonal Polarization (CALIOP, Winker et al. 2009) on CALIPSO, the Cloud Profiling Radar (CPR, Stephens et al. 2002) on CloudSat, and the Atmospheric Infrared Sounder (AIRS, Aumann et al. 2003) on Aqua. Each of these instruments has

unique measurement capabilities that greatly complement each other. Comparison and combination of their retrievals have the potential to significantly improve our understanding of the climatologies of mid-level clouds.

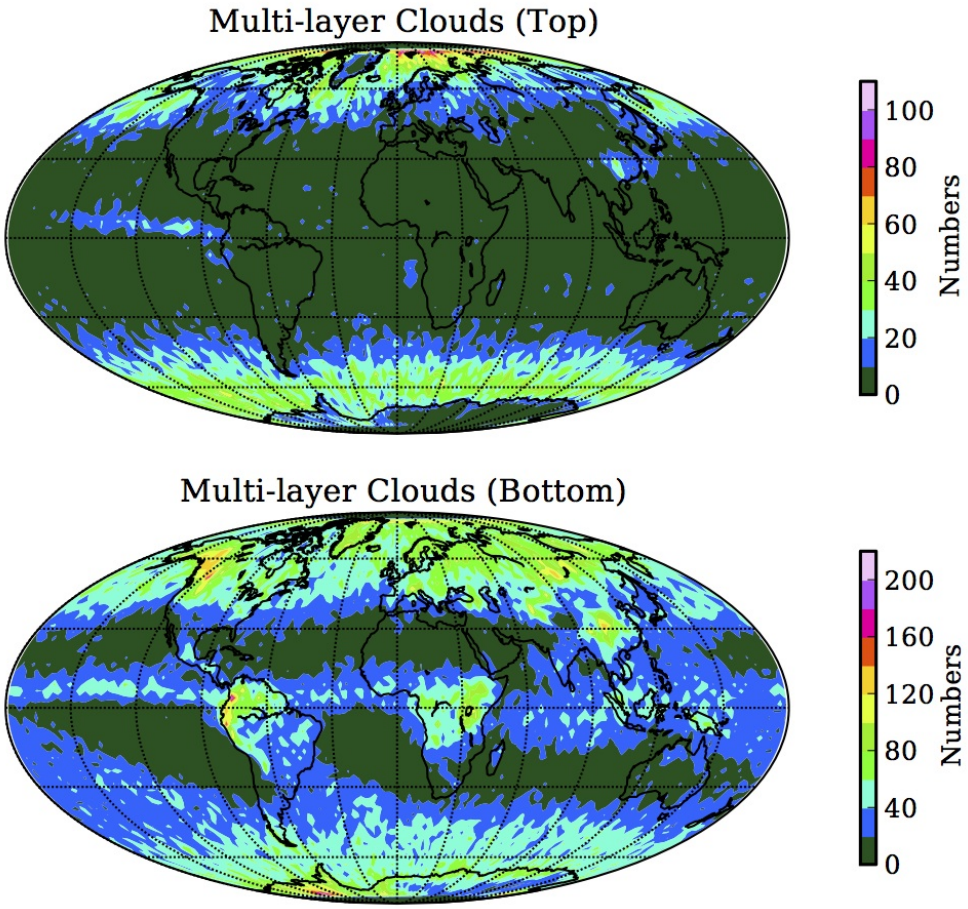

Figure 1.2 Global distributions of mid-level clouds for multi-layer cloud regimes using ISCCP classification from spatially collocated CALIPSO and CloudSat between July 2006 and December 2009. Mid-level clouds: 440 hPa < cloud top pressure (CTP) < 680 hPa. Top panel: top layer; bottom panel: bottom layer.

Along with these opportunities in improved understanding of mid-level clouds arise some new challenges. For example, with more than 2000 spectral channels, AIRS has a great spectral resolution and therefore provides more information in the vertical profiles of atmospheric temperature, moisture and minor gases (Aumann et

al. 2003; Tian et al. 2006). However, the volume of AIRS data is enormous because of its high-spectral resolution nature, which makes the interpretation of AIRS observations a challenging task. The capabilities for using high-spectral-resolution IR radiances, such as AIRS, to determine cloud thermodynamic phase has been explored by Nasiri et al. (2008). Their simulations show that hyperspectral measurements would serve an important role in refining estimates of cloud phase. A wealth of high-resolution IR emission measurements from several satellite instruments, including AIRS, the Infrared Atmospheric Sounding Interferometer (IASI, Chalon et al. 2001), as well as the Cross-track Infrared Sounder (CrIS), a part of the Suomi National Polar-orbiting Partnership (NPP), are available. Thus, the improvement of existing methods and the development of a new cloud phase retrieval algorithm for hyperspectral applications are challenging, yet rewarding, tasks.

The "A-Train" satellite constellation also provides an excellent opportunity to compare nearly simultaneous cloud retrievals from different satellite instruments. CALIPSO, AIRS, and Moderate Resolution Imaging Spectroradiometer (MODIS) within the "A-Train" can provide cloud thermodynamic phase. Because cloud phase plays an important role in determining cloud radiative properties, it is of interest to compare this important cloud parameter retrieved among these different instruments. Cho et al. (2009) compared MODIS IR cloud phase with CALIPSO cloud phase product. Another comparison between CALIPSO and AIRS will be presented later in this dissertation. Such comparisons will not only reveal differences between different cloud products, but may also help answer some crucial questions in satellite-based remote sensing of mid-level clouds. An important question, which may be answered through the comparison, is in what situation does cloud phase, as derived from passive remote sensing, lead to misclassification.

1.4 Organization of this dissertation

The main theme of this dissertation aims to use NASA "A-Train" satellites to study characteristics and thermodynamic phase of mid-level clouds. The rest of this dissertation is organized into four major sections, and each devoted to a particular issue that has been briefly introduced in the previous section.

In chapter 2, we investigate the impacts of overlapping clouds in the satellite remote sensing of clouds at different levels. In chapter 3, we look at the characteristics of mid-level clouds using spatially collocated CALIPSO and CloudSat dataset, including the relationships between cloud frequency, cloud top/base height and pressure, geometric thickness, and cloud top temperature. In chapter 4, we introduce a newly developed cloud thermodynamic phase determination algorithm using AIRS hyperspectral measurements. In chapter 5, we demonstrate the evaluation of the new AIRS IR cloud phase algorithm using CALIPSO cloud phase product and we also examine the thermodynamic phase of mid-level clouds. Finally, we present the summary and future work in chapter 6.

2. IMPACTS OF OVERLAPPING CLOUDS ON SATELLITE-BASED GLOBAL STATISTICS OF CLOUDS AT DIFFERENT LEVELS

2.1 Background

Satellite remote sensing is the only means to provide cloud climatology on a global scale (Rossow and Schiffer 1999). However, overlapping clouds have posed a major challenge in interpreting satellite data properly. For instance, traditional satellite imagers and sounders only see the uppermost cloud top in each vertical column. Passive satellite remote sensors provide information on cloud top height but often have some systematic errors, especially for optically thin cirrus clouds (Minnis et al. 1993; Rossow and Schiffer 1999; Naud et al. 2007). Additionally, some studies using passive remote sensing techniques assume all clouds are homogeneous and single-layered. One major problem with this assumption is that multi-layer clouds have been frequently observed by surface observers, radiosonde, and in-situ aircraft measurements, as well as satellite observations (Hahn and Warren 1999; Poore et al. 1995; Tian and Curry 1989; Verlined et al. 2004; Heidinger and Pavolonis 2005; Wang and Dessler 2006; Joiner et al. 2010). To improve our understanding of the multi-layer clouds, some approaches have been proposed to detect multi-layer clouds (Nasiri and Baum 2004; Chang and Li 2005).

Cloud overlap can cause large biases in the satellite retrievals of many cloud properties including cloud top height, thermodynamic phase, and radiative properties (Minnis et al. 1993; Baum and Wielicki 1994; Cho et al. 2009; Huang et al. 2005). Multi-layer clouds sometimes cause errors in cloud height retrievals that depend on specific algorithm and cloud properties (Naud et al. 2007). A thin cirrus cloud over a lower level water cloud is one of the most problematic overlapping cloud scenarios

for global cloud property retrievals, particularly for the retrieval of effective radius and optical depth (Nasiri 2004; Chang and Li 2005; Huang et al. 2005). In the case of high ice clouds over low water clouds, one of the greatest impediments to accurately determine cloud ice mass for a given atmospheric profile is the influence of the underlying liquid water clouds on the radiances observed in the visible and near-infrared wave-lengths at TOA (Minnis et al. 1993; Chang and Li 2005). Additionally, retrievals of cloud water path tend to be biased when an ice cloud overlaps a liquid water cloud (Minnis et al. 2007).

Clouds at different levels can have different radiative impacts. For instance, thick low clouds can reflect a significant amount of incoming SW solar radiation back to space, and thin high clouds can reduce outgoing LW radiation. Multi-layer clouds therefore behave radiatively differently compared to single-layer clouds. Cloud radiative effects (CRE) of high-level clouds depend on a number of factors, including cloud fraction, cloud top temperature, cloud optical properties, and cloud particle habit (Rossow and lacis 1990; Garrett et al. 2009; McFarquhar et al. 2002). Generally, the net CRE of high-level thin cirrus clouds is positive at TOA (McFarquhar et al. 2000), while the net CRE of thick anvils with visible optical depth larger than about 10 could be negative (Jensen et al. 1994). Low-level clouds typically have a cooling effect, because they can reflect more SW radiation to space and have a relatively small impact on the LW radiation (Chen et al. 2000; Dong et al. 2003). The impact of mid-level clouds depends on the strengths of these two radiative effects of high- and low-level clouds (Hartmann et al. 1992; Zhang et al. 2005; Zelinka et al. 2012).

Cloud vertical morphology contributes a major uncertainty in the analysis of satellite data used for climate studies (Heidinger and Pavolonis 2005; Wang and Dessler 2006; Li et al. 2011; Subrahmanyam and Kumar 2011). The ISCCP (Rossow and Schiffer 1999) has been collecting measurements of visible ($\sim$0.6 μm) and In-

frared (IR, $\sim$11 μm) radiances from the imaging radiometers on the international constellation of weather satellites since 1983. The ISCCP classification of clouds at high-level, mid-level, and low-level using cloud top pressure is widely used in the atmospheric community, even though there exist some uncertainties (Jin et al. 1996; Wylie et al. 2005; Rossow and Zhang 2010).

ISCCP builds a cloud climatology by relating the observed radiances to cloud radiative properties. Cloud top temperature is first retrieved by assuming that all clouds are opaque. Cloud top pressure is then determined from cloud top temperature using a profile of atmospheric temperature with pressure. If the cloud is opaque, it radiates likes a blackbody hence the emission temperature is equivalent to the cloud top temperature. However, if the cloud is optically thin, then the emission will appear to be larger than that for the cloud top temperature due to contamination by the radiation emitted by the warmer atmosphere and surface below. For clouds with visible optical depth between 2 and 6, the cloud top temperature is corrected by decreasing cloud top temperature (or increasing cloud top height) as a function of optical depth. This correction produces overestimations of cloud top temperature and pressure. During nighttime, however, semitransparent cirrus clouds may be falsely identified as mid-level clouds by not being able to use visible optical depth to correct cloud height. This leads to the general underestimation and overestimation of high- and mid-level clouds amounts in the ISCCP dataset, respectively (Jin et al. 1996; Rossow and Zhang 2010).

In contrast, the TOVS-B (Stubenrauch et al. 2006) dataset uses the IR radiances together with microwave observations and is more sensitive to high clouds. Similarly, the HIRS, which uses the CO_2 slicing analysis (Wylie and Menzel 1989; Wylie et al. 1994), also has better sensitivity to cirrus clouds. While the TOVS-B and HIRS are capable of detecting cirrus clouds, they do not detect low clouds ob-

scured by the high clouds. For instance, in the case of thin cirrus overlying mid- or low-level clouds, TOVS-B or HIRS provides the properties of the cirrus, whereas the use of visible channel by ISCCP leads to inference of a mid-level cloud. Discrepancies in the global coverage between ISCCP and TOVS-B (Stubenrauch et al. 2006) and between ISCCP and HIRS (Jin et al. 1996; Wylie et al. 2005) have been explained by differences in temperature profiles, horizontal heterogeneities (partial cloud cover) and vertical heterogeneities (multi-layer clouds).

In this chapter, we investigate the impacts of overlapping clouds in global statistics at different levels using the combined lidar and radar observations aboard the "A-Train" satellites. Comparisons of cloud amounts at different levels with the ISCCP dataset are also made for the same time period.

2.2 Dataset

New active sensors onboard the "A-Train" satellites, such as the CPR (Stephens et al. 2002) on CloudSat and CALIOP (Winker et al. 2009) on CALIPSO, are able to measure the multi-layer clouds lacking in the passive satellite measurements (Stephens et al. 2002). The CPR is a nadir-viewing instrument with an effective horizontal resolution of 1.4 km (Stephens et al. 2008). It transmits at 94-GHz (W-band) and has a maximum and minimum detectable radar reflectivity of 29 and -30 dBZ (Stephens et al. 2008). With this sensitivity, the radar detects the majority of clouds that significantly affect the radiation budget and critical elements of the water budget of the atmosphere. The primary instrument aboard the CALIPSO payload is CALIOP (Winker et al. 2003), which is a near-nadir viewing lidar operating at two wavelengths centered at 532 and 1064 nm. The measurements made by the 532 nm channel have good sensitivity to thin clouds and aerosols (Winker and Trepte 1998). Cloud vertical profiles from either CloudSat or CALIPSO alone, however, cannot

provide a complete picture of the cloud vertical structure. For instance, clouds containing relatively small particles, like cold cirrus or shallow water clouds that do not contain large particles or drizzle droplets, will not be detected by the CPR. The CALIOP signal, on the other hand, can be completely attenuated by the clouds with an visible optical depth greater than about 3 (Mace 2007; Mace et al. 2009).

A first step in using the information of multi-layer clouds from CloudSat and CALIPSO is to combine cloud vertical profiles derived independently from these two instruments. The combination of CALIPSO and CloudSat as well as other instruments has been widely used in the cloud-related research (Wang et al. 2010; Joiner et al. 2010; Li et al. 2011). The accuracy of overlapping CALIPSO and CloudSat footprints in the coordination of satellite pointing has been discussed in previous studies (Stephens et al. 2008; Mace et al. 2009), and shows that more complete information of clouds can be generated with the combination of these two instruments (Mace 2007; Mace et al. 2009). Kato et al. (2010) demonstrated a sophisticated method to merge CALIPSO, CloudSat, CERES, and MODIS data products into an integrated dataset named CCCM (available at: http://eosweb.larc.nasa.gov/).

The CCCM dataset spatially collocates CALIPSO, CloudSat and MODIS with near nadir view of the CERES instrument's footprints. The horizontal resolution of CCCM is the length of CERES footprint (approximately 20 km). The best estimate of the vertical profile of cloud properties is determined from CALIPSO and CloudSat. Kato et al. (2010) stated that the merged cloud profiles of CCCM are primarily based on CALIPSO derived cloud profiles, except when the CALIPSO signals are completely attenuated. The cloud layer top and base height are examined from TOA to the surface. The cloud boundary determination strategy is demonstrated in Table 2.1. Approximately 85% and 77% of cloud top and base heights are determined from CALIPSO according to Kato et al. (2010).

Table 2.1 Cloud profile merging strategy (obtained from Kato et al. 2010).

Cloud Boundary	CALIOP	CPR	Merged Boundary
Top	Detected	Detected	Higher cloud top
Top	Detected	Undetected	CALIOP cloud top
Top	Undetected	Detected	CPR cloud top
Base	Not completely attenuated	Undetected	CALIOP cloud base
Base	Not completely attenuated	Detected	CALIOP cloud base
Base	Completely attenuated	Detected	CPR cloud base
Base	Completely attenuated	Undetected	CALIOP lowest unattenuated cloud base

The CCCM keeps up to 16 cloud groups (i.e. 16 different sets of cloud top and base boundaries) in a CERES footprint. The clouds with the same cloud layering and the largest cloud fraction are grouped together into group one, and subsequently from group two to group sixteen. For each cloud group, there are up to a total of six cloud overlapping layers. Once cloud height profiles from CALIPSO and CloudSat are merged, we manually match the cloud top temperature and pressure for each cloud layer in an individual merged cloud group using the atmospheric pressure and temperature profiles from the Global Earth Observing System (GEOS) data product provided to the CALIPSO project by the NASA Global Modeling and Assimilation Office (GMAO) Data Assimilation System. A total of three and a half years (July 2006 - December 2009) of the CCCM data are selected for the analysis.

The ISCCP cloud amounts at high-, mid-, and low-level are used to make comparisons with the CCCM dataset for the same time period. The ISCCP D2 monthly

mean cloud amount is available at http://isccp.giss.nasa.gov/products/browsed2.html.

2.3 Identification of single-layer and multi-layer clouds

Cloud layering can have different meanings to the remote sensing and modeling communities. In remote sensing, cloud layering typically refers to the situations in which one cloud geometrically overlaps a lower level cloud within a Field of View (FOV) and it is frequently looked at as a potential source of errors (Baum and Wielicki 1994). A common assumption is that there is a cloud-free layer between the two cloud layers. In GCMs, the cloud overlap problem typically refers to different ways of arranging clouds in the prescribed layers of the vertical column within a GCM grid box - whether or not the cloud layers are separated by non-cloudy airs. Not surprisingly, changing the cloud overlap scheme in GCMs affects cloud radiative forcing (Weare 2001), but observational studies have shown that cloud layering is complicated and depends on location and local dynamics and radiation (Mace and Benson-Troth 2002; Falk and Larson 2007).

Table 2.2 Frequency of occurrence (%) of single-, double, triple, and four or more than four-layered clouds over the globe. Data are from Table 1 in Wang et al. (2000) and Table 1 in Subrahmanyam and Kumar (2011).

	Single-	Double-	Triple-	$\geq$ Four-layer
Want et al. (2000)	58	28	9	5
Subrahmanyam and Kumar (2011)	57	29	11	3

Because the CCCM dataset only provides cloud information for up to six layers, the single-layer clouds and multi-layer clouds are then manually derived from the merged cloud groups. When a CERES footprint contains only one cloud layer for each group, the cloud within this CERES footprint can be referred to "Single-layer cloud". "Multi-layer cloud", on the other hand, means all cloud profiles within

the corresponding CERES footprint contain more than one cloud layer for each profile. Several previous studies have reported statistically significant frequency of multi-layer cloud occurrence regionally and globally (Wang et al. 2000; Wang and Dessler 2006; Subrahmanyam and Kumar 2011). Table 2.2 shows the frequency of occurrence of single-layer and multi-layer clouds in two previous studies. In the Wang et al. (2000) investigation, they showed that multi-layer clouds occurred 42% of the time in a 20-year radiosonde dataset. Among all the multi-layer clouds, two-layered, three-layered, and clouds with more than 4 layers were present 28%, 9%, and 5%, respectively, of the time. Subrahmanyam and Kumar (2011), using the CloudSat 2B-GEOPROF-LIDAR data (Mace 2007) of the year 2007, studied multi-layer clouds across the globe. They found that multi-layer clouds occurred 43% globally and approximately 70% of the multi-layer clouds were two-layered clouds. Since two-layered clouds substantially dominate the multi-layer cloud systems, this dissertation will only focus on the two-layered cloud scenarios.

2.4 Results

In this study, only overcast satellite footprints are considered. Cloud amount in a given CERES footprint is defined as:

$$A = \frac{N}{T}$$

where A is the cloud amount, N represents the number of single- or multi-layer cloud profiles, and T is the total merged cloud profiles from combined CALIPSO and CloudSat observations. Similar definitions for cloud amounts of single- and multi-layer clouds can be found in Li et al. (2011).

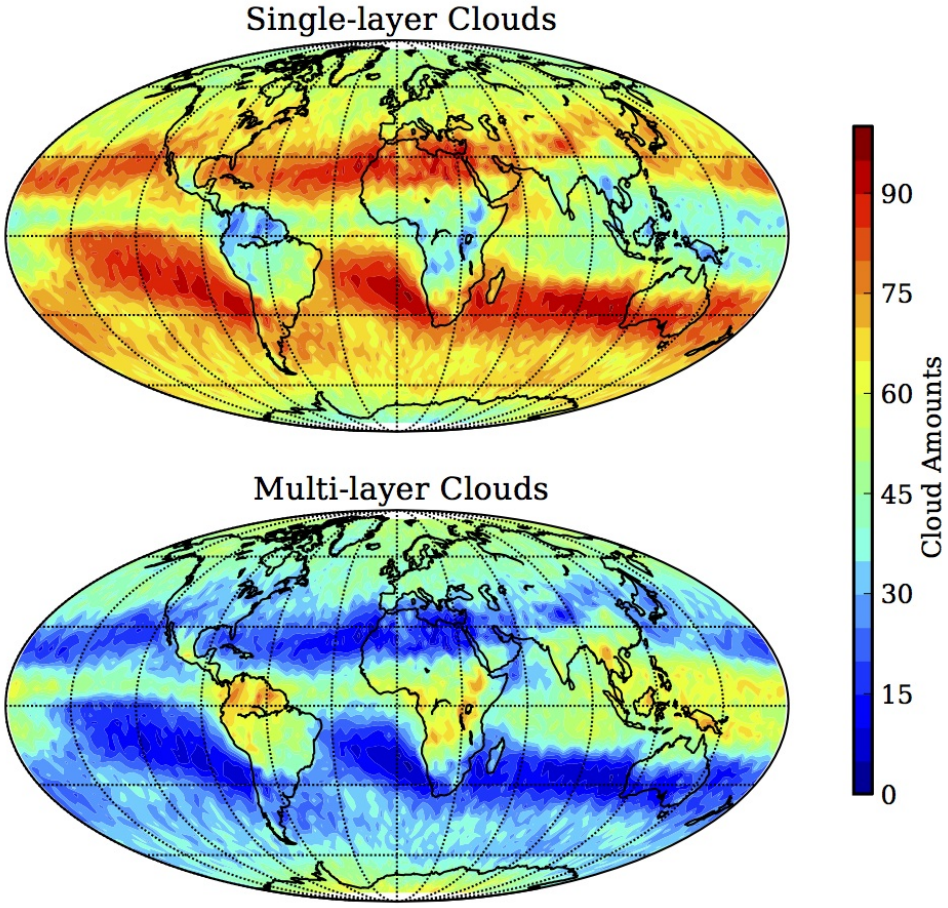

Figure 2.1 Global distributions of cloud amounts for single- and multi-layer clouds from collocated CALIPSO and CloudSat between December 2007 and November 2008. Cloud amount refers to in a given CERES footprint is defined as the ratio between the number of single- or multi-layer cloud profiles and the total merged cloud profiles from combined CALIPSO and CloudSat observations.

Figure 2.1 shows the global frequency maps of the determined single- and multi-layer cloud amounts. The distribution patterns of single- and multi-layer clouds in this figure are similar to the global maps of cloud fraction of these clouds in Li et al. (2011), even though clear sky cases were included in their calculations. Except for a few areas in the tropical region, the amount of single-layer clouds generally exceeds the multi-layer clouds over the globe for the entire period (three and a half years). Higher amounts of single-layer clouds occur between the latitudes of 10° and

30° in the NH. Greater values are also seen over the ocean on the western coast of continents between 0° S and 30° S, and at mid- and high-latitudes in the SH. Generally, more multi-layer clouds occur over oceans than over land. Looking at this figure, it is evident that multi-layer clouds occur more frequently than single-layer clouds in the low-latitudes, particularly over northern South America, central Africa, Southeast Asia, and the tropical western pacific. This feature is consistent with previous observations using the Advanced Very High Resolution Radiometer (AVHRR, Heidinger and Pavolonis 2005), and has been shown to lead to more complexity in deducing the radiative impact of clouds (Wielicki et al. 1995; Chen et al. 2000). High frequencies of multi-layer clouds can also be seen in high-latitudes. It is therefore of great importance to involve multi-layer clouds during the investigation of global cloud statistics.

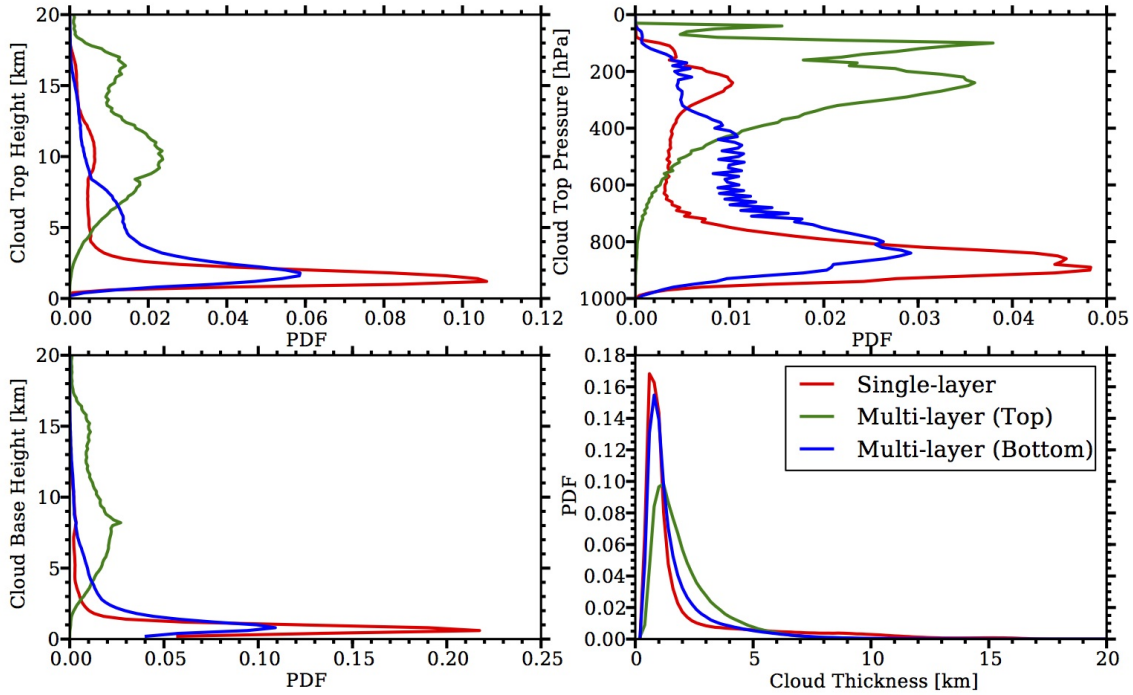

Figure 2.2 Probability distribution functions of cloud top and base height, cloud top pressure, and cloud thickness.

The factors that influence the radiative effects of clouds are numerous and complicated. When cloud overlap occurs, the determination of cloud microphysical and macrophysical properties is challenging (Nasiri 2004; Chang and Li 2005; Huang et al. 2005; Joiner et al. 2010). Because the discussion of microphysical properties is beyond the scope of this dissertation, only cloud macrophysical retrievals, including cloud top and base height, cloud top pressure, and cloud thickness, are analyzed in this section. Figure 2.2 shows the probability distribution function (PDF) of cloud top and base height, cloud top pressure, and cloud thickness for single- and multi-layer clouds. The single-layer clouds and top and bottom layers of multi-layer clouds are shown separately. The majority of the top layer clouds within the multi-layer cloud systems have cloud tops above approximately 4 km or 700 hPa, and cloud base heights are generally higher than 2km. The cloud top heights from the bottom cloud layer within the multi-layer cloud systems are lower than about 8 km or 400 hPa, and the cloud base heights are largely between 0 and 2 km. A notable amount of clouds have geometric thickness of larger than 5 km. Li et al. (2011) documented that the maximum single- and multi-layer cloud thickness occur in the tropical regions. Figure 2.3 shows the global average of cloud top height and pressure for the top and bottom layers of multi-layer clouds that corresponds to Figure 2.2. In the top two panels, it is evident that the top layer clouds are approximately above 13 km or 250 hPa in the tropics. From about 30^{o} N(S) to the polar regions, the cloud tops are generally between 7 and 11 km or between 300 and 450 hPa. Cloud tops of bottom layer clouds are generally lower than about 4 km or 750 hPa over oceans. Over northern South America, Africa, and tropical western pacific, the cloud tops of the bottom cloud layers can be up to 8 km or 400 hPa, which can be classified as mid-level clouds (Riihimaki et al. 2012).

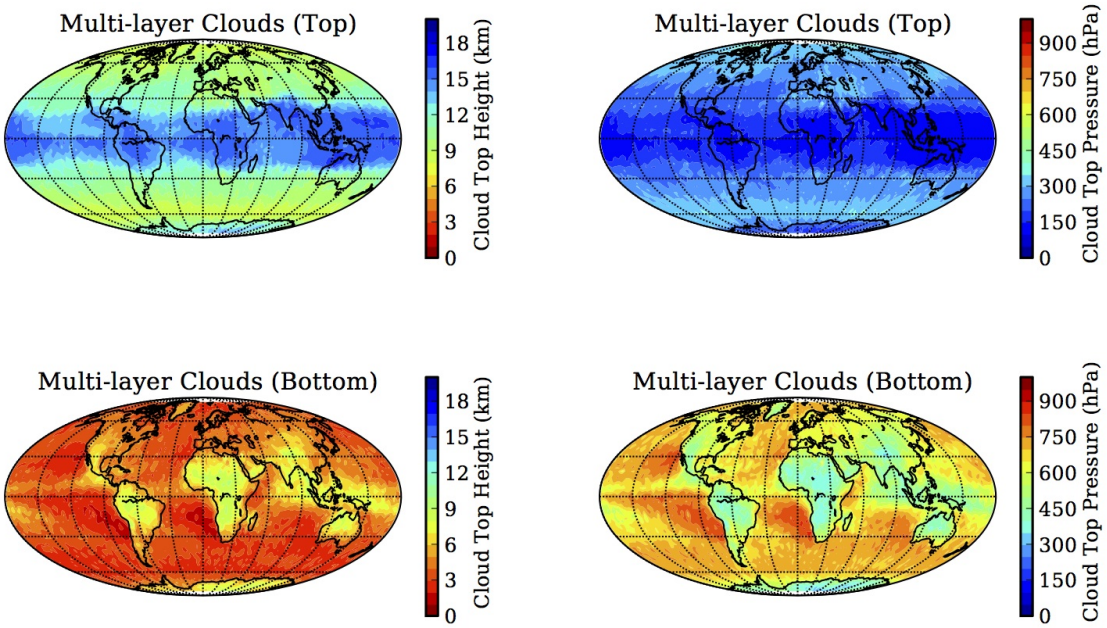

Figure 2.3 Global average of cloud top height and pressure for the top and bottom layers of multi-layer clouds.

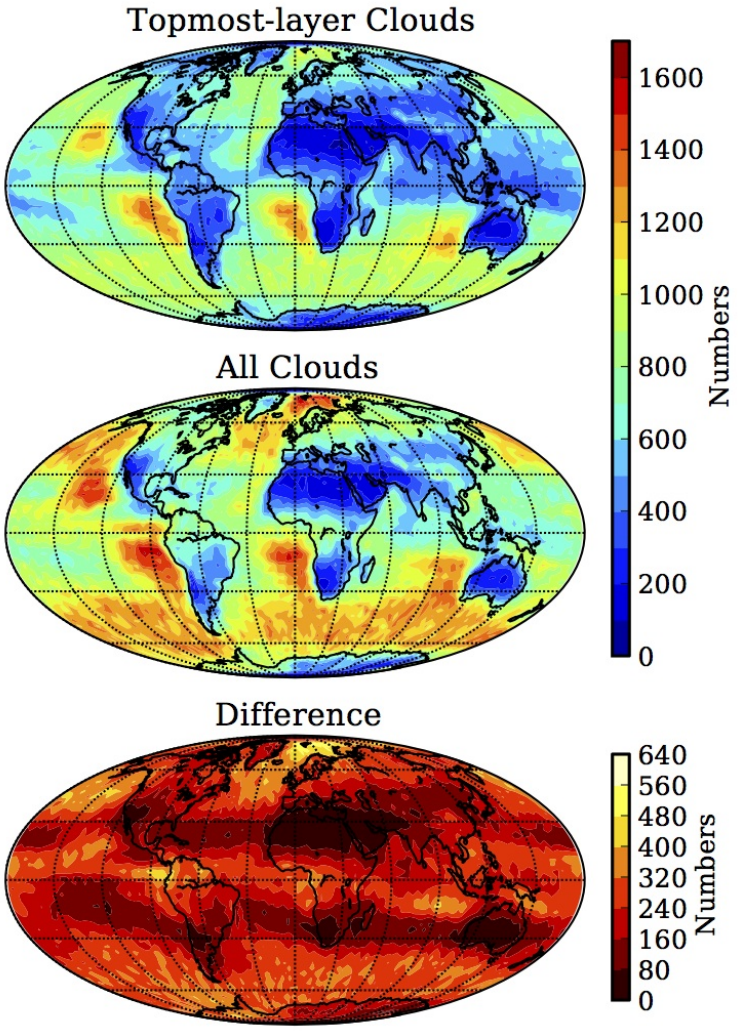

Figure 2.4 Global distributions of topmost-layer and all clouds as well as their difference. Single-layer and the top layer of multi-layer are included in the topmost-layer clouds; single- and multi-layer (top and bottom) clouds are included in all clouds. Difference: all clouds - topmost-layer.

Traditional satellite imagers and sounders only see the uppermost cloud top in each vertical column. If multi-layer clouds occur, the existing cloud statistics obtained from passive satellite techniques cannot accurately account for all the cloud information for climate-related applications. Rossow and Zhang (2010) developed a new statistical model using the statistics from a combination of the ISCCP dataset

and radiosonde profiles, and they classified clouds into high-, mid-, and low-level clouds based on cloud top pressure of the uppermost cloud layer in each profile. However, the use of only uppermost cloud layer can introduce significant errors in the analysis. Global maps of uppermost-layer clouds, all clouds, and their differences using the CCCM dataset are demonstrated in Figure 2.4. In our study, all clouds mean that both single-layer and multi-layer (top and bottom) clouds are included. The major differences between the uppermost-layer and all clouds are found over the mid- and high-latitude oceans and the Intertropical Convergence Zone (ITCZ). The lowest values are shown over the continents in northern Africa and Australia. Figure 2.5 shows the zonal distribution of the topmost-layer and all clouds at different levels using cloud top pressure (high: $P_t \geq 440$ hPa; middle: 440 hPa $< P_t <$ 680 hPa; low: $P_t \leq 680$ hPa, hereafter referred as ISCCP definition), of January and July averaged over the three years and a half period. The distribution patterns of clouds at different levels are similar for both January and July, although the ITCZ looks to shift northward in July. High-level clouds are the dominant cloud type in the tropical region. Mid-level clouds occur less frequent than high- and low-level clouds from tropics to high-latitudes. Larger differences of high- and low-level clouds between topmost-layer and all clouds can be found in winter season.

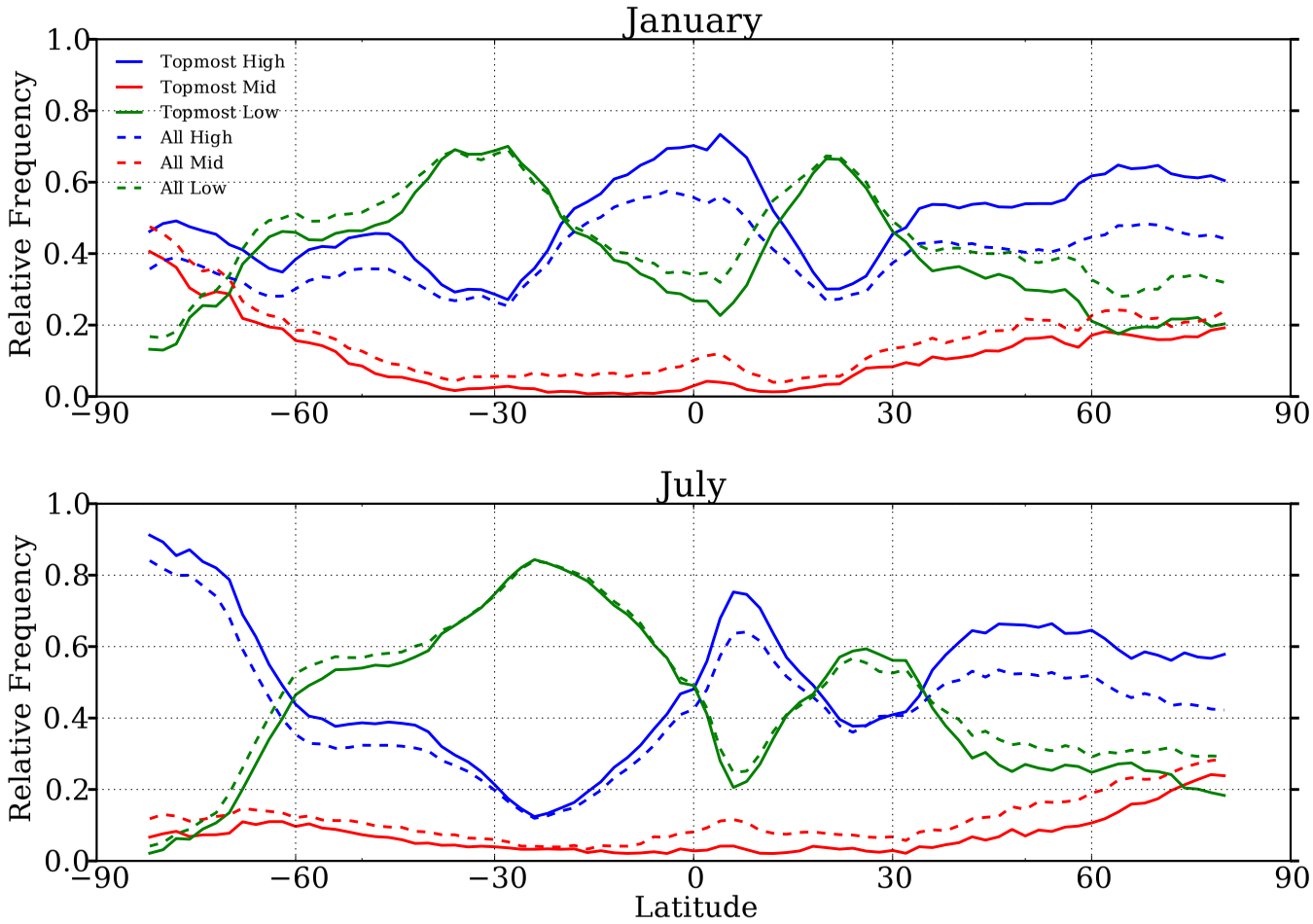

Figure 2.5 Zonal distributions of topmost-layer and all clouds at three levels using ISCCP definition for January and July . Upper panel: January; lower panel: July.

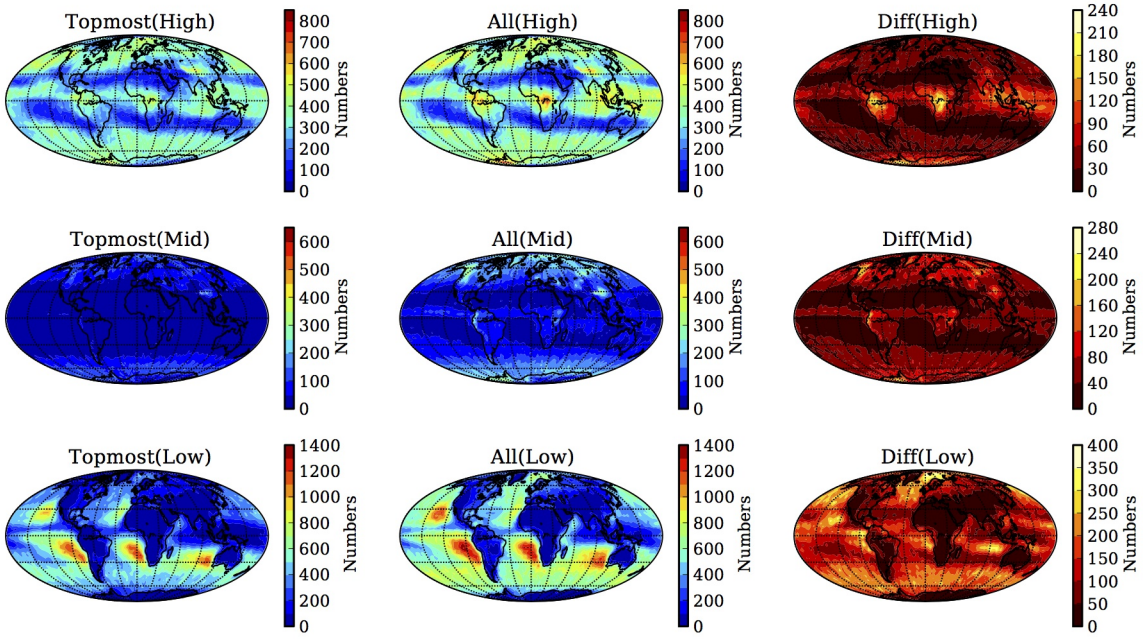

Figure 2.6 Global distributions of topmost-layer and all clouds at three levels using ISCCP. Diff: all clouds - topmost-layer.

From Figures 2.6 to 2.8, cloud at different levels for topmost-layer (left), all clouds (middle), and their difference (right) are presented. Figure 2.6 follows the ISCCP definition, and Figures 2.7 and 2.8 use cloud top height (high: $Z_t \geq 7$ km; middle: 3 km $< Z_t <$ 7 km; low: $Z_t \leq 3$ km, hereafter referred as cloud-top definition) and cloud base height (high: $Z_b \geq 5$ km; middle: 2 km $< Z_b <$ 5 km; low: $Z_b \leq$ 2 km, hereafter referred as cloud-base definition), respectively. Table 2.3 shows the number of footprints in different latitudes for clouds at different levels using three different classification schemes. As seen in Table 2.3, the high-level clouds, defined using cloud-base definition, are generally fewer than those determined by ISCCP and cloud-top definitions globally. The ISCCP definition identifies a comparable number of high-level clouds in the low- and mid-latitudes, as does the cloud-top definition, but not in the polar regions. From Figs 2.6 to 2.8, we know that the major difference of high-level clouds between topmost-layer and all clouds are in the low-latitudes,

particularly in South America, central Africa, Southeast Asia, and tropical western pacific, where multi-layer clouds occur frequently.

Table 2.3 Number of CERES footprints in different latitude zones for high-, mid, and low-level clouds of topmost-layer and all clouds. The numbers of all clouds are shown in the parenthesis. Rows in each level represent different classification definition. Top, middle, and bottom rows correspond to ISCCP definition, cloud-top definition, and cloud-base definition, respectively.

	Global	Tropical (30°S-30°N)	Mid-latitude (30-60°S, 30-60°N)	High-latitude (60-90°S, 60-90°N)
High-level	1,981,848	591,658	766,512	623,678
	(2,289,963)	(710,090)	(845,462)	(734,411)
	1,857,178	590,872	726,582	539,724
	(2,114,279)	(707,300)	(789,007)	(617,972)
	1,536,981	544,453	575,228	417,300
	(1,754,311)	(649,251)	(630,703)	(474,357)
Mid-level	372,529	33,769	142,106	196,654
	(766,262)	(116,701)	(285,461)	(364,100)
	519,514	46,371	193,606	279,537
	(989,447)	(146,802)	(366,008)	(476,637)
	415,392	40,970	151,631	222,791
	(749,007)	(126,130)	(261,982)	(360,895)
Low-level	1,970,448	784,961	867,030	318,457
	(2,821,247)	(1,033,764)	(1,220,496)	(566,987)
	1,948,163	773,145	855,473	319,545
	(2,773,797)	(1,006,453)	(1,196,422)	(570,922)
	2,367,251	824,506	1,046,139	496,606
	(3,365,863)	(1,084,312)	(1,454,446)	(827,105)

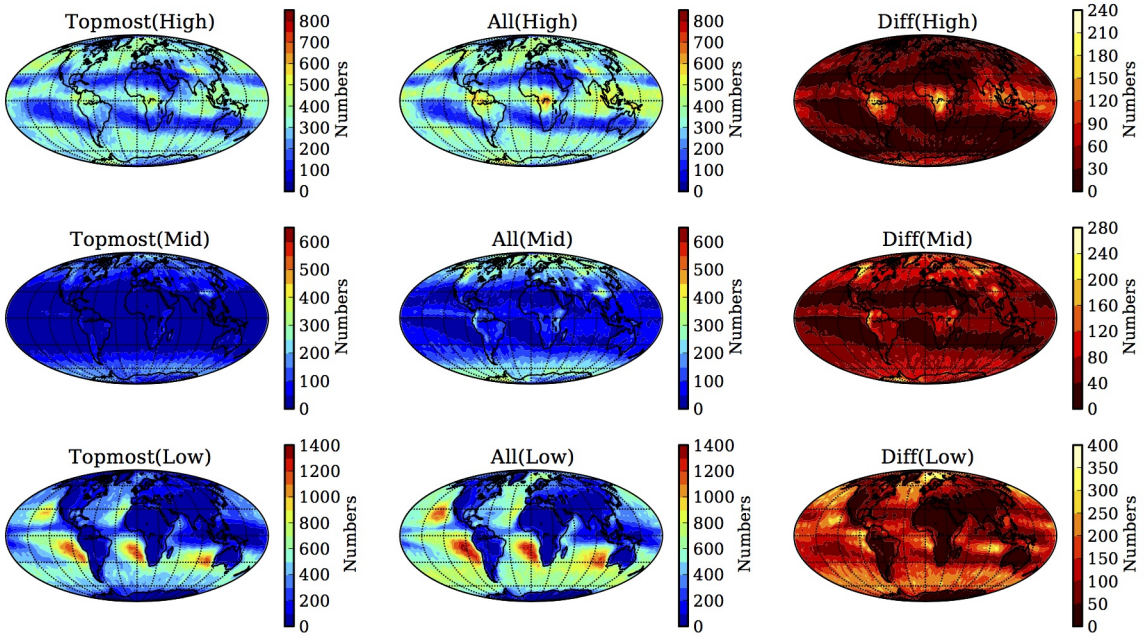

Figure 2.7 Similar as Figure 2.6. High-, mid-, and low-level clouds are defined using cloud top height (Z_t). High-level: $Z_t \geq 7$ km; Mid-level: 3 km $< Z_t <$ 7 km; Low-level: $Z_t \leq 3$ km. Diff: all clouds - topmost-layer.

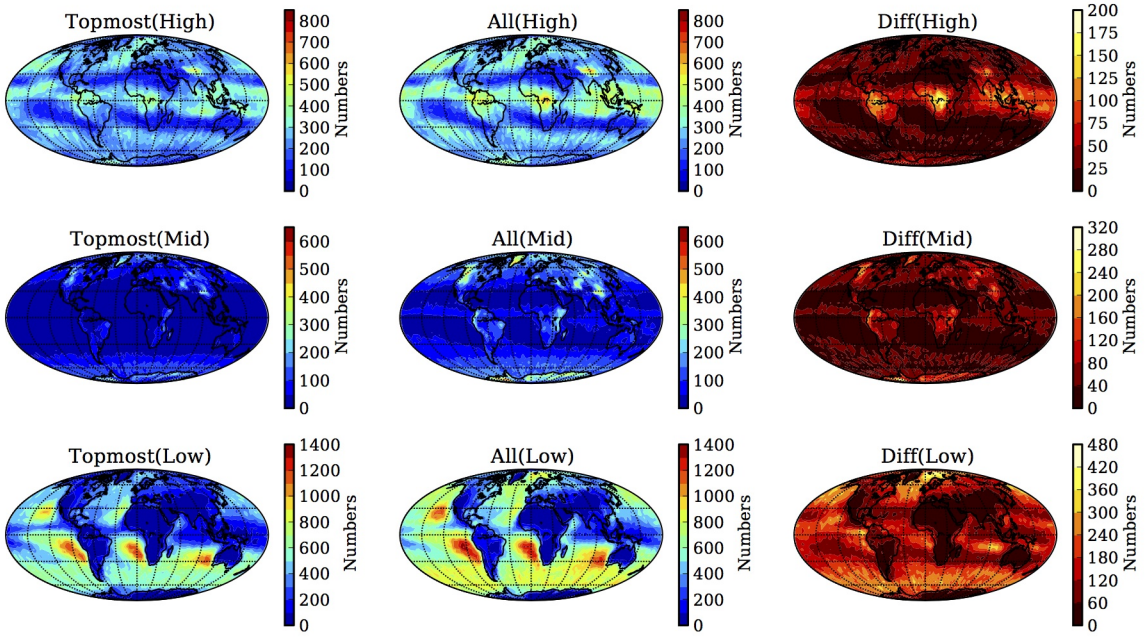

Figure 2.8 Similar as Figure 2.6. High-, mid-, and low-level clouds are defined using cloud base height (Z_b). High-level: $Z_b \geq 5$ km; Mid-level: 2 km $< Z_b <$ 5 km; Low-level: $Z_b \leq 3$ km. Diff: all clouds - topmost-layer.

Conversely, the number of low-level clouds determined by the cloud-base definition in Table 2.3 is much greater than compared to ISCCP and cloud-top definitions. This is likely due to some geometrically thick clouds, such as deep convective clouds or cumulus congestus with cloud bases less than 2 km, being classified as low-level clouds. The ISCCP definition, however, finds a similar amount of low-level clouds as the cloud-top definition does globally. A distinguishable feature shown in Figs 2.6 to 2.8 is the low level clouds have discriminated features over the oceans. Table 2.3 also shows that the largest variations are seen in the mid-level clouds. The number of mid-level clouds within all clouds account for approximately a factor of two compared to topmost-layer clouds. The sensitivity of mid-level cloud frequency varies greatly with observational techniques and definitions (Stubenrauch et al. 2006; Hahn and Warren 1999; Hahn and Warren 2003). Additionally, the ISCCP definition classifies less mid-level clouds than cloud-top and cloud-base definitions. Significant discrepancies exist in mid- and high-latitudes as well as ITCZ when multi-layer clouds are included (see Figs 2.6 to 2.8).

Through comparisons with CALIPSO and CloudSat observations, Rossow and Zhang (2010) found three major differences: 1) overestimation of mid-level clouds in polar regions; 2) overestimation of cloud top pressure of highest-level clouds, especially in the tropical regions; and 3) underestimation of low-level cloud amounts over southern mid-latitude oceans. However, in Rossow and Zhang (2010), they only considered the clouds in the uppermost-layer, whereas in our study, we include both the uppermost-layer and all clouds from the CCCM dataset in the analysis. Figure 2.9 shows normalized frequencies of ISCCP cloud mounts and CCCM cloud amounts of topmost-layer and their differences at three vertical levels using the ISCCP definition for the same time period. And similarly, Figure 2.10 shows cloud amounts at each level but uses all clouds from CCCM rather than only topmost-layer clouds.

The global distribution of high-level clouds of ISCCP and CCCM datasets are similar with high values over land and the tropical western pacific and low values over the west coast of continents. The largest discrepancy of high-level clouds between the two datasets is in the tropics, NH continents, and polar regions. Generally, the ISCCP data underestimate high-level clouds in Figure 2.9 and Figure 2.10, which is consistent with a few previous studies that made comparisons between the ISCCP and HIRS datasets (Jin et al. 1996; Wylie et al. 2005). The differences decrease when multi-layer clouds are included and compared to the topmost-layer clouds only. Significant differences between the ISCCP and CCCM are shown for the mid-level clouds, where the ISCCP in general overestimates mid-level clouds globally. With regard to low-level clouds, the two datasets show similar global distributions except at the South Pole because no data is obtained from ISCCP. The ISCCP dataset underestimates low-level clouds over oceans from about 30^o N southward to the South Pole. Additionally, the ISCCP finds more low-level clouds in the Sahara Desert region, and in contrast, the CCCM reports more high-level clouds there instead. The difference is likely due to the detection sensitivities of different instruments to clouds and aerosols in a region with a bright surface (e.g. deserts or snow-covered land) (Chen et al. 2010; Rossow and Zhang 2010).

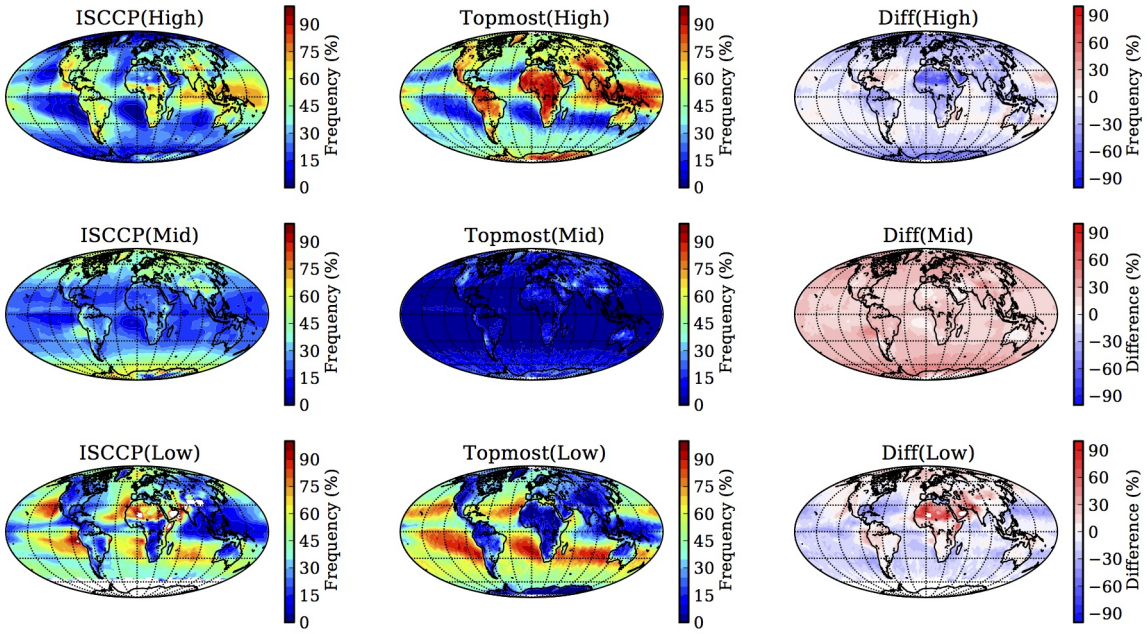

Figure 2.9 Normalized frequency of ISCCP cloud amounts and topmost-layer cloud amounts from CCCM as well as their difference at three levels using ISCCP definition. Diff: ISCCP - topmost-layer.

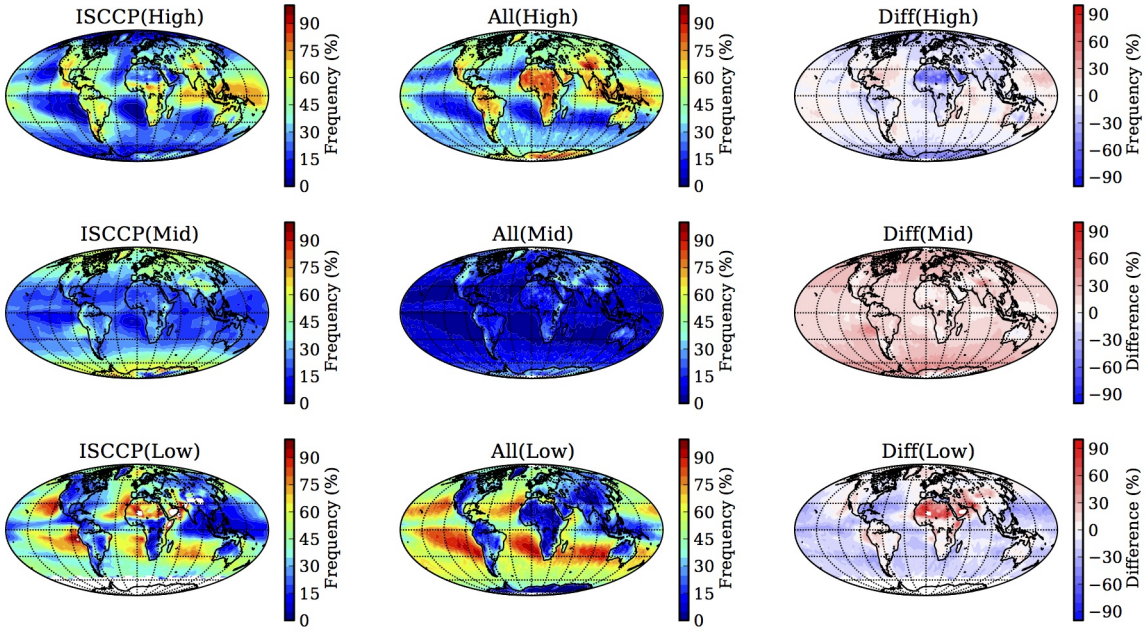

Figure 2.10 Normalized frequency of ISCCP cloud amounts and all cloud amounts from CCCM as well as their difference at three levels using ISCCP definition. Diff: ISCCP - all clouds.

3. CHARACTERISTICS OF MID-LEVEL CLOUDS

In the last chapter, we introduced a merged CCCM data set spanning July 2006 to December 2009. The active remote sensing datasets from CloudSat and CALIPSO allow us to deal with cases involving multiple cloud layers, which are a source of uncertainties in cloud studies based on purely passive observations. We statistically discussed the impacts of overlapping clouds at different vertical levels, and the results showed that it is fundamentally important to involve multi-layer clouds both in regional and global statistics. In this chapter, we focus on the characteristics of mid-level clouds. The three years and a half years of the CCCM dataset is also used in the analysis. Three major questions will be addressed: 1) Because multi-layer clouds occur frequently, what fraction of mid-level clouds tend to occur in the multi-layer cloud scenes? 2) What are the observed relationships between cloud frequency, cloud top height and pressure, geometrics thickness, and cloud top temperature for mid-level clouds? 3) How effective is cloud top temperature for classifying mid-level clouds?

3.1 Mid-level clouds in the multi-layer cloud regimes

Traditionally, satellite-based cloud retrievals were made under the assumption of a single cloud layer within a FOV. The presence of multiple cloud layers introduces errors in infrared-based cloud top pressure retrievals (Baum and Wielicki 1994) with the retrieved upper-cloud height lower than the actual upper-cloud height. A recent development is the assumption of up to two cloud layers in a FOV, such as the AIRS standard retrievals (Susskind et al. 2003). In this section, we will consider the frequency of cloud layering as it relates to mid-level clouds from the observational perspective.

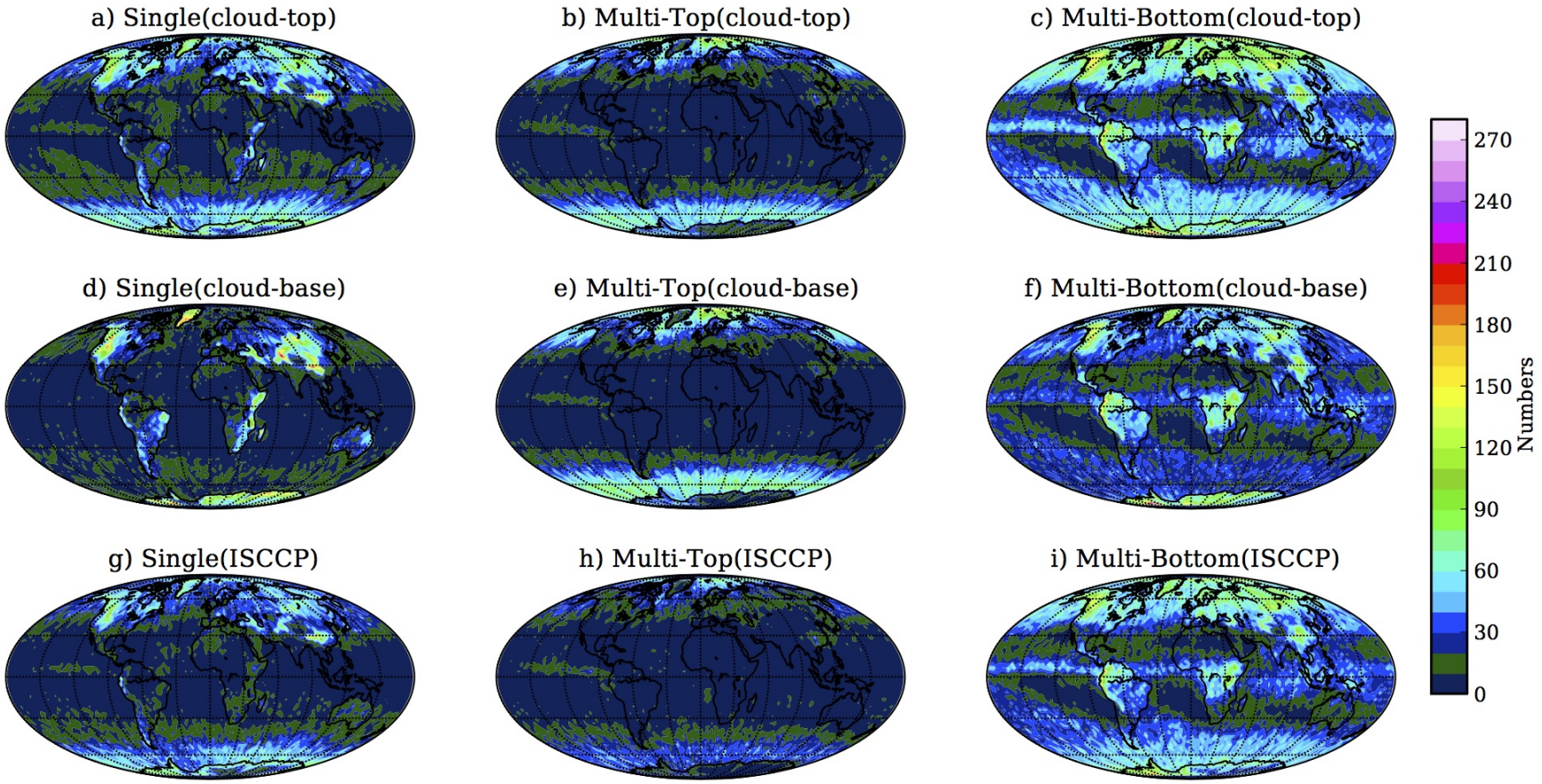

Figure 3.1 Global distributions of mid-level clouds using the ISCCP definition between 680 and 440 hPa, cloud-top definition between 3 and 7 km, and cloud-base definition between 2 and 5 km in the single-layer and multi-layer cloud scenes. Multi-Top: top layer of multi-layer clouds; Multi-Bottom: bottom layer of multi-layer clouds.

Figure 3.1 shows the global frequency distributions of mid-level clouds when using the cloud-top ($3\ \text{km} < Z_t < 7\ \text{km}$), cloud-base ($2\ \text{km} < Z_b < 5\ \text{km}$), and ISCCP ($440\ \text{hPa} < P_t < 680\ \text{hPa}$) definitions of the mid-level for single-layer (left panel), multi-layer top (middle panel), and multi-layer bottom (right panel), respectively. The global distribution patterns of mid-level cloud for single-layer cloud scenes are clearly different from the top and bottom layers within the multi-layer cloud regimes. It is important to point out that CALIPSO is more sensitive than most other satellite instruments to optically thin clouds, such as cirrus. Because of this sensitivity and the frequency of thin cirrus clouds, single-layered mid-level cloud scenes are not incredibly common in the low-latitude regions. When the top layer of multi-layer cloud scenes are determined as mid-level, it is clear that these clouds are mostly distributed over the high-latitudes. On the other hand, if the bottom layer of multi-layer cloud scenes are classified as mid-level clouds, it is easy to see that mid-level clouds are relatively common under cirrus in deep convection regions, such as the ITCZ and rain forest regions, as well as in the higher mid-latitudes.

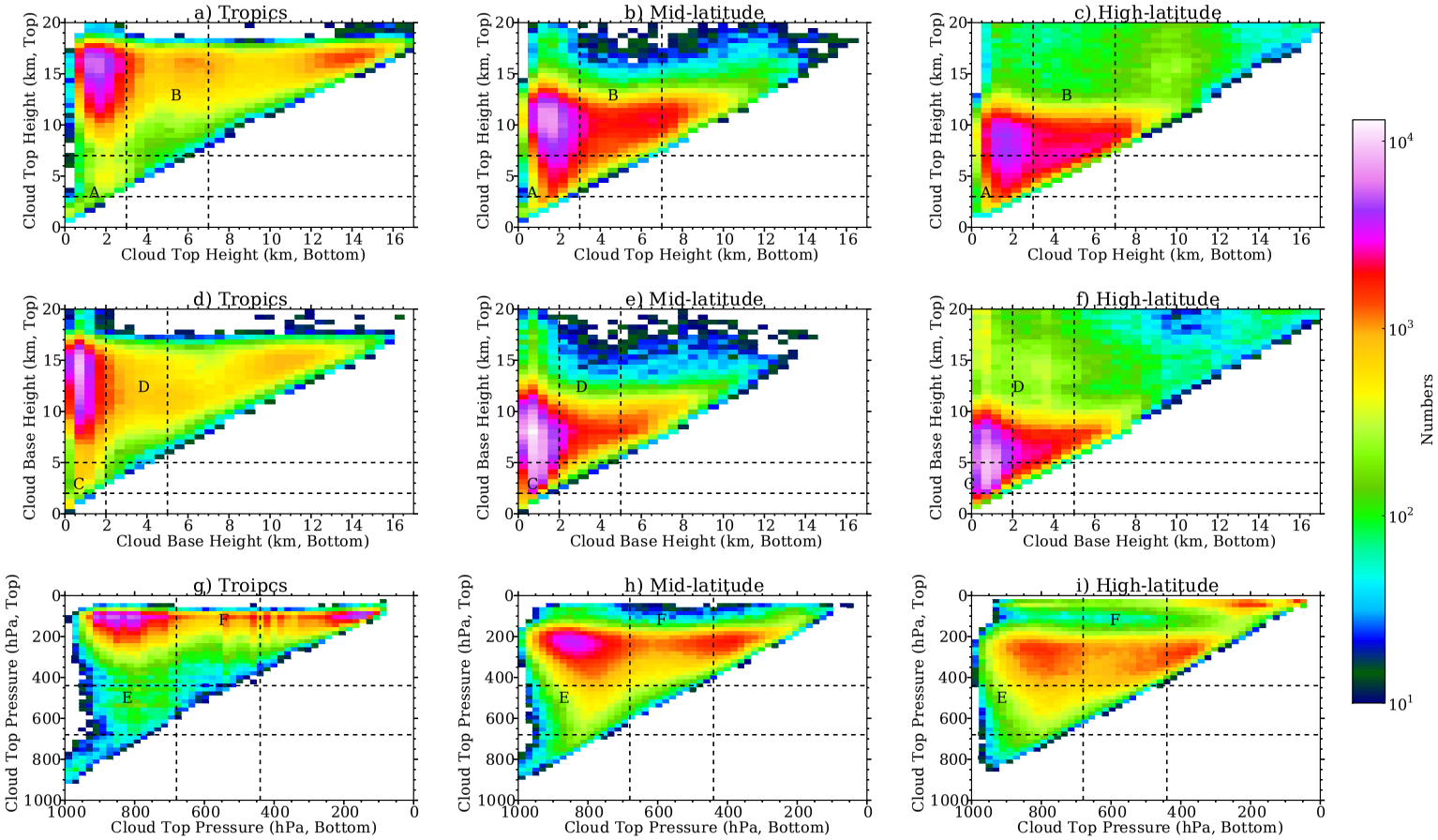

Figure 3.2 Joint histograms for top layer (y axis) and bottom layer (x axis) in the multi-layer cloud scenes. a), b), and c) are cloud top heights; c), d), and e) are cloud base heights; and g), h), and i) are cloud top pressures. Boxed A, C, and E are mid-level over low clouds, and boxes B, D, F are high clouds over mid-level.

Figure 3.2 shows the joint histograms for the top layer and bottom layer within the multi-layer cloud regimes as a function of cloud top height (top panel), cloud base height (middle panel), and cloud top pressure (bottom panel), respectively. Three categories of histograms are also plotted for different latitudinal regions (tropics: 30° N−30° S; mid-latitude: 30°−60° N(S); high-latitude: 60°−90° N(S)). Each subplot is sliced into nine boxes, two of which are labeled. We may associate boxes A, C, and E as mid-level over low-level clouds and boxes B, D, and F as high-level over mid-level clouds. These boxes are the main focuses for mid-level clouds here. We can see that the majority of the clouds of the multi-layer cloud scenarios are high-level over low-level. Table 3.1 lists the numbers and percentage of the corresponding boxes in each subplot in Figure 3.2 using the three definitions for mid-level clouds. Fewer mid-level clouds occur in the tropics than mid- and high-latitudes. Generally, the cloud-top and cloud-base definitions identify more mid-level cloud scenes than the ISCCP definition except the mid-level over low-level using cloud-base in the low latitudes. In the tropics, the high-level over mid-level clouds occur more frequently (approximately a factor of 8 or 9) than mid-level over low-level clouds. In mid- and high-latitudes, the high over middle cloud scenarios occur approximately as twice as much as the mid-level over low-level clouds with the cloud-top and ISCCP definitions, and on the other hand, the cloud-base definition shows a roughly comparable number of middle over low and high over middle clouds. Additionally, there are also notable amounts of mid-level over mid-level clouds in Figure 3.2; however, these cloud scenes occur much less frequent than the mid-level over low-level and high-level over mid-level scenes.

Table 3.1 Number of mid-level clouds in the multi-layer cloud scenes. The total number of multi-layer clouds is 1,552,671. A-F corresponds to boxes A-F in Figure 3.2. Percentage is shown in the parenthesis.

Definitions	Tropical (30°S-30°N)	Mid-latitude (30-60°S, 30-60°N)	High-latitude (60-90°S, 60-90°N)
cloud-top	A	A	A
	10,786	63,671	89,730
	(0.6%)	(4.1%)	(5.8%)
	B	B	B
	97,870	157,756	157,634
	(6.3%)	(10.2%)	(10.2%)
cloud-base	C	C	C
	9,534	81,906	118,468
	(0.6%)	(5.3%)	(7.6%)
	D	D	D
	84,204	105,817	123,832
	(5.4%)	(6.8%)	(8.0%)
ISCCP	E	E	E
	10,833	45,605	57,982
	(0.7%)	(3.0%)	(3.7%)
	F	F	F
	81,530	136,978	151,576
	(5.3%)	(8.8%)	(9.8%)

3.2 Characteritics

To investigate the characteristics of the mid-level clouds, we include all clouds (single-layer+multi-layer) in this section. Because the ISCCP definition of classifying mid-level clouds between 680 and 440 hPa is widely used in the climate model community, as a starting point, the ISCCP convention of mid-level clouds will first be followed. The ISCCP mid-level cloud pressures correspond to cloud top height

between 3.2 and 6.4 km in a standard mid-latitude winter atmosphere and between 3.4 and 6.9 km in a standard tropical atmosphere (McClatchey et al. 1972). To characterize mid-level clouds globally, the cloud top height range is expanded to between 3 and 7 km, even though other thresholds are often used in surface remote sensors (Mace et al. 2006; Riihimaki et al. 2012). Additionally, the characteristics of mid-level clouds defined by cloud-base definition as used in the last chapter are also examined. One of the main focuses of characterizing mid-level using the three definitions is to see whether the common mid-level cloud definitions find the same set of clouds. Moreover, to test the sensitivities of mid-level cloud frequencies to different definitions, a set of thresholds for cloud top and base boundaries are also investigated statistically.

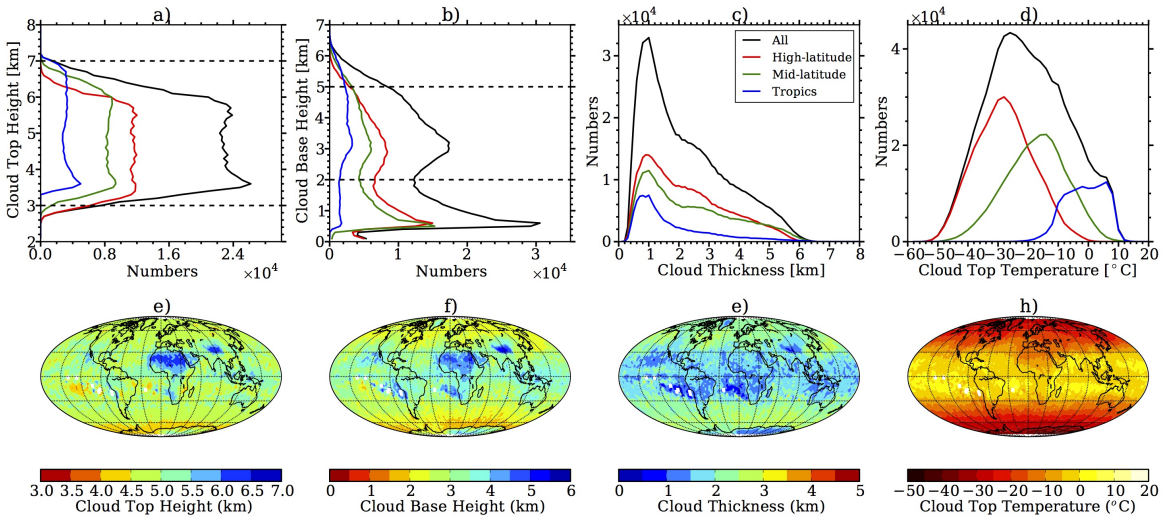

Figure 3.3 Probability distributions of mid-level clouds using the ISCCP definition between 680 and 440 hPa as a function of a) cloud top height, b) cloud base height, c) cloud thickness, and d) cloud top temperature. The four curves are for global (black), high-latitude (red), mid-latitude (green), and tropics (blue). e-h): Global averages of cloud top height, cloud base height, cloud thickness and cloud temperature.

Figure 3.3 shows mid-level cloud frequencies for the ISCCP definition between 680 and 440 hPa. These clouds are examined in terms of cloud top pressure, cloud

base height, cloud thickness, and cloud top temperature for different latitudinal bands (tropics: 30° N−30° S; mid-latitude: 30°−60° N(S); high-latitude:60°−90° N(S)). The global averages for the aforementioned quantities are also displayed. Figs 3.3a and 3.3b show the distribution of cloud top heights and cloud base heights for clouds with cloud top pressure between 680 and 440 hPa. Horizontal dashed lines show the traditional mid-level cloud top boundaries between 3 and 7 km (Fig 3.3a) and the base boundaries between 2 and 5 km (Fig 3.3b). Only a negligible amount of the mid-level clouds have cloud top height below 3 km and above 7km. The highest averaged values of cloud top height are found in northern Africa and northwestern China (Fig 3.3e). Figs 3.3b and 3.3f show that a notable amount of clouds have a cloud base height lower than 2 km over the oceans, which suggests that using the cloud-base definition will exclude these mid-level clouds determined by ISCCP definition. Figure 3.3c shows that geometrically thin mid-level clouds (< 2 km) are approximately 70%, 50%, and 50% of the amounts of mid-level clouds in the tropics, mid-latitude, and high-latitude, respectively. Geometrically thick clouds (cloud thickness > 2.5 km) are generally more common in mid- and high-latitudes. From Figs 3.3d and 3.3h, we can see that a significant amount of mid-level clouds, classified using the ISCCP definition, generally have cloud top temperature above -10°C in the tropics and below -10°C in the high-latitudes, whereas these clouds cover a large range between -50°C and 10°C in the mid-latitudes.

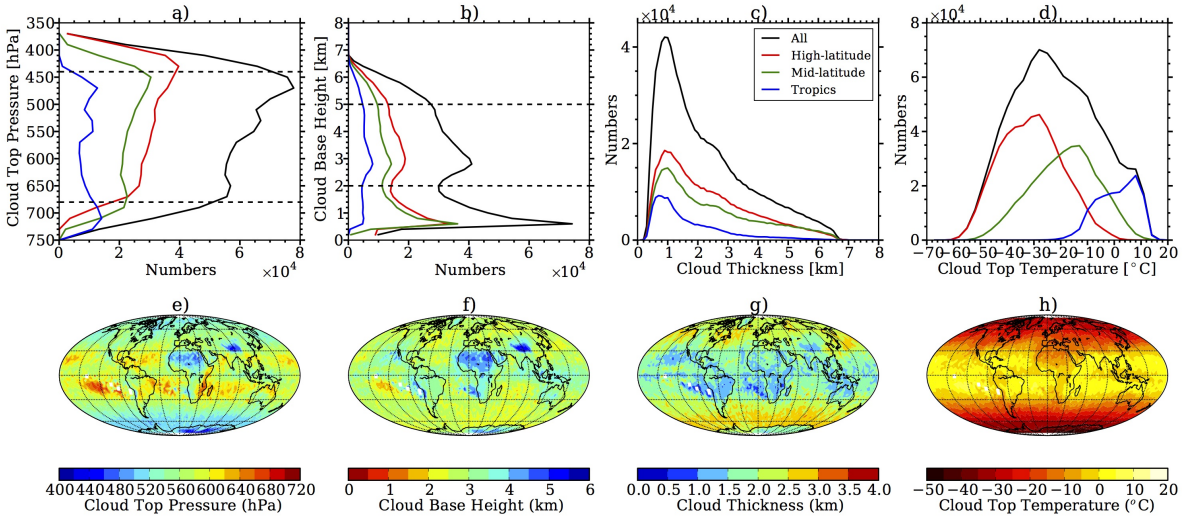

Figure 3.4 Similar to Figure 3.3, but for mid-level clouds using the cloud-top definition between 3 and 7 km.

Figure 3.4 is similar to Figure 3.3, but shows mid-level cloud frequencies using the cloud-top definition between 3 and 7 km. Figs 3.4a and 3.4b illustrate distribution of cloud top pressures and cloud base heights for clouds with cloud top heights between 3 and 7 km. Similarly, horizontal dashed lines show the mid-level cloud top and base boundaries between 680 and 440 hPa (Fig 3.4a) and between 2 and 5 km (Fig 3.4b). It is easy to see that although the majority of the mid-level clouds have cloud top pressure between 680 and 440 hPa, a notable amount of these clouds are above 680 hPa or below 440 hPa when cloud top height is used to identify mid-level clouds. The higher cloud top pressure values are found over the oceans in the low-latitudes and the low values are located in northern Africa and northwestern China (Figure 3.4e). The mid-level cloud frequency plots through Figs 3.4b to 3.4d are similar to Figs 3.3b to 3.3d except the magnitude changes, implying that further studies of the mid-level clouds defined by cloud-top definition are needed to understand the extent of regional variations.

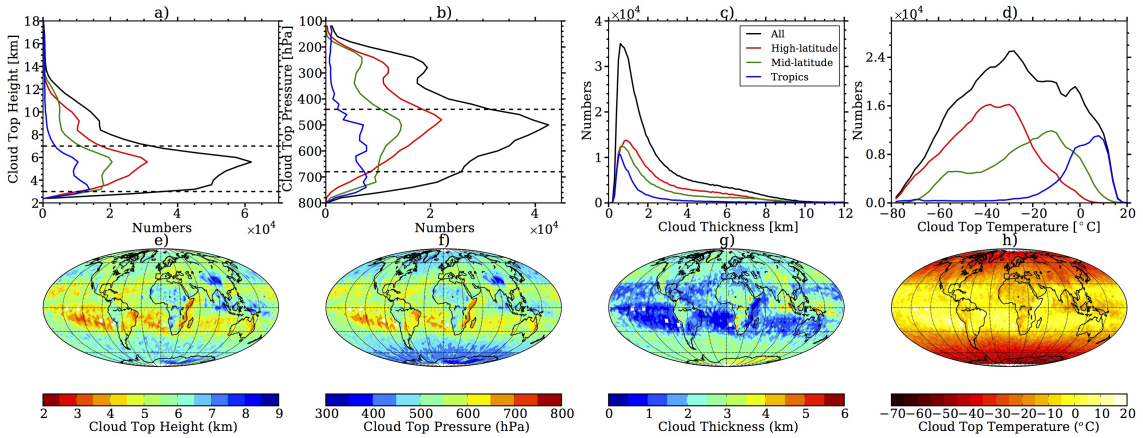

Figure 3.5 Similar to Figure 3.3, but for mid-level clouds using the cloud-base definition between 2 and 5 km.

Figure 3.5 shows mid-level cloud frequencies using the cloud-base definition between 2 and 5 km. Figs 3.5a and 3.5b show the distribution of cloud top heights and cloud top pressures. Horizontal dashed lines show the mid-level cloud top boundaries between 3 and 7 km (Fig 3.5a) and between 680 and 440 hPa (Fig 3.5b). It is obvious that this definition will treat some geometrically thick clouds with cloud top height as high as 14 km or 100 hPa, such as deep convective clouds, as mid-level clouds. This indicates that the cloud-base definition has the potential of overestimating mid-level clouds and needs more analyses to see whether it is from regional variations.

Mace et al. (2006) classified mid-level clouds using ground-based measurement at ARM program SGP site. They considered thin mid-level clouds as having cloud base height greater than 3 km, cloud top height less than 6.5 km, and optical depth less than 10; they also treated thick mid-level clouds as having cloud base height between 3 and 6.5 km and optical depth greater than 10. In their classification, it is also possible to include geometrically thick clouds within the mid-level determination. Due to the classification criteria of the cloud-base definition for mid-level clouds, the cloud thickness can be greater than 8 km. Additionally, the cloud top temperature

for mid-level clouds with this definition in tropics and high-latitude also overlap approximately at -10°C. These types of clouds in the mid-latitudes also cover a large temperature range of -80°C and 20°C.

Table 3.2 Number of mid-level clouds in the adjusted thresholds of the ISCCP definition for all cloud scenes (single-layer+multi-layer). The 6th column shows the number of mid-level clouds using the traditional ISCCP definition. The percentage shows in the parenthesis is the variation from the 6th column in each row.

CTP(hPa)	420−660	420−680	420−700	440−660	440−680	440−700	460−660	460−680	460−700
Global	780,303	846,101	920,068	700,464	766,262	840,229	621,782	687,580	761,547
	(1.8%)	(10.4%)	(20.1%)	(-8.6%)		(9.7%)	(-18.9%)	(-10.3%)	(-0.6%)
Tropics	113,948	126,020	140,873	104,629	116,701	131,554	91,707	103,779	118,632
(30°S-30°N))	(-2.4%)	(8.0%)	(20.7%)	(-10.3%)		(12.7%)	(-21.4%)	(-11.1%)	(1.7%)
Mid-latitude	292,880	317,377	346,140	260,964	285,461	314,224	231,366	255,863	284,626
(30-60°S, 30-60°N)	(2.6%)	(11.2%)	(21.3%)	(-8.6%)		(10.1%)	(-19.0%)	(-10.4%)	(0.3%)
High-latitude	373,475	402,704	433,055	334,871	364,100	394,541	298,709	327,938	358,289
(60-90°S, 60-90°N)	(2.6%)	(10.6%)	(18.9%)	(-8.0%)		(8.3%)	(-18.0%)	(-9.9%)	(-1.6%)

Table 3.3 Similar to Table 3.2, but changes cloud base and top boundaries of 50 hPa.

CTP(hPa)	390−630	390−680	390−730	440−630	440−680	440−730	490−630	490−680	490−730
Global	821,521	977,460	1,182,335	610,323	766,262	971,137	423,118	579,057	783,932
	(7.2%)	(27.6%)	(54.3%)	(-20.4%)		(26.7%)	(-44.8%)	(-24.4%)	(2.3%)
Tropics	111,238	140,733	182,813	87,206	116,701	158,781	58,704	88,199	130,279
(30°S-30°N))	(-4.7%)	(20.6%)	(56.7%)	(-25.3%)		(36.1%)	(49.7%)	(-24.4%)	(11.6%)
Mid-latitude	312,632	369,921	454,459	228,172	285,461	369,999	156,683	213,972	298,510
(30-60°S, 30-60°N)	(9.5%)	(29.6%)	(59.2%)	(-20.1%)		(29.6%)	(-45.1%)	(-25.0%)	(4.6%)
High-latitude	397,651	466,806	545,063	294,645	364,100	442,357	207,731	276,886	355,143
(60-90°S, 60-90°N)	(9.2%)	(28.2%)	(49.7%)	(-19.0%)		(21.5%)	(-42.9%)	(-24.0%)	(-2.5%)

The sensitivity of mid-level cloud frequency to different definitions of the mid-level is not known. Another goal of this study is to test the sensitivities of mid-level clouds to the cloud boundary thresholds. The adjusted cloud boundaries for mid-level clouds in terms of cloud top pressure, cloud top height, and cloud base height are listed from Table 3.2 to 3.7. First, the tests for mid-level clouds using the ISCCP definition are demonstrated in Tables 3.2 and 3.3. In the ISCCP climatology, cloud top pressure are biased high by about 20 hPa on average, equivalent to a high bias of cloud top temperature of about 2 degrees (Rossow et al. 1999; Koelemeijer

et al. 2002; Garay et al. 2008). Previous studies have shown that traditional passive remote sensing techniques can provide cloud top pressure estimations with uncertainties approximately between 30 and 50 hPa (Menzel et al. 2008; Eldering et al. 2008), therefore, we use two thresholds 20 hPa (Table 3.2) and 50 hPa (Table 3.3) to adjust the ISCCP definition and test the corresponding statistics for mid-level clouds. In Table 3.2, the sixth column shows the number of mid-level clouds between 680 and 440 hPa, and other columns are the adjustments. The changes discussed here are on the basis of the sixth column. If we fix one boundary and change the other boundary for $\pm$ 20 hPa (columns 3, 5, 7, and 9), the number of mid-level clouds increases or decreases by about 8 % to 11%. If we extend or shrink both boundaries (columns 4 and 8), then the changes in the number of mid-level clouds can be as high as approximately 20%. In columns 2 and 10, if the pressure band is shifted upward or downward, a slight change of less than approximately 3% in the total numbers can be seen. The sixth column in Table 3.3 also shows the number of mid-level clouds with cloud top pressures between 680 and 440 hPa. Again, if one cloud boundary is fixed, the variations can be between 20 and 30% except that the highest change (36.1%) is in the tropics with cloud top pressure between 730 and 440 hPa. If both boundaries are extended or shrunk by 50 hPa, changes of between 40% and 60% can be seen. Additionally, if we only shift the pressure band upward or downward, there are significant variations that are as high as about 10%.

Tables 3.4 and 3.5 show the global statistics for mid-level clouds using cloud top height definitions. As mentioned before, the ISCCP mid-level cloud pressures correspond to cloud top height between 3.2 and 6.4 km in a standard mid-latitude winter atmosphere and between 3.4 and 6.9 km in a standard tropical atmosphere (McClatchey et al. 1997). Riihimaki et al. (2012) defined mid-level clouds as having cloud top height between 4 and 8 km at the ARM TWP site at Darwin Australia.

Therefore, we choose 0.5 km and 1 km as thresholds to see how the statistics change correspondingly. Table 3.4 shows the adjustment with 0.5 km and Table 3.5 shows changes of cloud top for 1 km. Also, the sixth columns in Tables 3.4 and 3.5 are identical and show the number of mid-level clouds with cloud top height between 3 and 7 km. These statistics clearly show that a cloud top height-based definition of the mid-level has more variations than the ISCCP definition when perturbing the cloud boundaries, particularly in the tropical regions. The last column in Table 3.5 shows that the number of mid-level clouds between 4 and 8 km decreased 17.4% when using their definition compared to the traditional definition with cloud top height between 3 and 7 km.

Table 3.4 Similar to Table 3.2, but uses the cloud-top definition. The 6th column shows the number of mid-level clouds using the cloud top height between 3 and 7 km.

CTH(km)	2.5−6.5	2.5−7.0	2.5−7.5	3.0−6.5	3.0−7.0	3.0−7.5	3.5−6.5	3.5−7.0	3.5−7.5
Global	1,075,270	1,203,844	1,335,112	860,873	989,447	1,120,715	711,367	839,941	971,209
	(8.7%)	(21.7%)	(34.9%)	(-13.0%)		(13.3%)	(-28.1%)	(-15.1%)	(-1.8%)
Tropics	189,194	204,766	291,816	131,230	146,802	161,852	98,360	113,932	128,982
(30^{o}S-30^{o}N))	(28.9%)	(39.5%)	(49.7%)	(-10.6%)		(10.3%)	(-33.0%)	(-22.4%)	(12.1%)
Mid-latitude	401,794	450,969	501,871	316,833	366,008	416,910	261,078	310,253	361,155
(30-60^{o}S, 30-60^{o}N)	(9.8%)	(23.2%)	(37.1%)	(-13.4%)		(13.9%)	(-28.7%)	(-15.2%)	(-1.3%)
High-latitude	484,282	548,109	613,425	412,810	476,637	541,953	351,929	415,756	481,072
(60-90^{o}S, 60-90^{o}N)	(1.6%)	(15.0%)	(28.7%)	(-13.4%)		(13.7%)	(-26.2%)	(-12.8%)	(0.9%)

Table 3.5 Similar to Table 3.4, but changes cloud base and top boundaries for 1km.

CTH(km)	2.0−6.0	2.0−7.0	2.0−8.0	3.0−6.0	3.0−7.0	3.0−8.0	4.0−6.0	4.0−7.0	4.0−8.0
Global	1,348,073	1,600,926	1,863,009	736,594	989,447	1,251,530	464,263	717,116	979,199
	(36.2%)	(61.8%)	(88.3%)	(-25.6%)		(26.5%)	(-53.1%)	(-27.5%)	(-1.0%)
Tropics	301,238	332,958	361,346	115,082	146,802	175,190	61,158	92,878	121,266
(30^{o}S-30^{o}N))	(105.2%)	(126.8%)	(146.1%)	(-21.6%)		(19.3%)	(-58.3%)	(-36.7%)	(-17.4%)
Mid-latitude	526,203	622,140	725,241	270,071	366,008	469,109	169,805	265,742	368,843
(30-60^{o}S, 30-60^{o}N)	(43.8%)	(70.0%)	(98.1%)	(-26.2%)		(28.1%)	(-53.6%)	(-27.4%)	(0.7%)
High-latitude	520,632	6,45,828	776,422	351,441	476,637	607,231	233,300	358,496	489,090
(60-90^{o}S, 60-90^{o}N)	(9.2%)	(35.5%)	(62.9%)	(-26.3%)		(27.4%)	(-51.1%)	(-24.8%)	(2.6%)

Mace et al. (2006) classified mid-level clouds as having cloud base height

between 3 and 6.5 km using surface measurements at the ARM SGP site. Therefore, a third adjustment of 1 km is chosen to perturb the cloud base height (Table 3.7), and in order to show more contrasts, we also chose 0.5 km (Table 3.6). Again, the sixth columns in Tables 3.6 and 3.7 are identical and are show the number of clouds having cloud base heights between 2 and 5 km. Compared to the adjustments of the ISCCP and cloud-top definitions, the statistics of the mid-level clouds using the cloud-base definition show even more variations, with more high-level or low-level clouds included in the mid-level when adjusting the cloud boundaries. The last column in Table 3.7 shows the number of mid-level clouds with cloud base heights between 3 and 6 km. The value indicates a negligible change (∼0.4%) when we move the mid-level band upward.

Table 3.6 Similar to Table 3.2, but uses the cloud-base definition. The 6$^{\text{th}}$ column shows the number of mid-level clouds using the cloud base height between 2 and 5 km.

CBH(km)	1.5−4.5	1.5−5.0	1.5−5.5	2.0−4.5	2.0−5.0	2.0−5.5	2.5−4.5	2.5−5.0	2.5−5.5
Global	857,639	974,693	1,095,036	631,953	749,007	869,350	477,093	594,147	714,490
	(14.5%)	(30.1%)	(46.2%)	(-15.6%)		(16.1%)	(-36.3%)	(-20.7%)	(-4.6%)
Tropics	166,683	183,259	199,059	109,554	126,130	141,930	74,878	91,454	107,254
(30$^{\text{o}}$S-30$^{\text{o}}$N))	(32.2%)	(45.3%)	(57.8%)	(-13.1%)		(12.5%)	(-40.6%)	(-27.5%)	(-15.0%)
Mid-latitude	306,906	350,838	398,172	218,050	261,982	309,316	161,995	205,927	253,261
(30-60$^{\text{o}}$S, 30-60$^{\text{o}}$N)	(17.1%)	(33.9%)	(52.0%)	(-16.8%)		(18.1%)	(-38.2%)	(-21.4%)	(-3.3%)
High-latitude	384,050	440,596	497,805	304,349	360,895	418,104	240,220	296,766	353,975
(60-90$^{\text{o}}$S, 60-90$^{\text{o}}$N)	(6.4%)	(22.1%)	(37.9%)	(-15.7%)		(15.9%)	(-33.4%)	(-21.4%)	(-1.9%)

Table 3.7 Similar to Table 3.6, but changes cloud base and top boundaries for 1km.

CBH(km)	1.0−4.0	1.0−5.0	1.0−6.0	2.0−4.0	2.0−5.0	2.0−6.0	3.0−4.0	3.0−5.0	3.0−6.0
Global	1,269,029	1,497,796	1,739,236	520,240	749,007	990,447	236,166	464,933	706,373
	(69.4%)	(100.0%)	(132.2%)	(-30.1%)		(32.2%)	(-68.5%)	(-37.9%)	(-5.7%)
Tropics	310,285	343,073	374,201	93,342	126,130	157,258	34,756	67,544	98,672
(30$^{\text{o}}$S-30$^{\text{o}}$N))	(146.0%)	(172.0%)	(196.7%)	(-26.0%)		(24.7%)	(-72.4%)	(-46.4%)	(-21.8%)
Mid-latitude	487,309	571,786	670,003	177,505	261,982	360,199	78,049	162,526	260,743
(30-60$^{\text{o}}$S, 30-60$^{\text{o}}$N)	(86.0%)	(118.3%)	(155.8%)	(-32.2%)		(37.5%)	(-70.2%)	(-38.0%)	(-0.4%)
High-latitude	471,435	582,937	695,032	249,393	360,895	472,990	123,361	234,863	346,958
(60-90$^{\text{o}}$S, 60-90$^{\text{o}}$N)	(6.4%)	(22.1%)	(37.9%)	(-15.7%)		(15.9%)	(-33.4%)	(-21.4%)	(-1.9%)

3.3 Temperature

One key to predicting the occurrence of mid-level clouds is to understand what thermodynamic regimes favor their occurrence. We have characterized the occurrence of mid-level clouds by analyzing the frequencies in terms of cloud top and base boundaries and geometrical thickness. Moreover, understanding relationships between mid-level clouds and temperature is also important to numerical modeling studies because the distribution between liquid water and ice in clouds is frequently parameterized with respect to cloud temperature (Norris and Weaver 2001; Naud et al. 2006). Looking at mid-level clouds in terms of cloud temperature may remove some of the difficulties inherent in dealing latitudinal and/or seasonal variations in the relationships between atmospheric profile height, temperature, and pressure.

The interest is spurred by observed microphysical and radiative similarities between low-level Arctic stratus and mid-latitude mid-level altostratus (Fleishauer et al. 2002). Johnson et al. (1999) categorized the mid-level cumulus congestus clouds in the tropical cloudiness as having cloud tops near the 0°C melting level, which is approximately 6-7 km. However, Haynes and Stephens (2007) identified a bimodal distribution of tropical mid-level clouds and Riley and Mapes (2009) reported a second peak in cloud top height around 8-9 km ($\sim$-15°C) with measurements from CloudSat. This bimodal feature existed in cumulus congestus clouds, altocumulus, and altostratus clouds at corresponding levels. Many mid-level clouds occur at temperatures in which mixed-phase clouds are possible and cloud remote sensing is difficult (Cho et al. 2009).

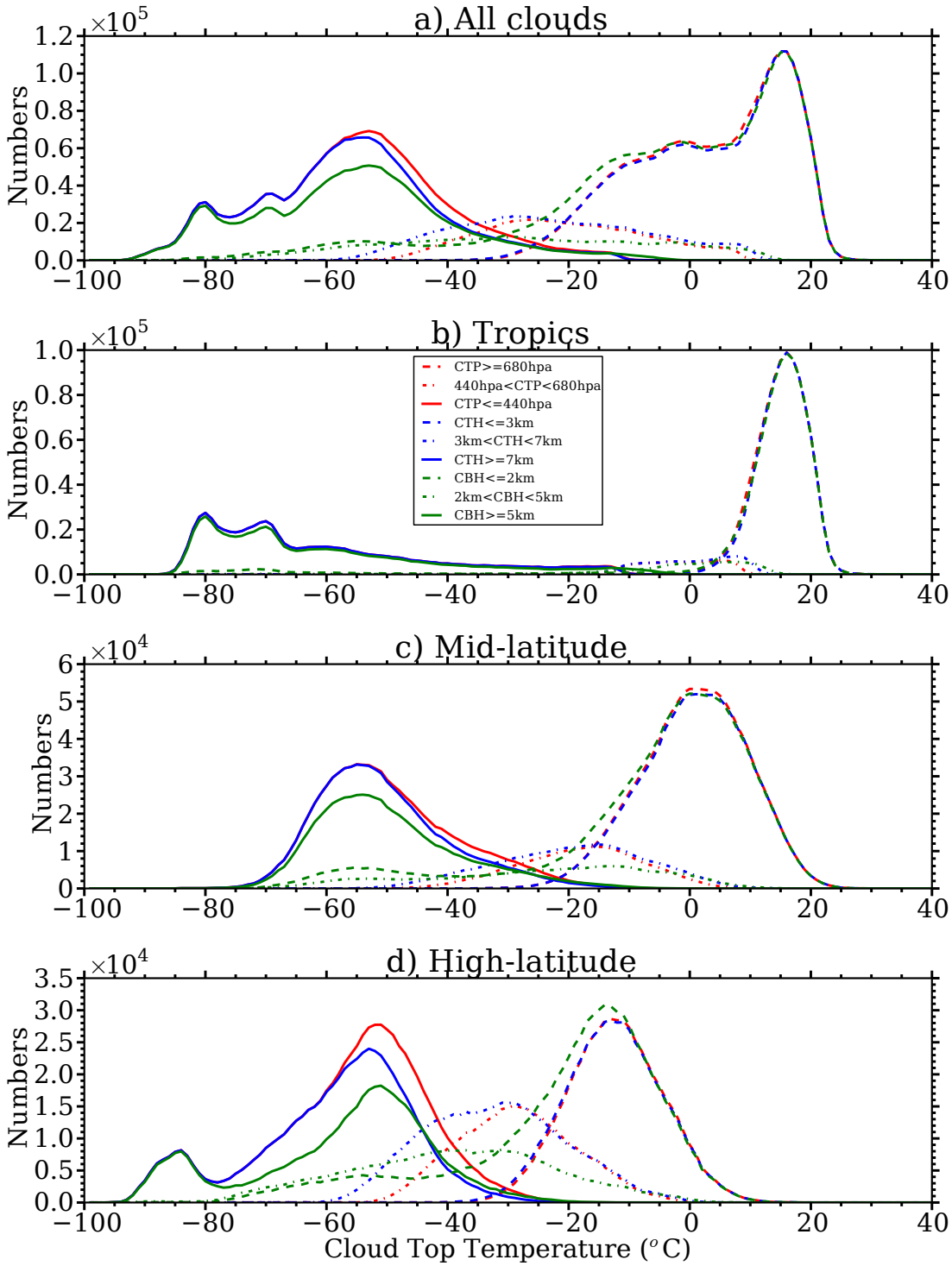

Figure 3.6 Probability distributions for high-, mid-, and low-level clouds using the ISCCP, cloud-top, and cloud-base definitions as a function of cloud top temperature.

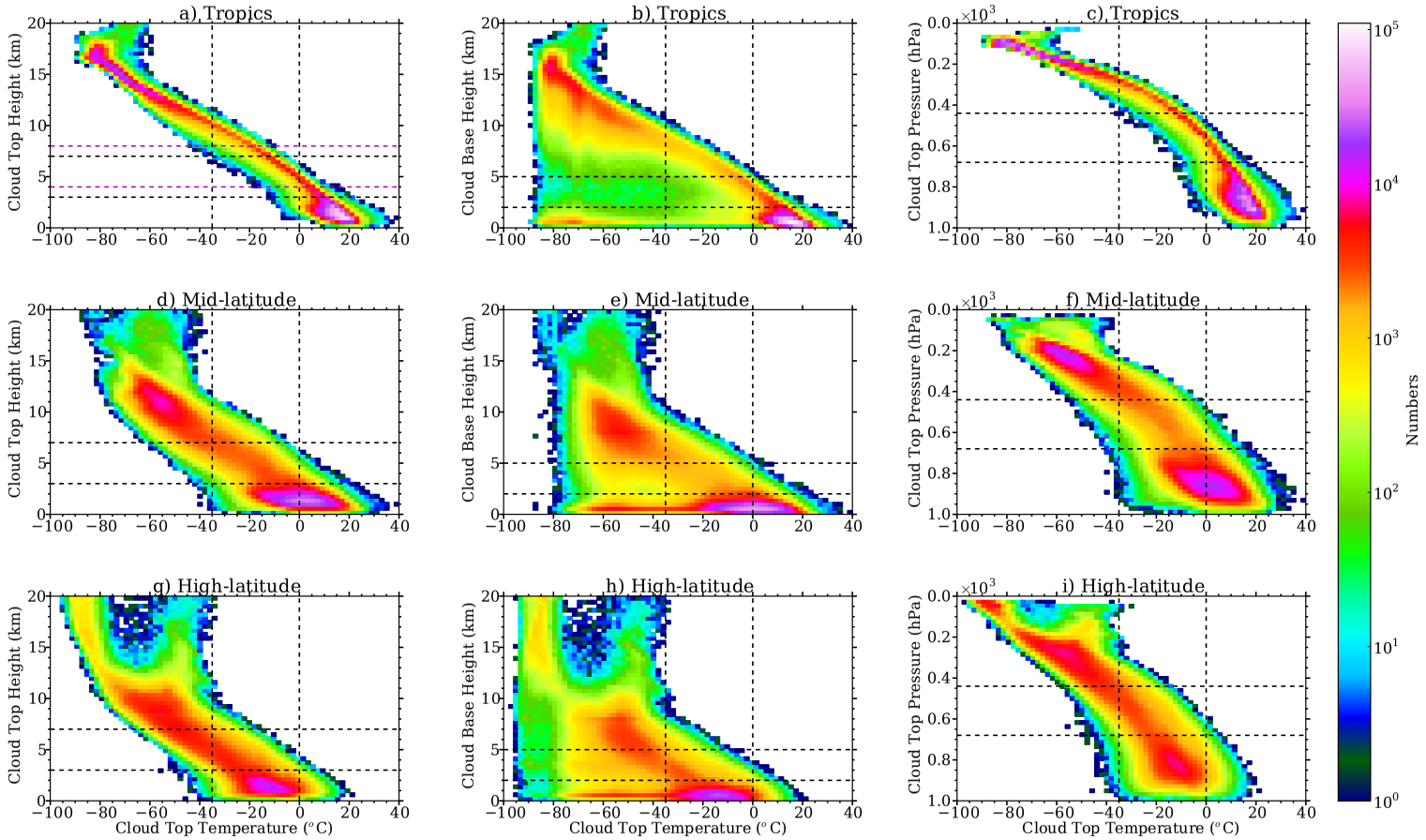

Figure 3.7 Joint histograms between cloud top height, cloud base height, and cloud top pressure and cloud top temperature in the tropics, mid-latitudes, and high-latitudes. Vertical dashed lines are 0°C and -35 °C; and horizontal dashed lines are the cloud heights for mid-level clouds in each corresponding definition.

Cloud distribution for different latitudinal bands (tropics: 30° N−30° S; mid-latitude: 30°−60° N(S); high-latitude: 60°−90° N(S)) are demonstrated in Figures 3.6 and 3.7 using the CCCM dataset. Figure 3.6 shows the cloud top temperature distributions for high-level (solid), mid-level (dashed dot), and low-level clouds (dashed) for the ISCCP, cloud-top, and cloud-base definitions, respectively. It is evident that the peaks and overlaps shift towards lower temperature when moving from low-latitudes to polar regions. The high-level clouds and low-level clouds can be roughly separated at around 0°C, -22°C, and -30°C in the tropics, mid-latitude, and high-latitudes, respectively.

The cloud top temperature shows difficulties in determining the mid-level clouds, because they cover a fairly board temperature range from about -80°C to 15°C. Figure 3.7 shows the joint histograms for clouds as a function of cloud top and base boundaries and cloud top temperature. In the tropics, cloud-top and ISCCP definition show good correlations between cloud top temperature and cloud top height and pressure. While not shown, the cloud-base definition treats some deep convection systems (∼8%) with cloud top height above 10 km as mid-level clouds according to the cloud top height and cloud top temperature. In the mid- and high-latitudes, the distributions of cloud-top and ISCCP definitions become broader, making the determination of mid-level clouds using cloud temperature more difficult. Similar to Figures 3.6 and 3.7, cloud distributions using the ground-based measurements at the ARM TWP Darwin site is shown in Figure 3.8. The figures clearly show that the cloud top temperature has fairly good correlation with cloud top height and cloud top pressure in the tropical western pacific region. The mid-level clouds correspond fairly well to cloud temperatures between -15°C and 10°C.

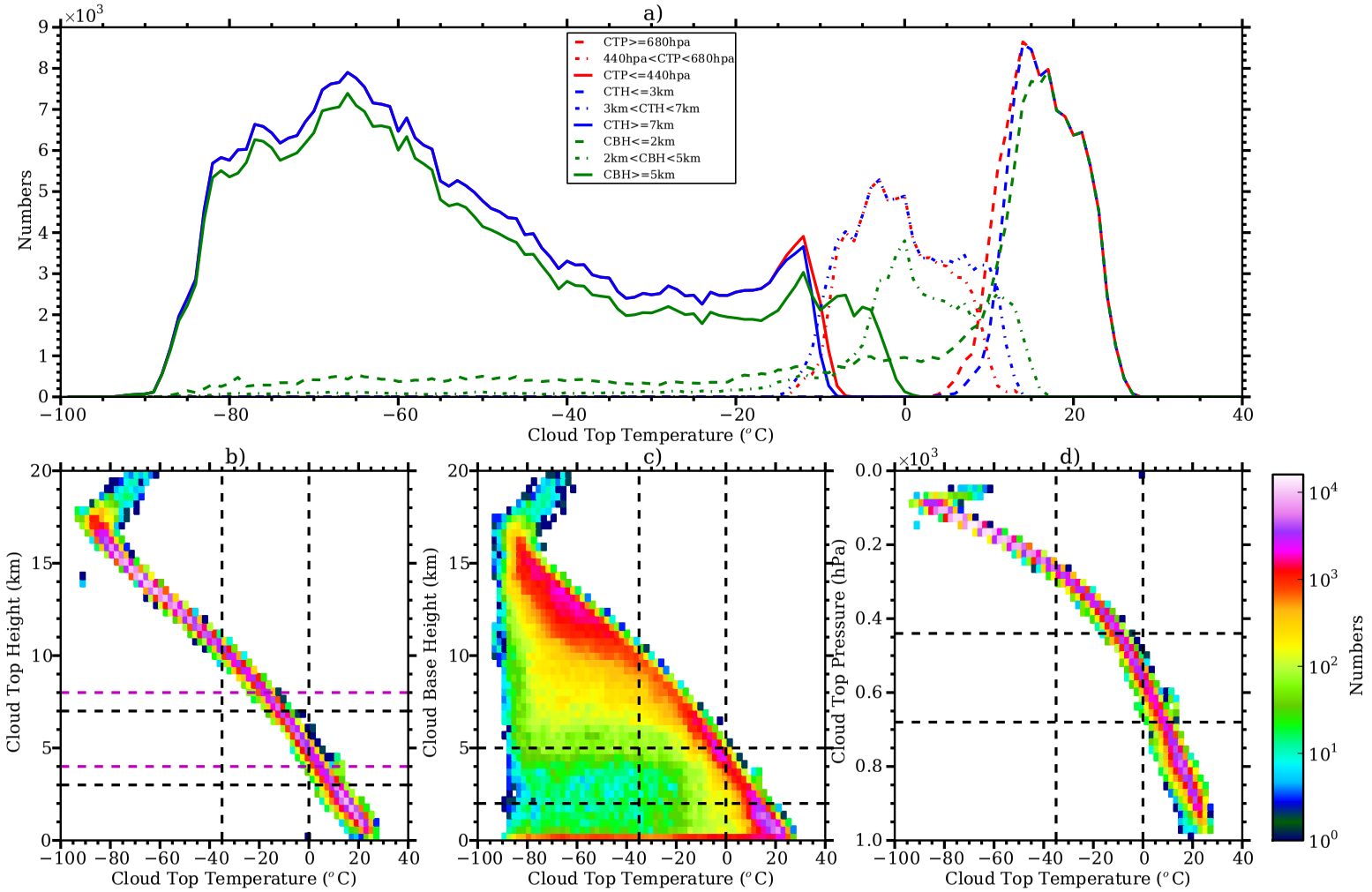

Figure 3.8 Mid-level clouds at ARM TWP site (data was obtained from ground-based measurements at Darwin, Australia). a) is similar to Figure 3.6; b), c), and d) are similar to Figure 3.7.

We show the relationships between cloud top height and pressure and cloud top temperature in Figure 3.7. We can easily see that there are overlaps of cloud temperatures for clouds at different levels. Because the tropical region has different correlation features compared to mid- and high-latitudes, it may be useful to see the temperature difference between clouds at different levels. Figure 3.9 shows the average temperature difference between mid-level and low-level clouds (left) and high-level and mid-level clouds (right) for the cloud-top, cloud-base, and ISCCP definitions of clouds using the 3.5-year CCCM dataset. While the cloud temperature difference between mid-level and low-level does not show a great deal of organization with the cloud-top and ISCCP definitions, the cloud-base definition indicates a distinct feature that the positive difference are mainly distributed over the continents except a few areas over the oceans in the tropics. There is a strong zonal signature to the averaged cloud temperature difference between high clouds and mid-level clouds using the three definitions. This is fairly useful when we know the long-term climatology of cloud temperature of high-level clouds, and we can statistically characterize mid-level clouds using the cloud temperature difference between high-level and mid-level. However, another question that needs to be answered is that how the cloud thermodynamic phase impacts the cloud temperature difference between clouds at different levels. I will come back to this point and address the issue in chapter 5.

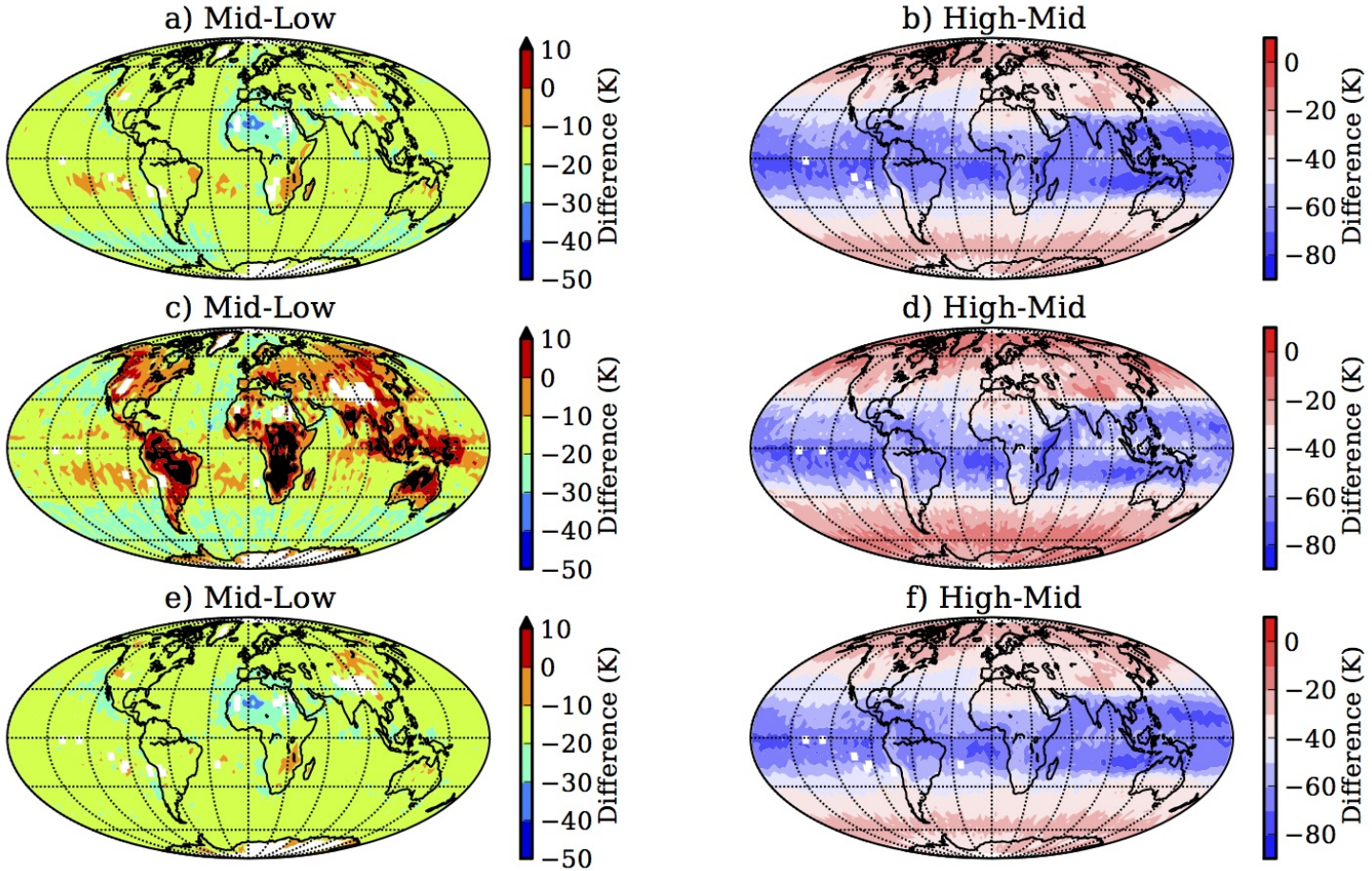

Figure 3.9 Cloud top temperature difference between mid-level and low-level (left) and between high-level and mid-level (right). a) and b): cloud-top definition; c) and d): cloud-base definition; e) and f): ISCCP definition.

4. DETECTION OF CLOUD THERMODYNAMIC PHASE USING ATMOSPHERIC INFRARED SOUNDER (AIRS)

4.1 Background

Although considerable efforts have been made to improve the characterization of cloud feedbacks, clouds are still a major source of uncertainty in climate projections by GCMs and even in contemporary satellite observations (Cess et al. 1990; Wielicki et al. 1995; Dessler 2010). A highly uncertain observable is the cloud thermodynamic phase, which is the classification of cloud composition as liquid water droplets, ice crystals, or a mixture of the two phases of hydrometeors (i.e., mixed-phase). Cloud phase can significantly impact the planetary radiation energy budget (Ackerman et al. 1988; Hartmann et al. 1992; Yang et al. 2003; McFarquhar and Cober 2004), because the cloud radiative properties, which are closely coupled to the cloud particle size and optical depth, vary according to the corresponding thermodynamic phase of the hydrometeors. Knowledge of cloud phase is therefore of fundamental importance to both remote sensing and climate simulations.

The determination of cloud thermodynamic phase is challenging for satellite cloud remote sensing. Assuming water droplets instead of ice crystals when retrieving cloud properties from satellite data can lead to biases in cloud height, optical depth, and microphysical properties (Minnis et al. 1993; Mischenko et al. 1996). Numerous efforts to derive cloud phase from satellite observations have been made for the past decade (Key and Intrieri 2000; Goloub et al. 2000; Platnick et al. 2003; Hu 2007). From passive sensors such as MODIS, the classification of cloud phase typically utilizes the spectral absorption and/or scattering differences between liquid water droplets and ice crystals (Baum et al. 2000; Platnick et al. 2003). Active

sensors like the CALIOP onboard the CALIPSO payload (Winker et al., 2009) can differentiate cloud particle phase based in part on the relationship between the depolarization ratio and attenuated backscatter of liquid droplets and ice crystals (Hu et al. 2009). Due to the complexity of different cloud compositions and instrument sensitivities, however, no single-phase determination approach is optimal for all cloud types and regimes. Combinations of different instruments and techniques are therefore both desirable and necessary. For example, McFarlane et al. (2005) developed a retrieval scheme to derive cloud particle phase and ice crystal habits using a combination of Multiangle Imaging Spectroradiometer (MISR) and MODIS observations and Riedi et al. (2010) inferred cloud phase from merged MODIS and Polarization and Directionality of the Earth Reflectance (POLDER) observations. Both of these investigations demonstrated the added value of instrument synergy to obtain cloud phase estimates.

Until recently, cloud thermodynamic phase determination methods have emphasized cloud phase assessments using only reflected solar radiation measurements. Several approaches using the near-infrared measurements (Pilewskie and Twomey 1987; Riedi et al. 2000; Knap et al. 2002; Platnick et al. 2003; Chylek et al. 2006) or in combination with mid-infrared brightness temperatures (BTs; Kokhanovsky et al. 2006) have been developed. Solar reflectance-based retrievals essentially reply on spectral differences in how liquid water droplets and ice crystals absorb solar radiation at the wavelengths near 1.6, 2.1 and/or 3.7 μm. These techniques, however, are highly sensitive to the solar zenith angle and satellite position and are only applicable during daytime.

Purely infrared-based methods to determine cloud thermodynamic phase have the advantage of being applicable to both daytime and nighttime because these techniques have no dependence on solar radiation. Currently, few approaches use only IR

observations to distinguish cloud phase. The bi-spectral IR cloud phase technique used in the MODIS Collection 5 (C5) (Strabala et al. 1994; Baum et al. 2000) has been used operationally for more than a decade with excellent global coverage. The bi-spectral method is adequate for classifying cloud phase as either "ice" or "water" for about 80% of the cloudy pixels globally. Using the supplementary information contained in the visible and near-infrared bands, the MODIS bi-spectral IR cloud phase algorithm has facilitated the retrieval of cloud optical and microphysical properties (Platnick et al. 2003).

Recent investigations using radiative transfer simulations and MODIS C5 cloud products have indicated that the MODIS bi-spectral IR technique is limited, particularly for optically thin cirrus and clouds with cloud top temperatures between 250 and 265 K (Nasiri and Kahn 2008; Cho et al. 2009). Nasiri and Kahn (2008) explored the use of high-spectral-resolution IR measurements, such as the AIRS, to determine cloud phase. Their model simulations showed cloud phase sensitivities of at least 0.5 K using the brightness temperature difference (BTD) between 1231 cm^{-1} and 960 cm^{-1} (abbreviated as $BTD_{1231\text{-}960}$). Their results are generally applicable to other high spectral IR instruments, such as the Infrared Atmospheric Sounding Interferometer (IASI) and Cross-track Infrared Sounder (CrIS), although these instruments contain additional spectral coverage missing in AIRS.

In this chapter, we introduce a newly developed cloud thermodynamic phase determination algorithm using the high-spectral IR radiances from AIRS (referred to as AIRS phase). This work is a further development of Nasiri and Kahn (2008) to determine cloud phase using high-spectral IR observations. The AIRS phase algorithm is initiated and developed based on radiative transfer simulations of a cloudy atmosphere. A newly developed high-spectral-resolution cloudy-sky radiative transfer model (HRTM, Wang et al. 2012) is used to simulate the brightness temperature

(BT) for single-layer water and ice clouds at different vertical levels. Using the model simulations and CALIPSO cloud phase products, four AIRS channels are analyzed thoroughly. A computationally fast AIRS phase algorithm is proposed to use four major parallel tests with different BT and/or BTD combinations to distinguish ice and water clouds. It will be implemented operationally into the AIRS Version 6 (V6) Level 2 (L2) support product in late 2012. A detailed discussion of the algorithm and theoretical basis is in development (Nasiri et al. 2012), but will be summarized here in this chapter.

4.2 Data

4.2.1 AIRS

The Atmospheric Infrared Sounder (AIRS) on the NASA EOS-Aqua platform has acquired global observations of outgoing thermal infrared spectra since 2002 (Aumann et al. 2003). The AIRS instrument is a high-resolution ($\lambda/\triangle\lambda$=1200) grating spectrometer that observes the atmosphere at both visible and infrared wavelengths. The infrared spectral coverage covers between 3.7 and 15.4 μm with a few spectral gaps for a total of 2378 channels. These high-spectral resolution measurements have a spatial resolution of about 13.5 km at a nadir view. AIRS scans out to $\pm$ 48.95^{o} from nadir, with 90 cross-track scan angles, yielding a swath width of approximately 1650 km at the surface. AIRS can measure approximately 2.9 million spectra per day with excellent calibrations (Pagano et al. 2003; Schreier et al., 2010). Near global coverage can be accomplished in a single day. The high-resolution spectra of AIRS can provide a better global view of clouds than other sensors with only narrow spectral bands.

The AIRS spectrum covers the 700-1300 cm^{-1} atmospheric window region, which will be examined in the current study, although the spectral coverage between

1050 and 1250 cm^{-1} is not complete. Window channels are preferable for the remote sensing of clouds because absorption line effects that can complicate the interpretation of cloudy IR spectra are either minimized or eliminated. However, because the volume of AIRS data is enormous due to its high-spectral resolution, only a limited number of channels are used in the AIRS phase algorithm. A few channels are selected by manual inspection of the water and ice indices of reflection in Figure 4.1 using the approach presented in Kahn et al. (2005). The channels are chosen to minimize the channel noise and maximize the sensitivity to cloud phase signatures in IR radiances. The trade-offs between index of refraction and atmospheric transmissivity are considered in the selection. For this study, we focus on the nine channels listed in Table 4.1 because these channels minimize the effects of absorption lines and channel noise. Each selected channel is averaged between two or three AIRS individual channels. Subsequently, four channels are selected in the algorithm based on the radiative transfer simulations. A detailed method is introduced briefly later in this chapter.

Table 4.1 Nine selected AIRS channels. Each channel is averaged over two or three individual channels in the AIRS spectrum that are shown in the third row.

Channels (cm^{-1})	857	868	926	930	960	1082	1096	1227	1231
Channels (μm)	11.66	11.62	10.80	10.75	10.42	9.24	9.12	8.15	8.12
Averaged channels	627	663	812	821	902	1157	1185	1284	1291
	628	664	813	822	903	1158	1186	1285	1292
				823					

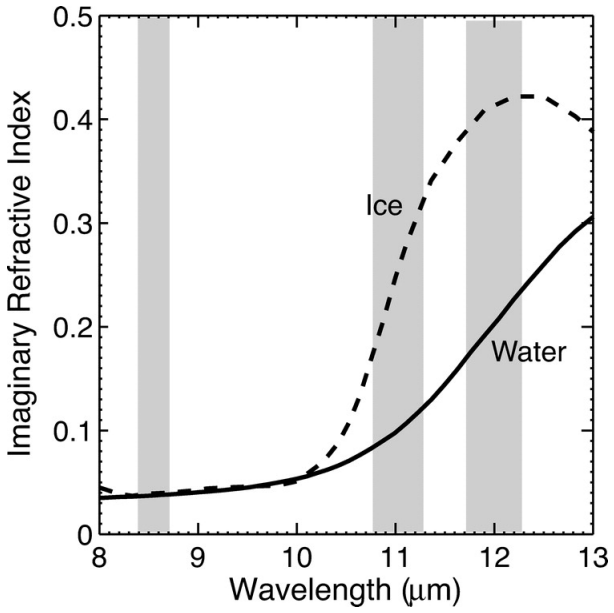

Figure 4.1 Imaginary part of index of refraction for water (solid line) and ice (dashed line). Gray regions indicate of the MODIS bands centered at 8.5, 11, and 12 μm (bands 29, 31, and 32, respectively). Adapted from Nasiri and Kahn (2008).

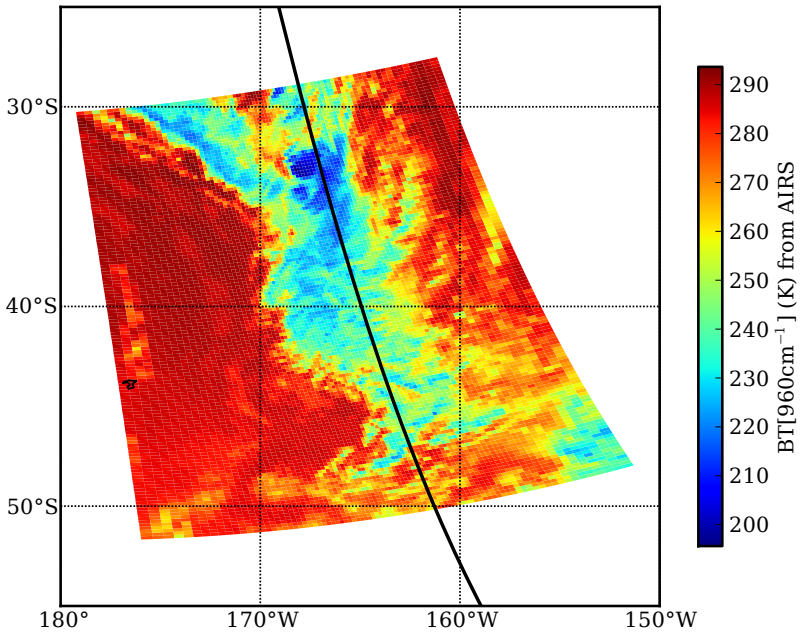

Figure 4.2 An example of one AIRS granule. Color scale represents brightness temperature at 960 cm^{-1}. The solid black is the CALIPSO ground track.

4.2.2 CALIPSO

The CALIPSO satellite is located about 100 seconds behind Aqua, and the two satellites provide near simultaneous observations of clouds along the CALIPSO ground track. Figure 4.2 demonstrates an example of AIRS and CALIPSO observations, which clearly shows that CALIPSO has only near-nadir views.

CALIPSO cloud profiles are obtained from the backscattered light generated at the dual wavelengths 532 and 1064 nm. The measurements made by the 532 nm channel provide high sensitivity to thin clouds and aerosols (Winker and Trepte 1998). One of the main features of CALIOP's 532 nm channel is its dual polarization capability (Sassen 1991). It assumes that backscattered light from ice crystals is depolarizing, whereas liquid water droplets, being spherical, result in minimal depolarization. The CALIPSO measurements include a number of quantities, such as layer-integrated attenuated backscatter, volume depolarization ratio, and integrated attenuated total color ratio. Specifically, the layer-integrated depolarization ratio (δ) and the total layer-integrated attenuated backscatter (γ) at 532 nm, which are defined as follows:

$$\delta = \frac{\int_t^b \beta_\perp \, dz}{\int_t^b \beta_\parallel \, dz}$$

$$\gamma = \int_t^b [\beta_\perp + \beta_\parallel] \, dz$$

where $\beta_\perp$ and $\beta_\parallel$ are the perpendicular and parallel components of the attenuated backscatter, respectively.

Hu (2007) and Hu et al. (2009) introduced a powerful approach to determine cloud thermodynamic phase exploiting these lidar capabilities. Water clouds consisting of spherical liquid droplets typically demonstrate positive correlation between δ

and γ, whereas the correlations for ice clouds tend to be negative. It should be pointed out that although a single water droplet does not depolarize the backscattered light, multiple scattering events within a water cloud do tend to depolarize lidar signals. Therefore, the depolarization ratio associated with water clouds increases with increasing backscatter and is positively correlated to the optical depth. Cloud phase is differentiated using the spatial correlation of layer-integrated depolarization ratio and attenuated backscatter. The procedure includes two steps: 1) use of a simple two dimensional threshold method to provide a preliminary identification of ice clouds containing randomly oriented ice crystals, horizontally oriented ice crystals, and possible water clouds, and 2) application of a spatial coherence analysis to distinguish water clouds from ice clouds containing horizontally oriented crystals. Extra information, like cloud temperature, color ratio and vertical variation of depolarization ratio, is also considered by Hu et al. (2009). Their method has been implemented operationally in the CALIPSO version 3 products.

For each cloud layer found in the CALIPSO cloud layer products (version 3, 1-km horizontal resolution), CALIPSO reports a set of feature classification flags including feature type (e.g. cloud or aerosol) and cloud phase (referred to as CALIPSO phase). The CALIPSO phase classification contains four categories: water, ice, horizontally oriented ice crystals, and unknown. In November 2007, the CALIOP viewing angle was increased from 0.3^{o} to 3^{o} off nadir to reduce specular signal returns from clouds containing horizontally oriented ice crystals, which can result in uncertainties of cloud phase retrievals. The angle change resulted in a decrease in the number of clouds classified as horizontally-oriented ice. In this dissertation, we only consider measurements at the 3^{o} off-nadir angle.

Because the CALIPSO phase is not part of the AIRS phase determination algorithm, it can serve as a powerful tool for assessment of the AIRS algorithm. In

Figure 4.2, AIRS and CALIPSO showed different observing potentials due to the large differences of spatial resolutions between the two instruments. We spatially collocated one month (January) of CALIPSO 1-km cloud layer products and AIRS L1B radiances data with AIRS surface footprints. The detailed collocation strategy is introduced in the next chapter. As mentioned before, because an AIRS footprint is about 15 km on the surface, the CALIPSO phase is reassigned within the AIRS footprint as ice, water, and mixed-phase. CALIPSO mixed-phase means that CALIPSO retrievals of both water and ice are found within the collocated AIRS footprint.

4.3 Algorithm development

4.3.1 Radiative transfer model simulations

To detect cloud thermodynamic phase using high-spectral IR measurements, a computationally efficient high-spectral-resolution cloudy-sky radiative transfer model (HRTM, Wang et al. 2012) in the infrared region (700-1300 cm^{-1}, 0.1 cm^{-1} spectral resolution) has been used in this study. The model is sensitive to atmospheric pressure and temperature profiles, cloud particle size, optical depth, and cloud phase. The HRTM takes into accounts the gas absorptions by major atmospheric absorption gases (i.e., H_2O, CO_2, O_3, O_2, CH_4, CO, and N_2O), spherical water droplets, and ice cloud bulk single-scattering properties (Baum et al. 2007).

BT from 700 cm^{-1} to 1300 cm^{-1} are simulated for single-layered water and ice clouds. Ice crystals and liquid water droplets have different absorption and scattering properties in the infrared window region. Additionally, Nasiri and Kahn (2008) demonstrate good phase sensitivity using channels at 1231 cm^{-1} and 960 cm^{-1}. It is important to point out that the high-level clouds and/or "upper" portion of opaque clouds contribute significantly in AIRS measurements, therefore, the main objective of the AIRS phase algorithm is to identify as many ice clouds as possible.

Like many cloud-phase algorithms, a priori assumptions of relationships between cloud temperature and cloud phase have been made in this algorithm. A few thresholds of BT and BTD are quantified, and four major tests are simultaneously conducted to infer cloud phase:

1. The first test uses simulated BTs at 960 cm^{-1} (abbreviated as BT_{960}). Pixels with very cold BT_{960} are assumed to be ice. This works because the BT_{960} of a cloudy scene is usually warmer than the cloud top temperature due to the contributions to radiance from the atmosphere below the cloud and the surface. Figure 4.3 shows the simulated BT_{960} as a function of particle effective diameter and optical depth for ice and water clouds at different cloud top temperatures. For simulated clouds with optical depth > 5, only ice clouds have BT_{960} less than 235 K. Both water and ice clouds can have high BT_{960} even for optically thin cirrus, thus a warm scene is assigned if a pixel has BT_{960} greater than 280 K. Therefore, detection of optically thin cirrus clouds will require criteria other than BT_{960} threshold.

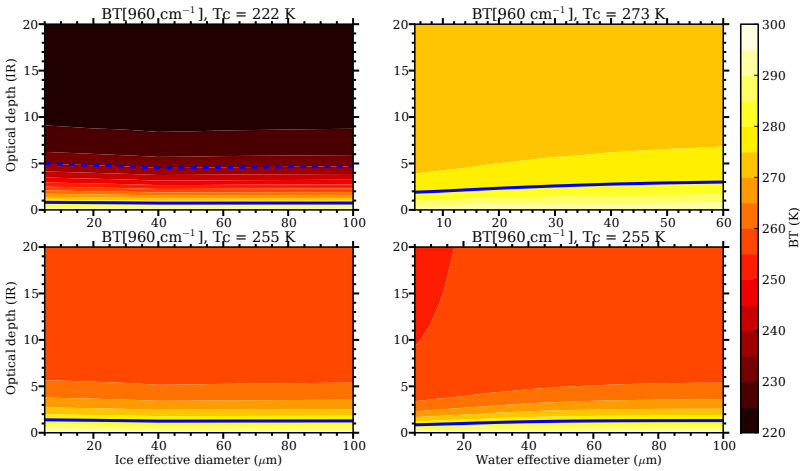

Figure 4.3 HRTM simulated BT_{960} for ice (left panel) and water (right panel) clouds. T_c: cloud top temperature. Dashed blue line: 235 K; Solid blue line: 280 K.

2. The second test uses simulated $BTD_{1231\text{-}960}$. If we only consider absorption at these two channels, $BTD_{1231\text{-}960}$ will always be positive. But for small particles (ice or water), scattering is important, thus $BTD_{1231\text{-}960}$ can be negative. Figure 4.4 shows simulated $BTD_{1231\text{-}960}$. Water clouds typically have negative $BTD_{1231\text{-}960}$ (about -1 K). Only a small fraction of simulated water clouds show positive $BTD_{1231\text{-}960}$ for cloud optical depth less than 2. For clouds with low to moderate optical depth, ice clouds with larger ice crystals show positive $BTD_{1231\text{-}960}$, whereas only opaque ice clouds with small ice particles have negative $BTD_{1231\text{-}960}$ characteristics of water clouds. The cold ice test compensates for this limitation, and should prevent many misclassifications of ice as water.

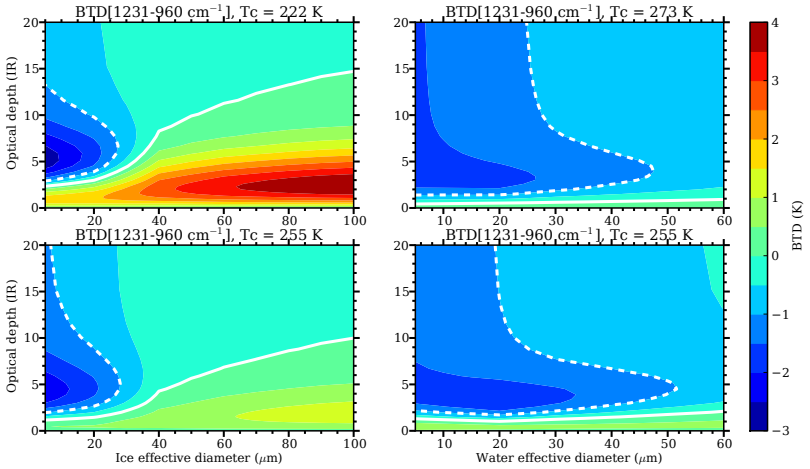

Figure 4.4 HRTM simulated $BTD_{1231\text{-}960}$ for ice (left panel) and water (right panel) clouds. T_c: cloud top temperature. Dashed blue line: -1 K; Solid blue line: 0 K.

3. The third test uses simulated BTD between 1231 cm^{-1} and 930 cm^{-1} (abbreviated as $BTD_{1231\text{-}930}$). Figure 4.5 shows that the $BTD_{1231\text{-}930}$ is more sensitive to optically thin ice clouds with small ice crystals compared to water clouds. These features are capable of detecting ice clouds ($BTD_{1231\text{-}930} > 1.75$ K) with ice crystal sizes that are small or large. Water clouds, on the other hand, gen-

erally have $BTD_{1231\text{-}930}$ less than -0.6 K. This is a weaker test compared to the first water test.

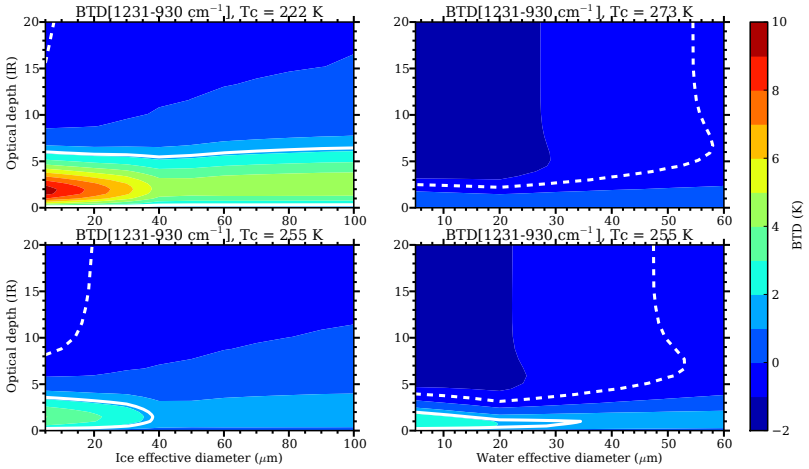

Figure 4.5 HRTM simulated $BT_{1231\text{-}930}$ for ice (left panel) and water (right panel) clouds. T_c: cloud top temperature. Dashed blue line: 235 K; Solid blue line: 280 K.

4. Additionally, the fourth test using simulated $BTD_{1227\text{-}960}$ is also shown in Figure 4.6. This figure indicates similar features as Figure 4.3. The channel centered at 1227 cm^{-1} has a weak water vapor absorption, and is helpful for finding optically thin ice clouds with $BTD_{1227\text{-}960}$ greater than - 0.5 K in the tropics.

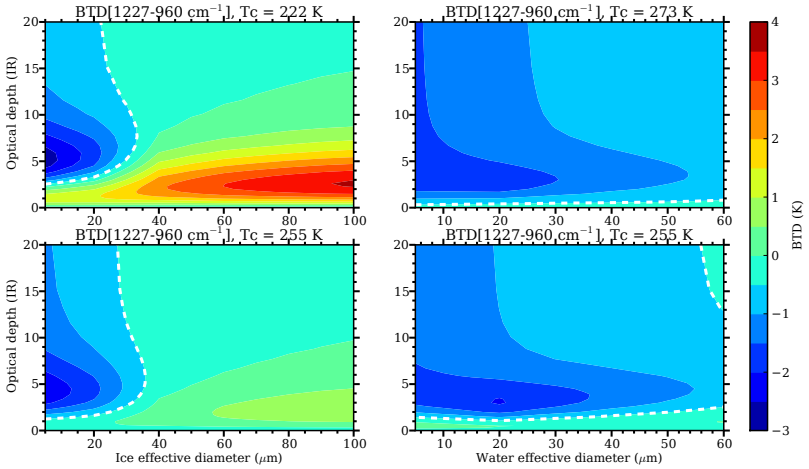

Figure 4.6 HRTM simulated $BTD_{1227\text{-}960}$ for ice (left panel) and water (right panel) clouds. T_c: cloud top temperature. Dashed blue line: -0.5 K.

4.3.2 CALIPSO observations

The one-month spatially collocated CALIPSO phase dataset is investigated and used to assess the sensitivities of the AIRS phase algorithm.

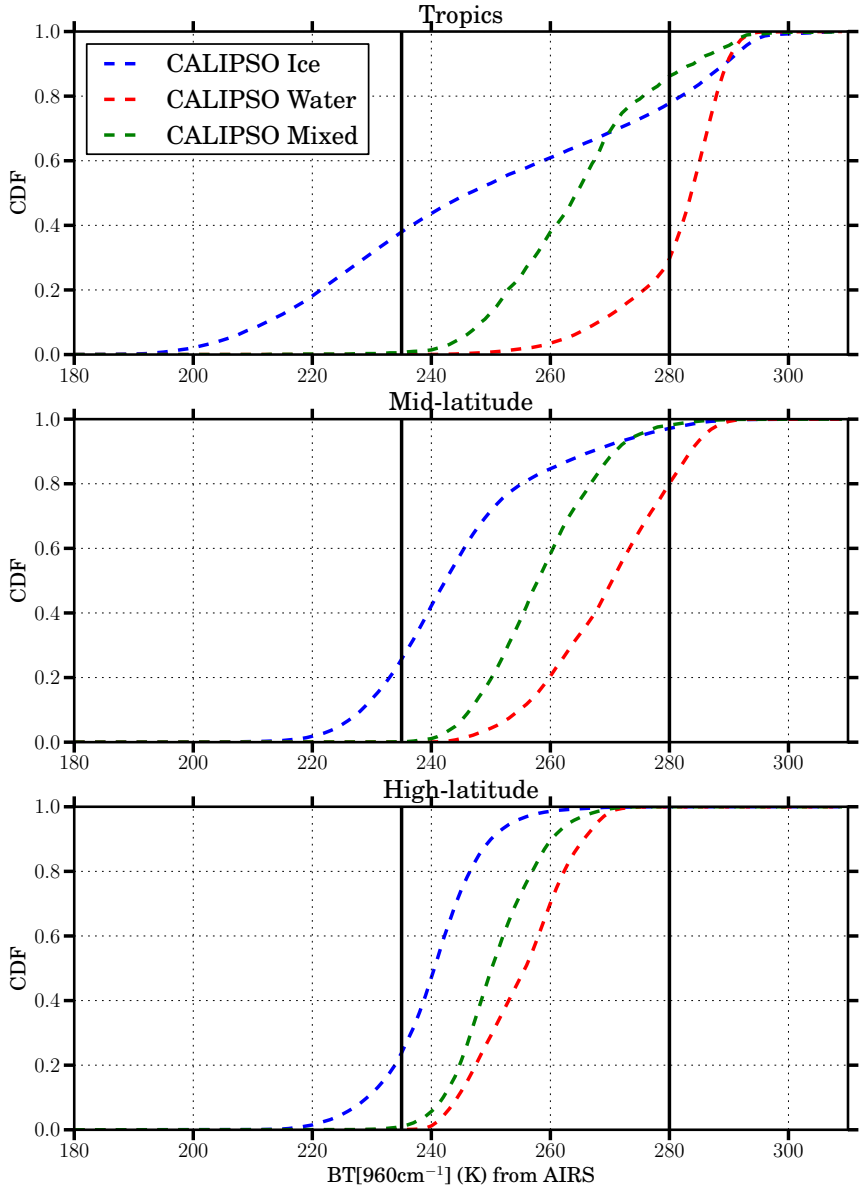

Figure 4.7 Cumulative distribution function (CDF) for AIRS BT_{960} of spatially collocated CALIPSO cloud phase of January 2009. Tropics: 25° S−25° N; Mid-latitude: 25° N(S)−60° N(S); High-laitude: 60° N(S)−90° N(S). Two solid vertical lines: 235 and 280 K.

The basis for the cold cloud test is shown in Figs 4.7 and 4.8. Essentially, we look for opaque cold clouds that have $BT_{960} < 235$ K. In Figure 4.7, nearly 40%, 25%, and 20% of CALIPSO's ice phase can be identified with this BT test in tropics, mid-latitude, and high-latitude, respectively. The fraction of ice clouds found by this step alone decreases poleward due to decreasing tropopause height and less deep convection. The lidar depolarization ratio and backscatter relationships shown in Figure 4.8 indicate that this test does not misclassify water clouds as ice (Hu 2007; Hu et al. 2009). Some optically thin cirrus clouds have $BT_{960} > 280$ K in the tropics, and they cannot which cannot be identified solely by this test.

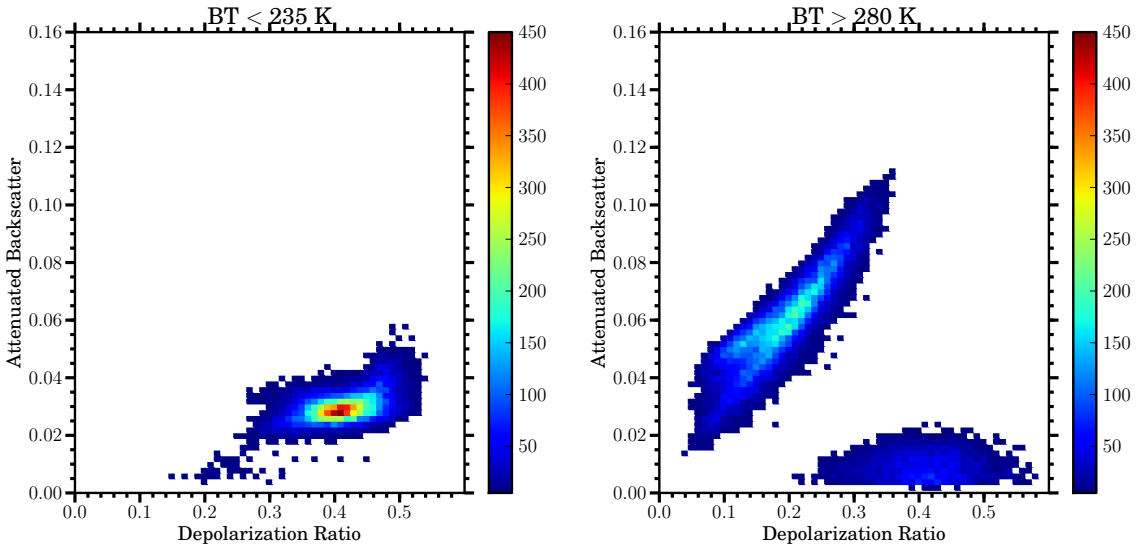

Figure 4.8 Relationships between layer-integrated depolarization ratio and layer-integrated attenuated backscatter at 532 nm for clouds with $BT_{960} < 235$ K (left) and > 280 K (right) for the collocated CALIPSO and AIRS dataset of January 2009.

The application of the second test to AIRS data is demonstrated in Figs. 4.9 to 4.11. From Figs 4.9 and 4.10, we can see that most ice clouds have $BTD_{1231\text{-}960} > 0$ while water clouds have $BTD_{1231\text{-}960} < 0$. The peaks of the ice and water probability distributions move left (more negative) as the tests move poleward. It is evident that there are overlaps between the water and ice PDFs (Figure 4.9) and

the joint histograms (Figure 4.10) within the range between - 1 and 0 K. Here, we consider strongly positive (> 0 K) and negative values (< -1 K) of $BTD_{1231\text{-}960}$ as thresholds for ice and water. Similarly, the relationships between lidar depolarization ratio and attenuated backscatter shown in Figure 4.11 indicate that this test barely shows misclassification of both ice and water clouds. While the PDFs are not shown, approximately 80%, 60%, and 40% of CALIPSO ice clouds in tropics, mid-latitudes, and high-latitudes can be found using this test, respectively.

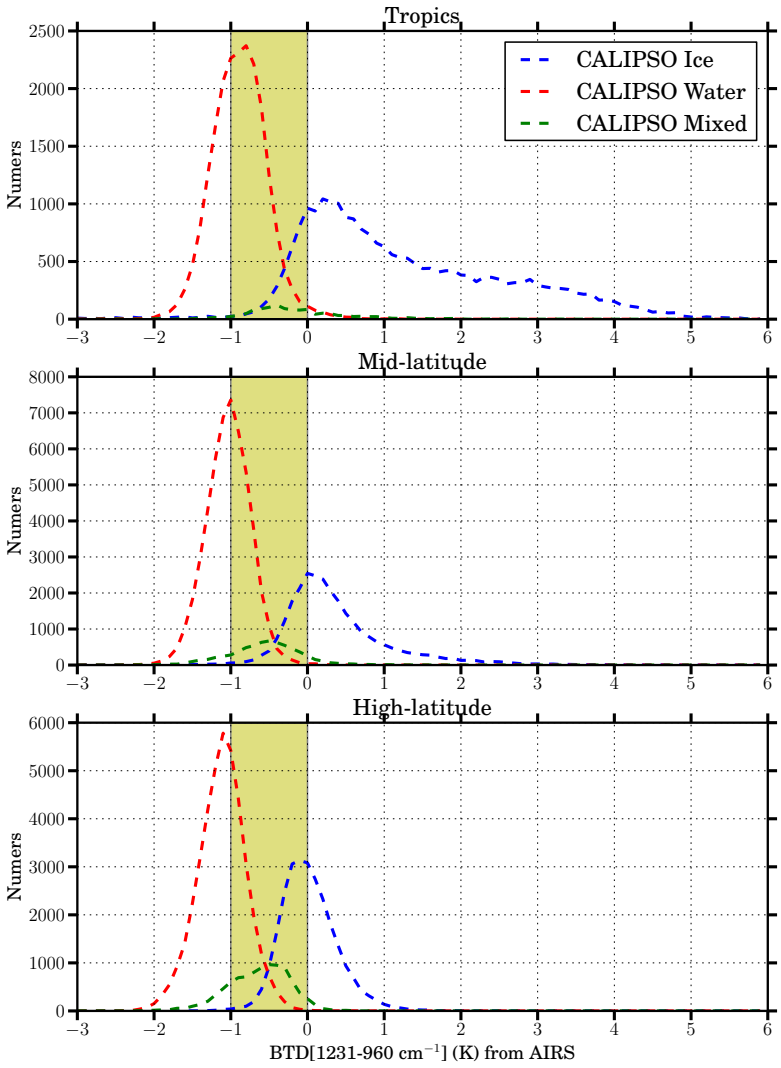

Figure 4.9 Similar to Figure 4.7. Probability distribution for AIRS $BTD_{1231\text{-}960}$ of spatially collocated CALIPSO cloud phase of January 2009.

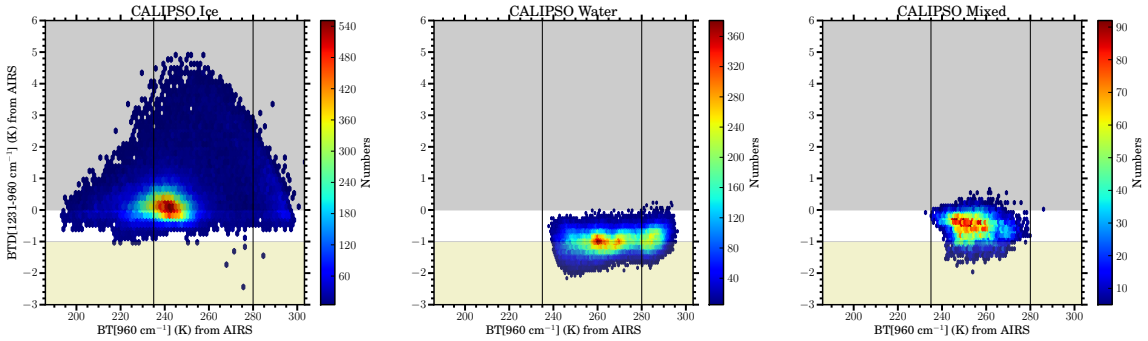

Figure 4.10 Joint histograms of BT_{960} and $BTD_{1231\text{-}960}$ for CALIPSO cloud phase of January 2009. Ice: left; Water: middle; and Mixed-phase: right.

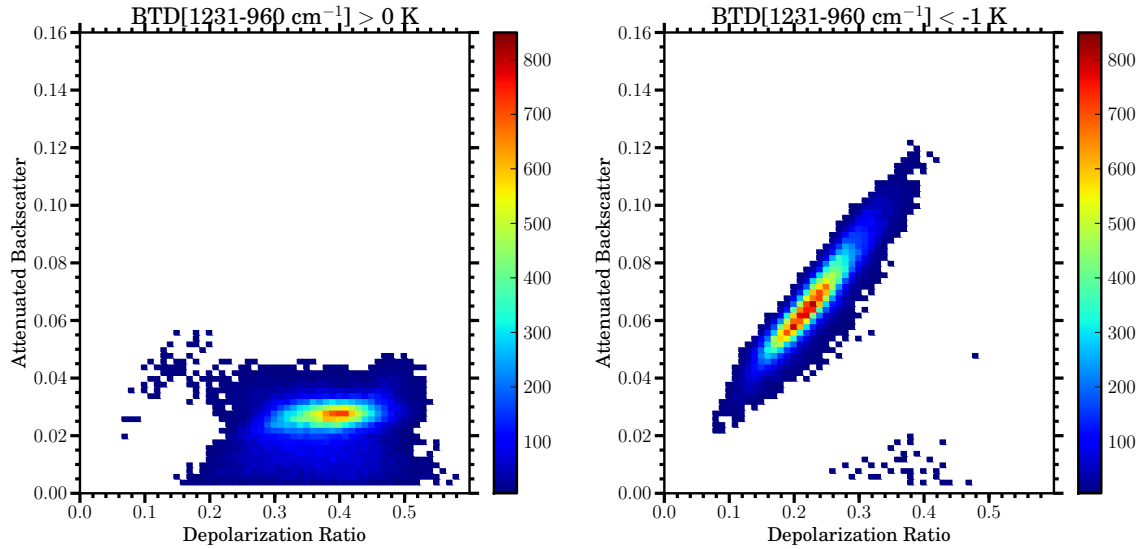

Figure 4.11 Relationships between layer-integrated depolarization ratio and layer-integrated attenuated backscatter at 532 nm for clouds with $BTD_{1231\text{-}960} > 0$ K (left) and < -1 K (right) for the collocated CALIPSO and AIRS dataset of January 2009.

The effects of third ice and second water tests are displayed from Figs. 4.12 to 4.14. The distributions of $BTD_{1231\text{-}930}$ in Figure 4.12 of ice and water are similar to $BTD_{1231\text{-}960}$, but the peaks are different. Although the shaded area between -0.6 and 1.75 K shows some overlaps between CALIPSO water and ice, this BTD is strongly correlated with $BTD_{1231\text{-}960}$ in Figure 4.13, and only a very small number of misclassification in the water and ice plots. For scenes classified as mixed-phase by

CALIPSO, more mixed scenes are classified as water by this test than are classified as ice. In practice, because of strong correlations with $BTD_{1231\text{-}960}$ in Figure 4.13, it is more useful for finding clouds that most likely are water. Thus, we consider these two values as thresholds for water and ice. The layer-integrated backscatter at 532 nm and layer-integrated depolarization ratio relationships in Figure 4.14 also show negligible amount of misclassification for water and ice.

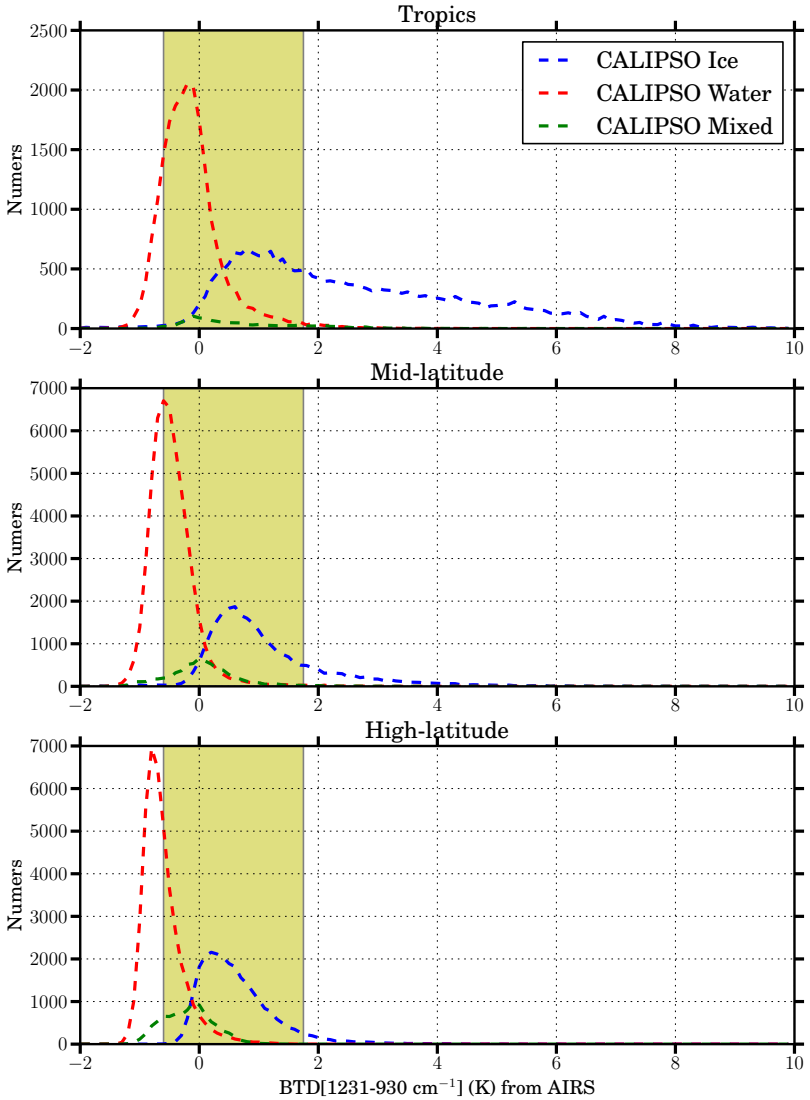

Figure 4.12 Similar to Figure 4.9. Probability distribution for AIRS $BTD_{1231\text{-}930}$ of spatially collocated CALIPSO cloud phase of January 2009.

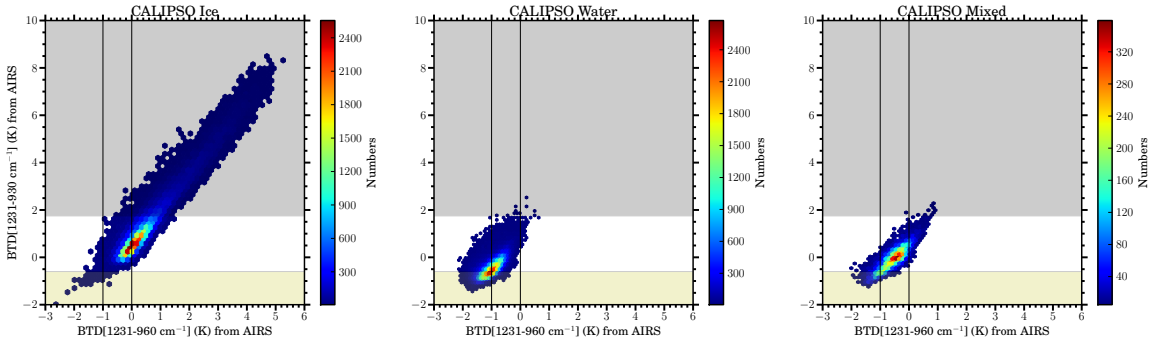

Figure 4.13 Similar to Figure 4.10. Joint histograms of $BTD_{1231\text{-}960}$ and $BTD_{1231\text{-}930}$ for CALIPSO cloud phase of January 2009. Ice: left; Water: middle; and Mixed-phase: right.

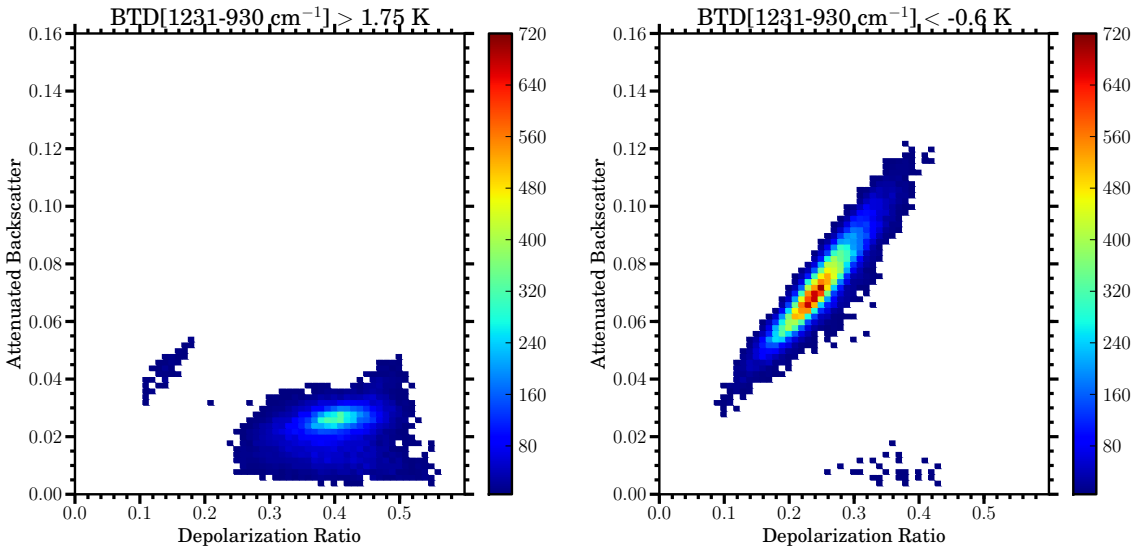

Figure 4.14 Similar to Figure 4.11. Relationships between layer-integrated depolarization ratio and layer-integrated attenuated backscatter at 532 nm for clouds with $BTD_{1231\text{-}930} > 1.75$ K (left) and < -0.6 K (right) for the collocated CALIPSO and AIRS dataset of January 2009.

The last test is based on the BTD between 1227 cm^{-1} and 960 cm^{-1}($BTD_{1227\text{-}960}$) and is used to identify ice in the tropics. Kahn et al. (2011) used BTD (1231-1227 cm^{-1}, $BTD_{1231\text{-}1227}$) and $BTD_{1231\text{-}960}$ to study the impacts of subpixel cloud heterogeneity on infrared thermodynamic phase assessment and showed a strong relationship between $BTD_{1231\text{-}1227}$ and total column water vapor. In Figure 4.10, a threshold

of $BTD_{1231\text{-}960}$ > -0.5 looked useful for finding many ice clouds, but there were problems with misidentification of water clouds as ice. The $BTD_{1227\text{-}960}$ helps with that ambiguity by essentially broadening the separation between ice and water (Figs 4.15 and 4.16), but at the expense of missing some optically thin ice clouds in the tropics (not shown). The layer-integrated backscatter at 532 nm and layer-integrated depolarization ratio relationships in Figure 4.17 indicate that this test can be useful to classify ice clouds.

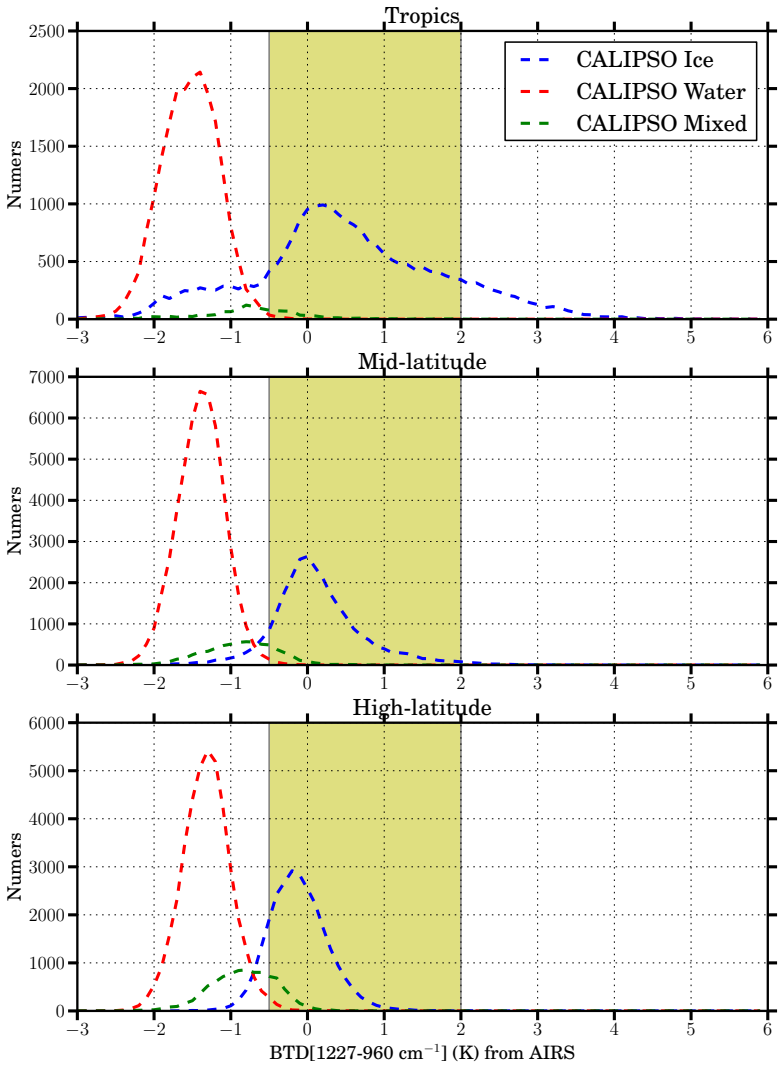

Figure 4.15 Similar to Figure 4.9. Probability distribution for AIRS $BTD_{1227\text{-}960}$ of spatially collocated CALIPSO cloud phase of January 2009.

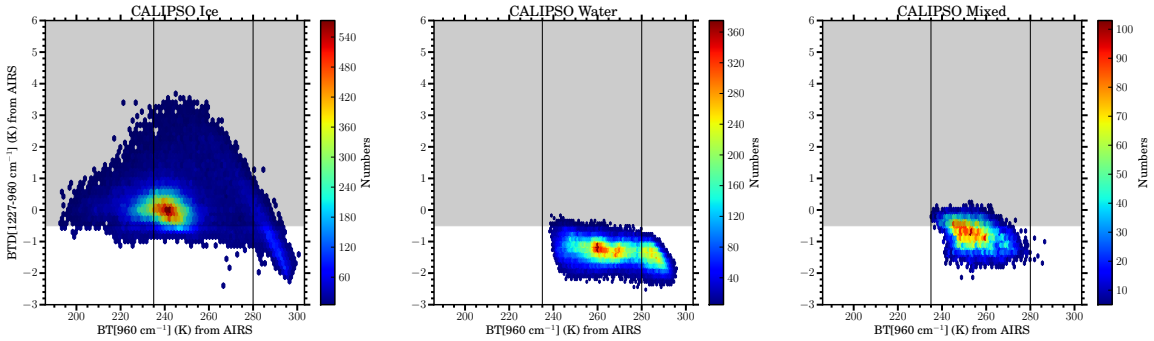

Figure 4.16 Similar to Figure 4.10. Joint histograms of BT_{960} and $BTD_{1227\text{-}960}$ for CALIPSO cloud phase of January 2009. Ice: left; Water: middle; and Mixed-phase: right.

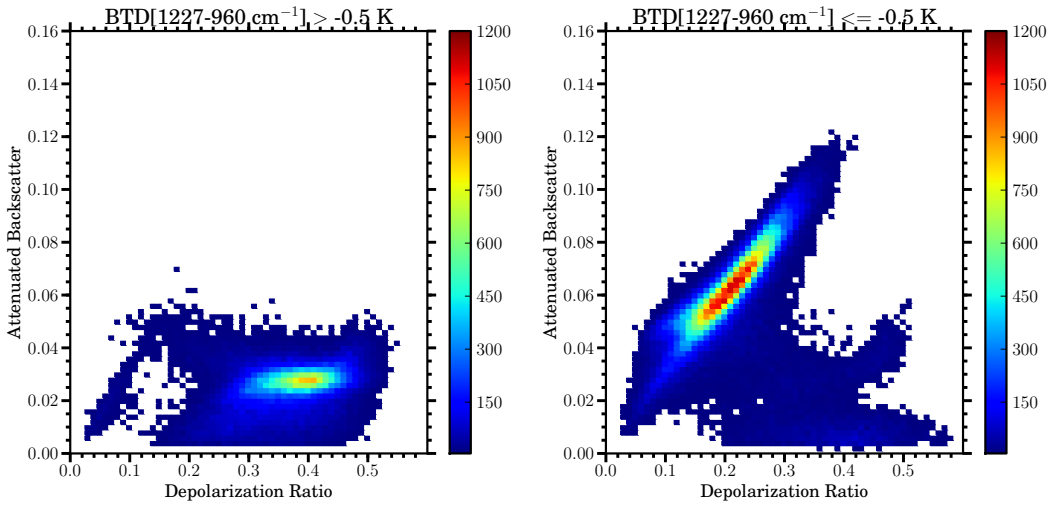

Figure 4.17 Similar to Figure 4.11. Relationships between layer-integrated depolarization ratio and layer-integrated attenuated backscatter at 532 nm for clouds with $BTD_{1227\text{-}960}$ > - 0.5 K (left) and ≤ -0.5 K (right) for the collocated CALIPSO and AIRS dataset of January 2009.

4.3.3 Schematic view of the algorithm

Based on the discussions of the radiative transfer simulations and CALIPSO observations in the previous two sections, the four potential tests appear promising for determining cloud thermodynamic phase, − particularly for ice. Therefore, we propose an AIRS cloud phase algorithm based on the four tests.

The flowchart for the AIRS phase algorithm is illustrated in Figure 4.18. The algorithm requires the following input data: AIRS L1B geolocated and calibrated radiances, AIRS-retrieved effective cloud fraction (ECF), and surface emissivity near the 8-μm region (Seemann et al. 2008). AIRS ECF is used as a proxy to determine the presence of clouds in an AIRS footprint. The AIRS ECF is a convolution of both cloud coverage and emissivity, unlike the traditional cloud mask, which represents coverage only. Because the phase algorithm depends on channels 1231 cm^{-1} and 1227 cm^{-1}, a spectral region especially sensitive to surface emissivity, no phase detection is performed in desert regimes with emissivity values at 1231 $cm^{-1} < 0.9$ (Jin and Liang 2006).

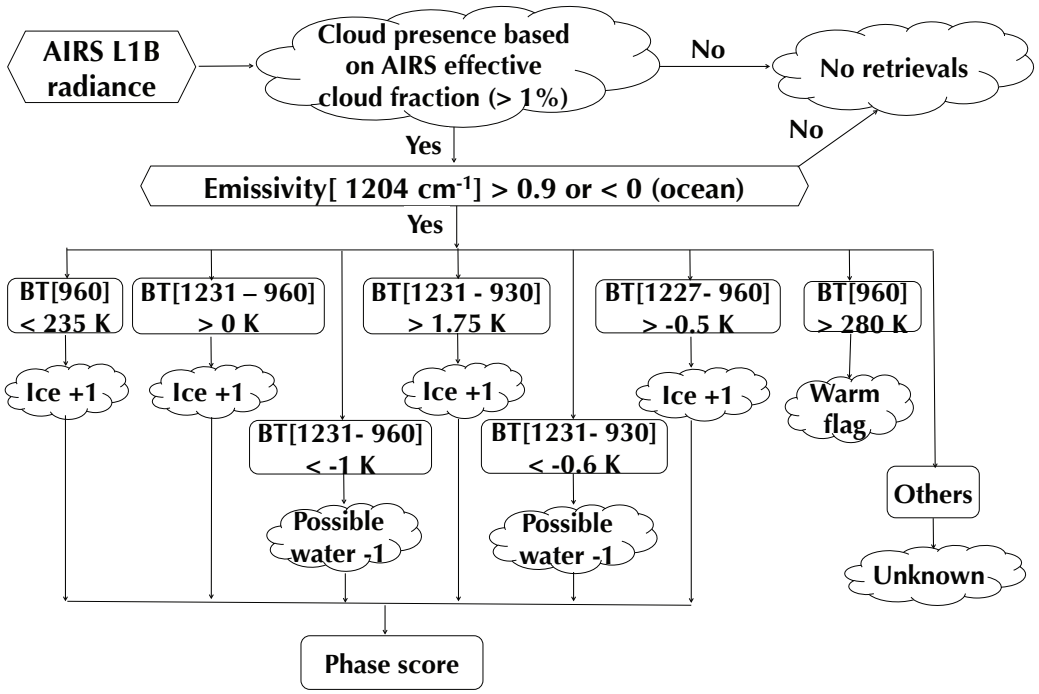

Figure 4.18 Flow chat for AIRS cloud phase.

The individual test outputs provide a measure of confidence. The phase score is a summation of ice and water tests, which can be simultaneously triggered in some

circumstances, while the warm scene is only tested and not used in the final phase determination. The algorithm has three possible cloud phase classifications: ice, water, and unknown. The higher the positive value (1−4), the higher the confidence the cloud is in the ice phase. Conversely, the lower the negative value (-1 or -2), the higher the confidence the cloud is composed of water. The unknown category results from no tests passing, or 1 or 2 positive tests each of ice and water. For instance, if one ice test and one water test simultaneously pass, the AIRS phase algorithm calls it unknown rather than ice or water. However, this situation occurs approximately less than 1% of the time according to Nasiri et al. (2012).

4.4 Case studies

To illustrate the performance of the newly developed AIRS phase algorithm, the algorithm is applied to two individual AIRS granules and compared to the CALIPSO phase products. A more comprehensive evaluation process will be discussed in the next chapter.

Figure 4.19 shows AIRS and CALIPSO observations corresponding to the 0112 UTC January 1, 2009 AIRS granule over the southern Pacific Ocean. The BTs for measured AIRS IR radiations at 960 cm^{-1} in Fig 4.19a show relatively low values along the CALIPSO track, represented by a line through the AIRS granule, indicating the likelihood of the occurrence of ice clouds. The AIRS phase retrievals (Fig 4.19b) are also displayed for this granule with the color scale representing the cloud phase scores. Figure 4.19c shows the cloud phase determination from CALIPSO (bottom) and AIRS (top) along the CALIPSO track. The color map for AIRS in Fig 4.19c is the same as the one in Fig 4.19b. It is clear that both AIRS and CALIOP identify the high clouds at approximately 10∼15 km from 45° to 29° S as ice phase. Additionally, AIRS classifies CALIPSO liquid water clouds as unknown phase be-

tween 50.5° and 47° S. Because CALIPSO has better phase sensitivity than AIRS, if there is not enough spectral information in such classification, AIRS phase prefers to call it unknown other than misclassification.

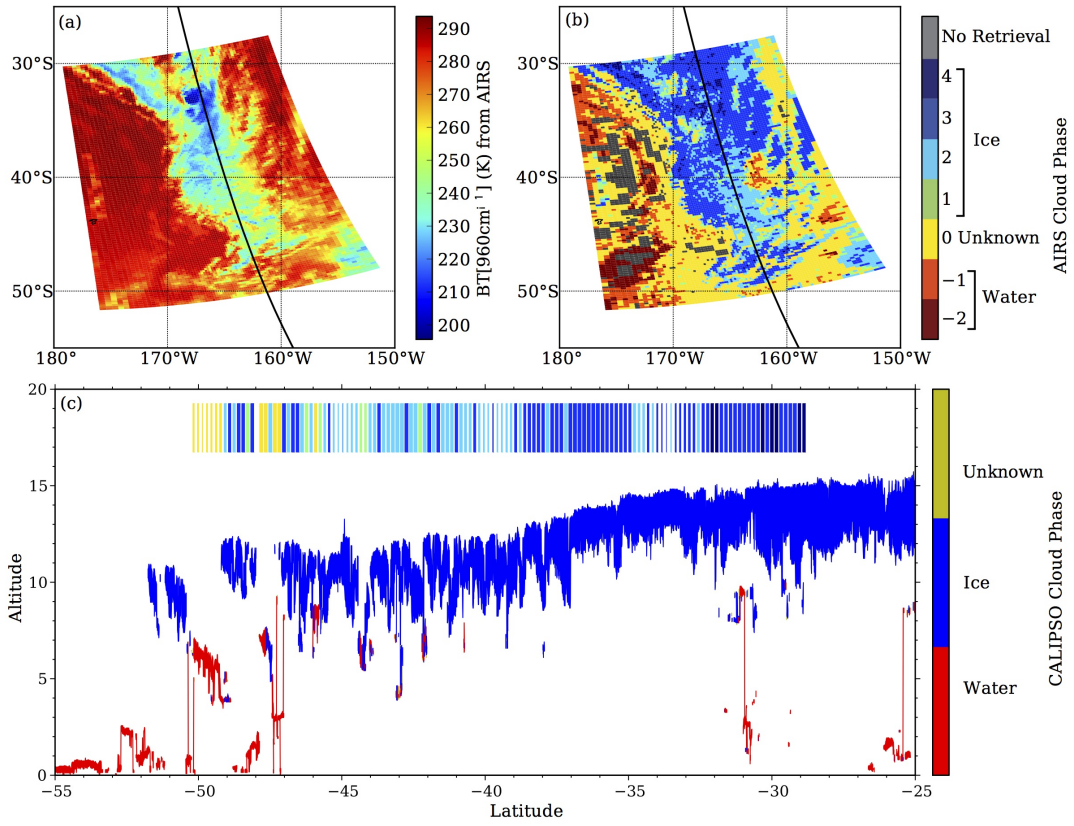

Figure 4.19 First case: the 12th AIRS granule and CALIPSO footprints at 0112 UTC on January 1 2009. a) shows the brightness temperature at 960cm^{-1} from AIRS, and the solid black line is the CALIPSO ground track; b) is the cloud phase scores from AIRS. Positive values are ice, negative values are water, and 0 represents unknown; c) is the cloud phase classification along the CALIPSO track. In c), the upper colors represents AIRS phase, and lower colors are CALIPSO phase..

The second case shown in Figure 4.20 focuses on the 1936 UTC on January 12, 2007 AIRS granule. Three cloud types classified by CloudSat (not shown, Wang and Sassen 2007) dominate this scene: cirrus, nimbostratus, and altostratus. Along the CALIPSO track, AIRS ice phase agrees well with the CALIPSO ice phase between 27° and 30° N and between 33° and 40° N. The AIRS phase identifies the clouds

as unknown phase rather than ice or water because there is not enough spectral information between 40° and 42° N, whereas CALIPSO shows thin cirrus cloud (ice phase) over mid-level water clouds.

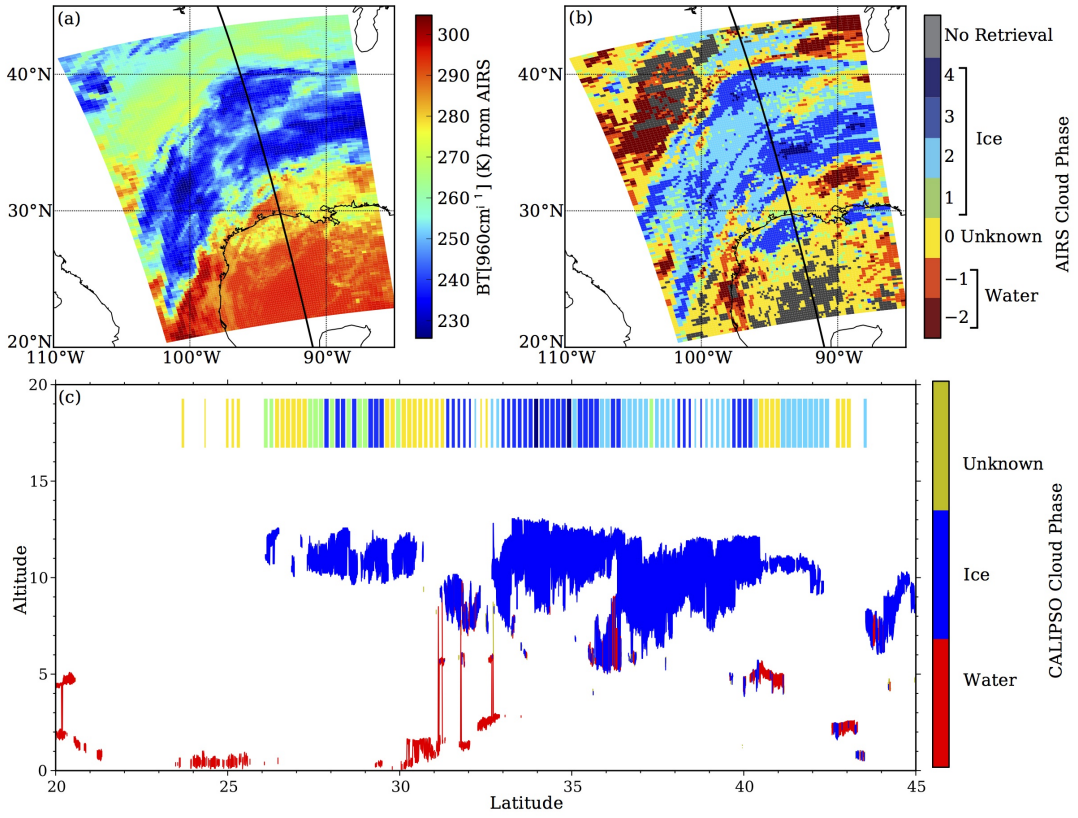

Figure 4.20 Similar to Figure 4.11, but for the 196 granule at 1936 UTC on January 12 2007.

5. EVALUATION OF AIRS CLOUD PHASE USING CALIPSO OBSERVATIONS AND THERMODYNAMIC PHASE OF MID-LEVEL CLOUDS

5.1 Introduction

In the last chapter, we introduced a new cloud thermodynamic phase determination algorithm using the high spectral resolution IR radiances from AIRS. To make use of the AIRS phase algorithm operational, we will need a more comprehensive evaluation to quantify the high-spectral IR cloud phase assessments.

A proper assessment of AIRS cloud phase retrievals requires comparisons with independent datasets of well-characterized measurements having global coverage and, preferably, vertical profiling. The CALIOP instrument on the CALIPSO payload can measure cloud vertical profiles and provide a 3D view of the ice and water distributions in clouds, which is useful for the evaluation of IR based cloud phase retrievals. Cho et al. (2009) demonstrated the usefulness of CALIPSO cloud phase retrievals to evaluate the MODIS C5 bi-spectral IR phase. A recent study by Nasiri and Kahn (2008) using radiative transfer model simulations showed a number of limitations of the MODIS C5 bi-spectral IR phase: 1) MODIS to classify optically thin cirrus as water clouds, mixed, or unknown; 2) opaque ice clouds composed of small particles to be classified as water clouds; 3) mid-level (approximately 4-7 km) or mid-temperature (between 250 and 265 K) water or ice clouds would be classified as mixed-phase or unknown. Cho et al. (2009) supported several hypotheses presented by Nasiri and Kahn (2008).

In this chapter, we conduct an evaluation of the AIRS cloud phase retrievals using the CALIPSO cloud phase product. The comparisons between the AIRS and

CALIPSO are made for a year (December 2007-November 2008). Cho et al. (2009) focused primarily on single-layer clouds. However, as discussed in chapter 2 and 3, overlapping clouds occur frequently over the globe (Poore et al. 1995; Wang et al. 2000; Li et al. 2011; Subrahmanyam and Kumar 2011). Additionally, heterogeneous clouds are also often observed globally and can have significant impacts on cloud phase assessments (Kahn et al. 2011). Therefore, we first choose three cloud configurations as single-layer, heterogeneous, and multi-layer cloud regimes within the AIRS footprints, respectively. The methodology for determining these scenes is presented and discussed later in this chapter. The robustness of the AIRS phase approach is then evaluated with respect to the single-layer, heterogeneous, and multi-layer cloud scenes. We will address that whether the AIRS cloud phase approach can improve the IR-based cloud phase retrievals, especially for optically thin cirrus and clouds in the mid-temperature.

The second major objective of this dissertation is to quantitatively characterize the thermodynamic phase of mid-level clouds. We have discussed that the use of the ISCCP convention of mid-level clouds occurring between 680 and 440 hPa is more appropriate for global studies than the cloud-base definition often used in ground-based studies. In this chapter, we investigate the phrase of mid-level clouds as defined by both the ISCCP cloud top pressure and the cloud-top height definitions of the mid-level.

5.2 Data and methodology

In the CALIPSO version 3 Level 2 1-km cloud layer products, up to ten cloud layers are profiled vertically. A "Cloud layer" means that there are signal returns from both the top and base boundaries of the cloud feature, as well as separations of "clear air" from other layers. The spatial, optical, and phase characteristics of

each cloud layer are reported including layer base and top altitudes, layer-integrated attenuated backscatter at 532 nm, layer-integrated volume depolarization ratio, and cloud top temperature and pressure. The cloud top temperature and pressure are derived at the top of the each vertical layer based upon the version 5 GEOS data product provided to the CALIPSO project by the NASA GMAO Data Assimilation System. To avoid breaking up the vertically continuous cloud features sometimes observed in the CALIPSO products, we combine cloud layers that have vertical separation of less than 400 m and treat them as a single layer following the approach in Cho et al. (2009). Figure 5.1 shows an example of the separation distances between multiple cloud layers from CALIPSO for 2008. Only a fairly small fraction of the multi-layer cloud profiles have a vertical separation of less than 400 m, and the vast majority of cloud layers are well separated.

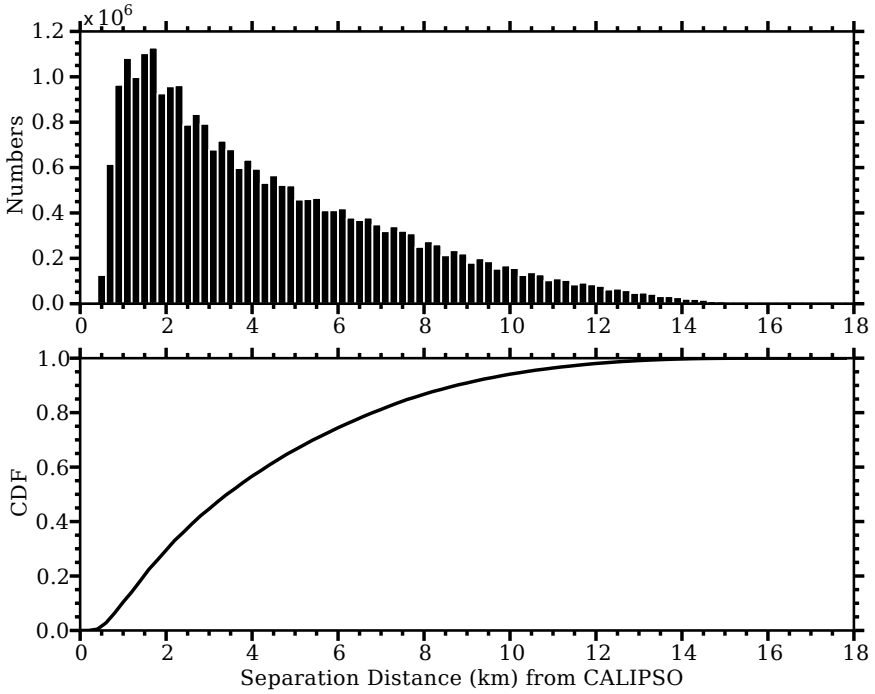

Figure 5.1 Separation distance between adjacent layers in the CALIPSO 1km cloud-layer product for 2008. The bottom panel shows the cumulative distribution function (CDF) of the histogram.

CALIPSO cloud phase products (version 3.01) are used to evaluate and assess the AIRS cloud phase algorithm we have developed in chapter 4. One of the main limitations of CALIPSO is that the lidar cannot penetrate clouds with visible optical depth greater than about 3, thus the vertical profiles are incomplete in thick clouds due to strong lidar return-signal attenuation. Therefore, CALIPSO is much more sensitive to the presence of optically thin clouds, and can typically provide vertical information of a cloud by penetrating through thin cirrus and the tops of opaque clouds.

It is important to point out that only the topmost layer within the multi-layer cloud scenes is included in the collocated AIRS and CALIPSO dataset. In chapter 2 and 3, we showed that the bottom layer within the multi-layer cloud systems also contributes significantly in the mid-level clouds amounts. Therefore, an extra dataset accounting for cloud phase of the multi-layer cloud scenes (top+bottom) is necessary to address the cloud phase information of mid-level clouds. In this study, we include an independent dataset of only CALIPSO 5-km cloud phase product for the same time period. This independent dataset reports cloud phase for two cloud layers.

5.2.1 AIRS/CALIOP collocation strategy

The CALIPSO cloud product that we are using has a horizontal resolution of 1 km which is enough to resolve many common cloud systems. As CALIPSO only makes nadir measurements, its track passes through the central part of the AIRS swath. An example of coincident AIRS and CALIPSO observations is shown in Figure 4.2, and a typical AIRS FOV (15 km) will fall into one of three cloud cover categories: 1): clear sky; 2) partially overcast; 3): completely cloudy. Along the CALIPSO track, up to 15 CALIPSO phase retrievals may fall within one AIRS FOV (Figure 5.2). The coincident observations between AIRS and CALIPSO are spatially

collocated using a nearest neighbor approach. The collocation criteria adopted here requires that the distance between the center of an AIRS FOV (assumed to be a circle, Figure 5.2) and CALIPSO pixels is less than 7.5 km.

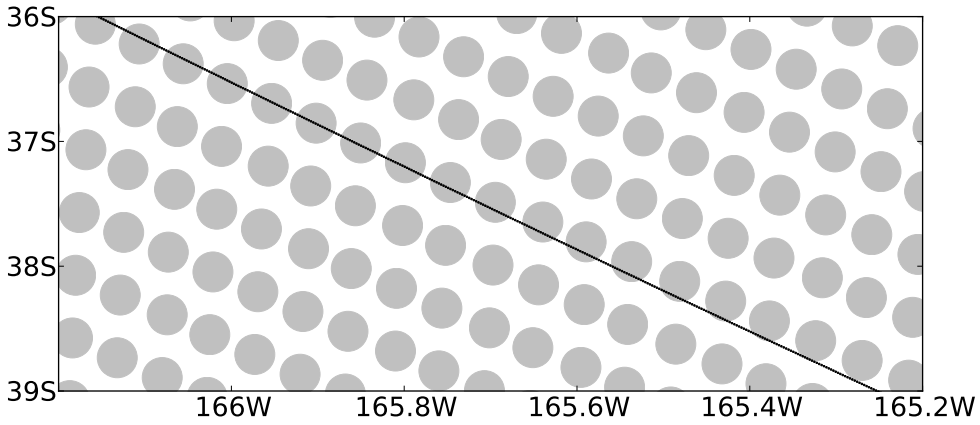

Figure 5.2 A zoomed in view of AIRS and CALIPSO obsevations. AIRS: grey dot; CALIPSO: black dot.

Since this study targets cloud phase, the clear sky scenes are ignored if there are no cloud layers found by the CALIPSO within the AIRS FOV. The cloudy match-ups are separated into three categories: single-layer, heterogeneous, and multi-layer scenes. We define single-layer cloud scenes to be those AIRS FOVs contain more than ten CALIPSO cloudy pixels with each CALIPSO pixel having only one cloud layer. Multi-layer cloud scenes, on the other hand, also containing more than ten CALIPSO cloudy pixels, but each CALIPSO pixel has at least two cloud layers. Heterogeneous scenes are defined as having $3-10$ CALIPSO cloudy pixels within the AIRS FOV. The heterogeneous scenes have more difficulty in the assessment of cloud phase than homogeneous cloud scenes (Kahn et al. 2011).

Two assumptions have been made for the three cloudy scenes: 1) a cloudy

CALIPSO 1-km cloud layer retrieval is assumed to be horizontally homogeneous; 2) the limited number of CALIPSO cloud retrievals is a statistically representative sub-sample of the AIRS FOV (Kahn et al., 2008). One caveat here is that, in some circumstances, AIRS considers the corresponding FOV as clear even though a number of cloudy CALIPSO pixels are identified. For example, contrails can be horizontally distributed along the CALIPSO track, and because the AIRS ECF may be less than 1%, the AIRS FOV is treated as clear sky and is not included in the statistics that follow.

Table 5.1 Number of collocated AIRS FOVs in different latitude zones for single-layer, heterogeneous, and multi-layer clouds for 2008.

	Total	Tropical (25°S-250°N)	Mid-latitude (25-60°S, 25-60°N)	High-latitude (60-90°S, 60-90°N)
Single-layer	2,379,807	459,400 (19.3%)	1,057,129 (44.4%)	863,278 (36.3%)
Heterogeneous	2,249,974	636,046 (28.3%)	928,819 (41.3%)	685,109 (30.4%)
Multi-layer	274,964	51,871 (18.8%)	120,024 (43.7%)	103,069 (37.5%)

Table 5.1 lists the sample sizes of collocated AIRS FOVs for the entire globe, and for different latitude bands (tropics: 25° N−25° S; mid-latitude: 25°−60° N and S; high-latitude: 60°−90° N and S). Approximately 19.3%, 44.4%, and 36.3% of the single-layer clouds are likely to occur in the tropics, mid-latitudes, and high-latitudes, respectively. Heterogeneous scenes, on the other hand, occur 23.8%, 41.3% and 30.5% from low-latitude to high-latitudes. Multi-layer cloud scenes are approximately 10% of the single-layer clouds, and shows similar frequency of occurrence as the single-layer clouds when moving from tropics towards polar regions. The heterogeneous

clouds dominate the statistics in the Tropics, but cloud phase discrimination is a much less ambiguous problem at low latitudes.

Because multiple CALIPSO phase retrievals occur within an AIRS FOV, it is possible for more than one CALIPSO phase to correspond to a single AIRS phase retrieval. In the 1-km CALIPSO cloud phase products, ice (randomly-oriented), water, horizontally-oriented ice crystals, and unknown phases are reported. If all of the selected CALIPSO pixels have one phase (i.e., ice or water), the CALIPSO phase category is straightforward. When the AIRS FOV has different cloud phases (i.e., both ice and water are found simultaneously), we refer to the collocated CALIPSO phase as "mixed-phase". This mixed-phase category is over the AIRS FOV, rather than at the 1-km CALIPSO pixel-scale. The CALIPSO quantities such as layer top/base altitudes and cloud top temperature/pressure are averaged within the AIRS FOV for single-layer scenes, whereas the uppermost layer for heterogeneous scenes and multi-layer scenes are used.

Additionally, no cloud-height or AIRS zenith angle correction is made herein, and it is possible that small collocation errors and scan angle biases are introduced. Cho et al. (2009) estimated that for MODIS and CALIPSO collocations, the errors would be small for low clouds, but in some circumstances could be up to 5 km for cirrus clouds. Kahn et al. (2011) quantify phase BTD sensitivities to scan angle and show that ice and water clouds are affected in different and non-intuitive ways, suggesting no easy implementation or fix for scan angle dependence, which therefore warrants further investigation.

5.3 Evaluation of AIRS phase

Table 5.1 shows that the number of collocated AIRS FOVs for one year (December 2007-November 2008) was approximately 5 million in total, and single-layer,

heterogeneous, and multi-layer scenes accounted for approximately 48.5%, 45.9%, and 5.6% of those FOVs, respectively. The joint histograms in Fig. 5.3 show the global distributions of the corresponding cloudy scenes. Figure 5.3a is the number density of the total cloudy scenarios, whereas Figs. 5.3b−5.3d indicate the relative fractions of occurrence for single-layer, heterogeneous, and multi-layer cases. The high frequencies of heterogeneous clouds mainly occur in the tropical region. The low fractions of single-layer scenes in Fig. 5.3b correspond to the high values of Fig 5.3c, with relatively high frequencies of occurrence of 40%-60% in the mid and high latitude regions. In the case of multi-layer clouds, the magnitude of frequency decreases notably by about a factor of two compared to single-layer and heterogeneous clouds. The multi-layer clouds occur most frequently in the tropics and mid latitudes, demonstrating a similar pattern to Figure 2.1.

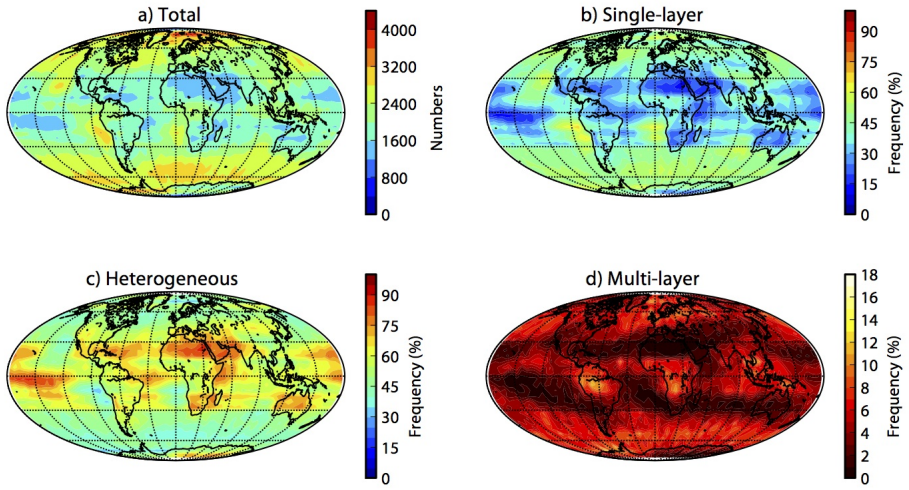

Figure 5.3 The joint histogram of global distributions of cloudy scenes for one year of collocated AIRS and CALIPSO observations. The grid size is 5°x5°. a) shows the number density of the total cloud scenarios (single-layer+heterogeneous+multi-layer). The other figures show the fraction of cloudy data within each grid that match the single-layer (b), heterogeneous (c), and multi-layer (d) for each grid cell, and the sum of b), c), and d) equals to 1. The color ranges for b) and c) are the same from 0 to 1, whereas the color scale for d) is from 0 to 0.18.

Table 5.2 Cloud phase of AIRS and CALIOP for single, heterogeneous, and multi-layer clouds for 2008. Percentage represents the faction of each cloud phase category of AIRS or CALIPSO.

		Ice	Water	Mixed	Unknown
Single-layer	AIRS	800,489	522,283		1,057,035
		(33.64%)	(21.95%)		(44.41%)
	CALIPSO	868,103	1,077,638	434,066	
		(36.48%)	(45.28%)	(18.24%)	
Heterogeneous	AIRS	738,196	409,183		1,102,595
		(32.81%)	(18.19%)		(49.00%)
	CALIPSO	601,999	1,011,031	630,944	
		(26.76%)	(44.94%)	(28.31%)	
Multi-layer	AIRS	162,865	11,660		100,439
		(59.23%)	(4.24%)		(36.53%)
	CALIPSO	65,103	16,711	193,150	
		(23.68%)	(6.08%)	(70.25%)	

Table 5.2 summarizes the cloud phase statistics of AIRS and CALIPSO. The CALIPSO phase used here for heterogeneous and multi-layer clouds are from the uppermost layer. In general, CALIPSO classified more clouds as water clouds than AIRS in the three cloudy scenarios. AIRS and CALIPSO classified comparable numbers of ice clouds in the single-layer and heterogeneous scenes, while in the multi-layer cases, AIRS classified twice as many clouds as ice phase than CALIPSO.

We now compare collocated AIRS and CALIPSO phase retrievals by latitude, BT at 1231 cm^{-1} (abbreviated as BT_{1231}), and cloud top temperature (CTT). Here in the comparisons, we focus on the channel 1231 cm^{-1} because this channel has low channel noise and the atmosphere is relatively transparent. Figures 5.4 to 5.8 show the comparisons for single-layer, heterogeneous, and multi-layer scenes, respectively.

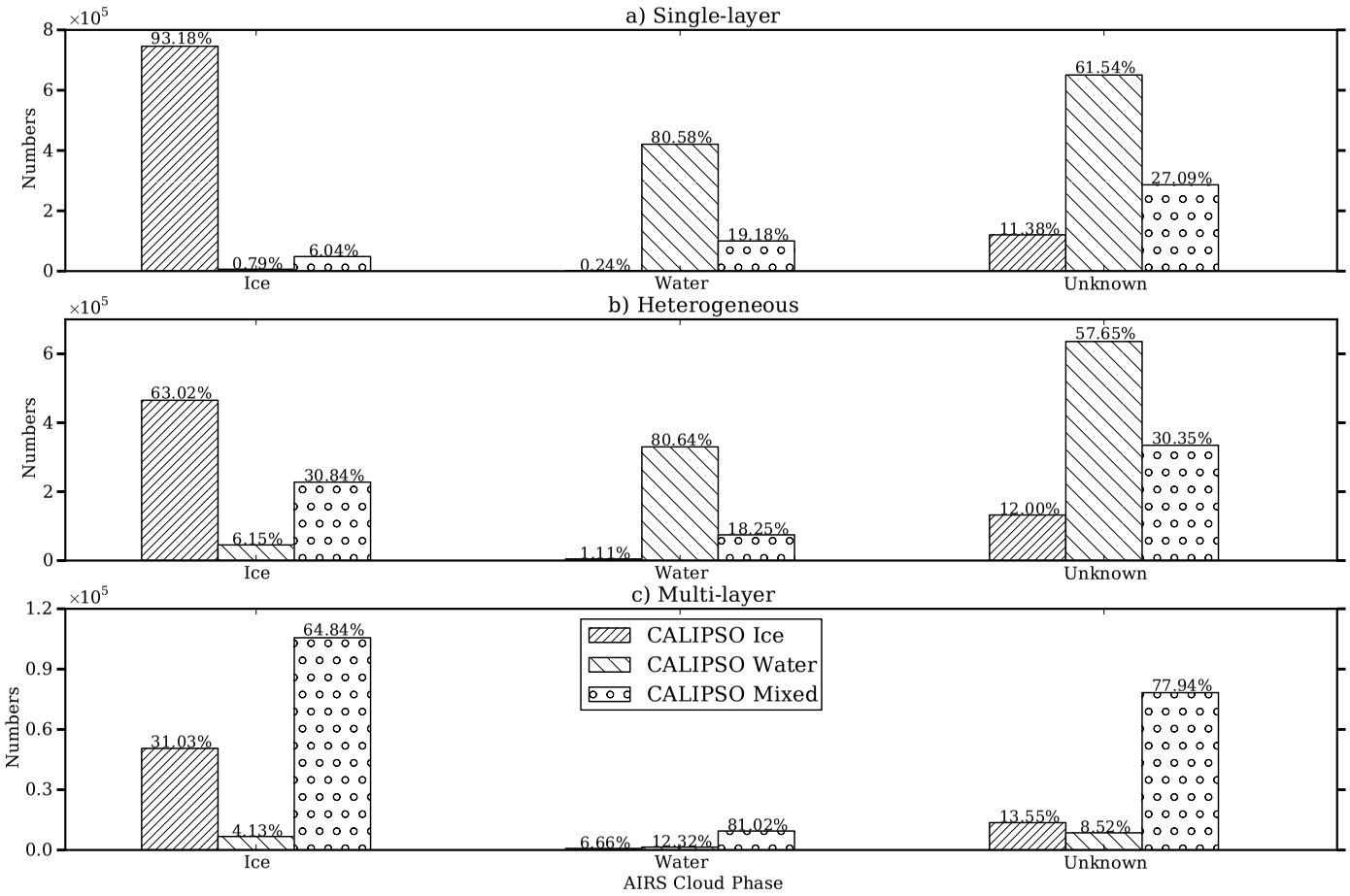

Figure 5.4 Comparisons of CALIOP and AIRS phase retrievals for a): single-layer; b): heterogeneous; c) multi-layer scenes. The x-axis shows the AIRS categories, while the different bars show the co-located CALIOP retrievals within each AIRS category. The sum of the CALIOP percentage is 100% for each AIRS category.

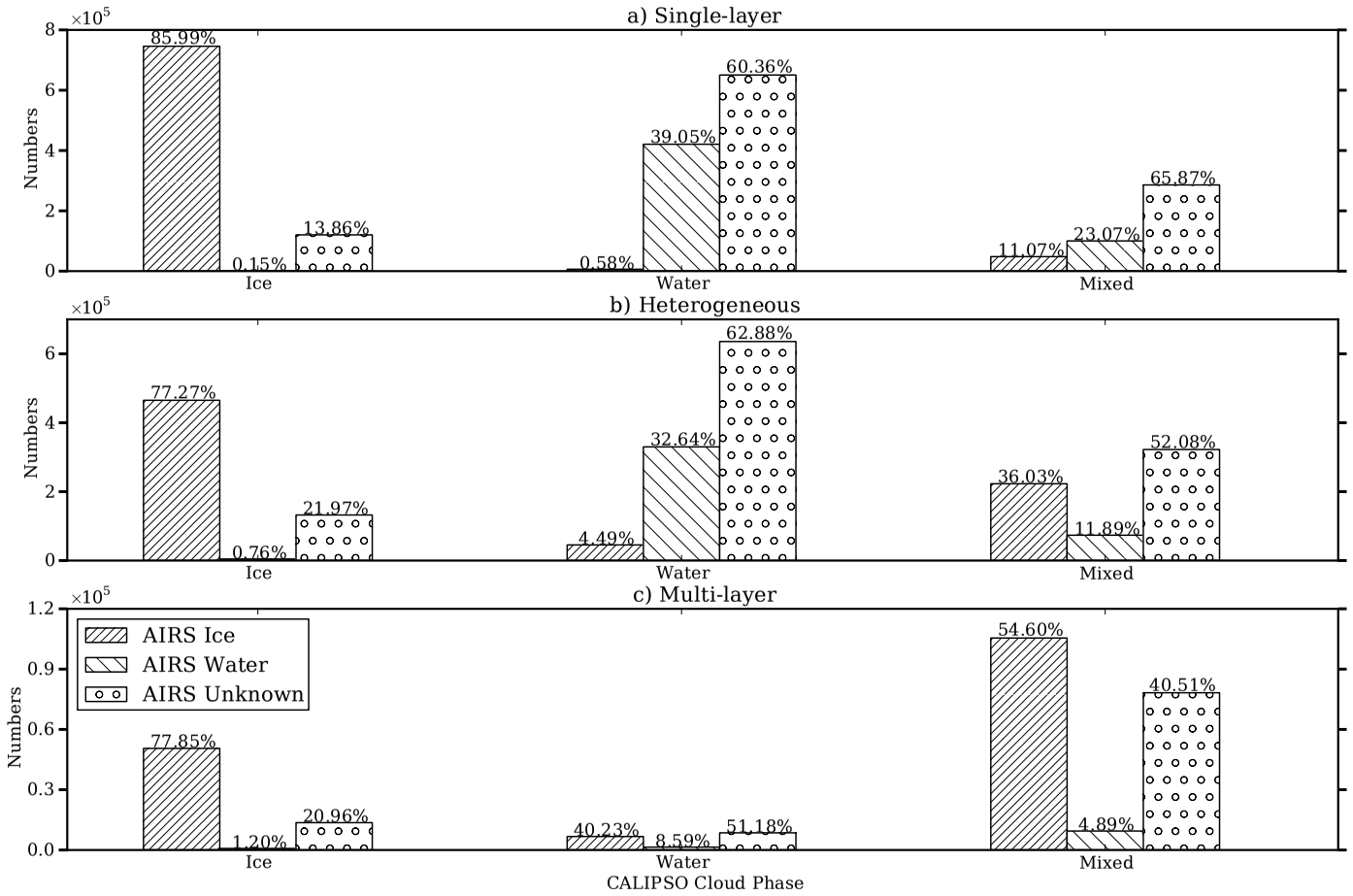

Figure 5.5 Similar to Figure 5.3, but CALIOP phases are on the horizontal axis, and the bars represent AIRS cloud phase.

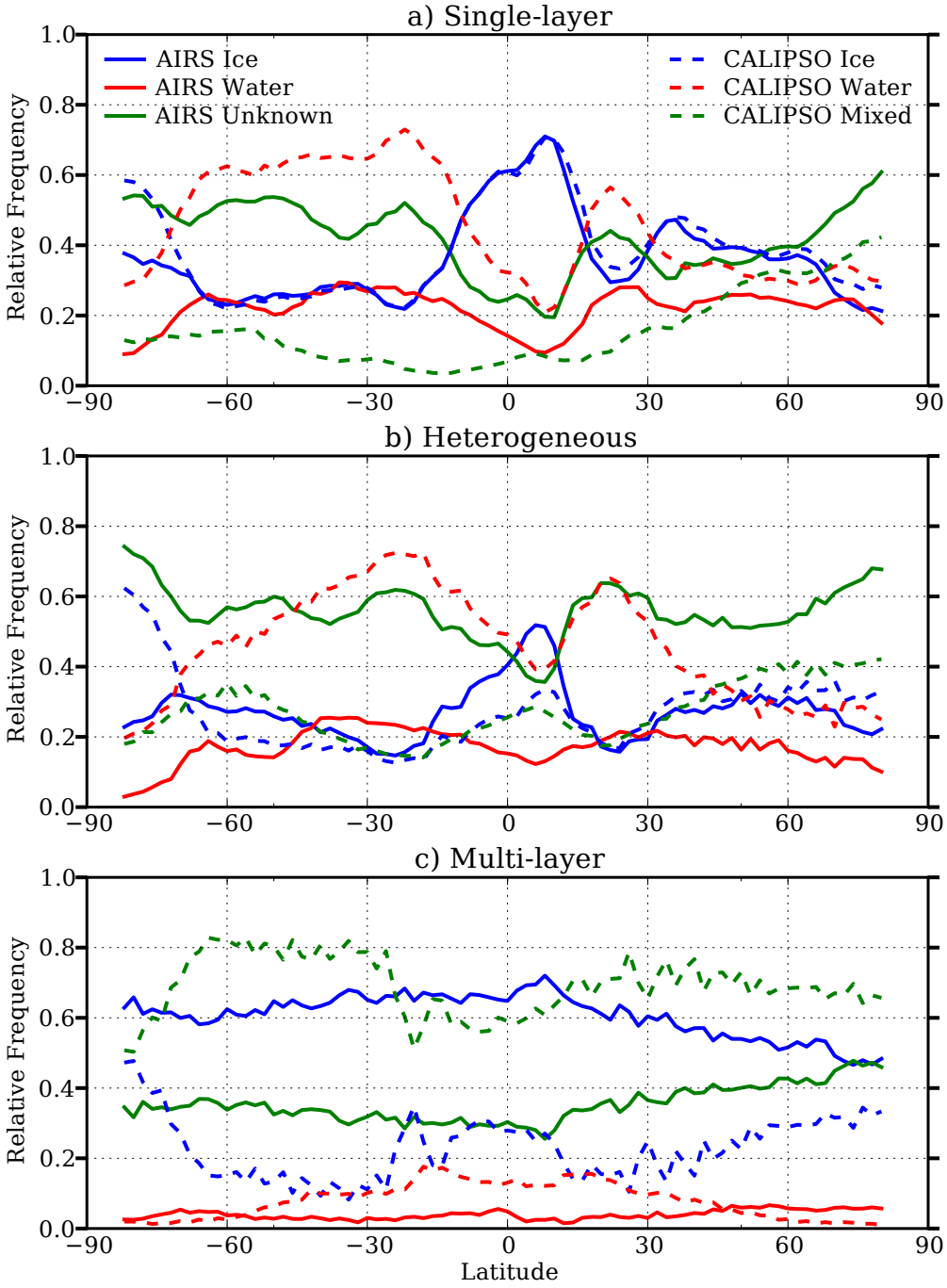

Figure 5.6 The relative zonal frequencies of AIRS (solid) and CALIOP (dashed) cloud phases. a) single-layer; b) heterogeneous; c) multi-layer.

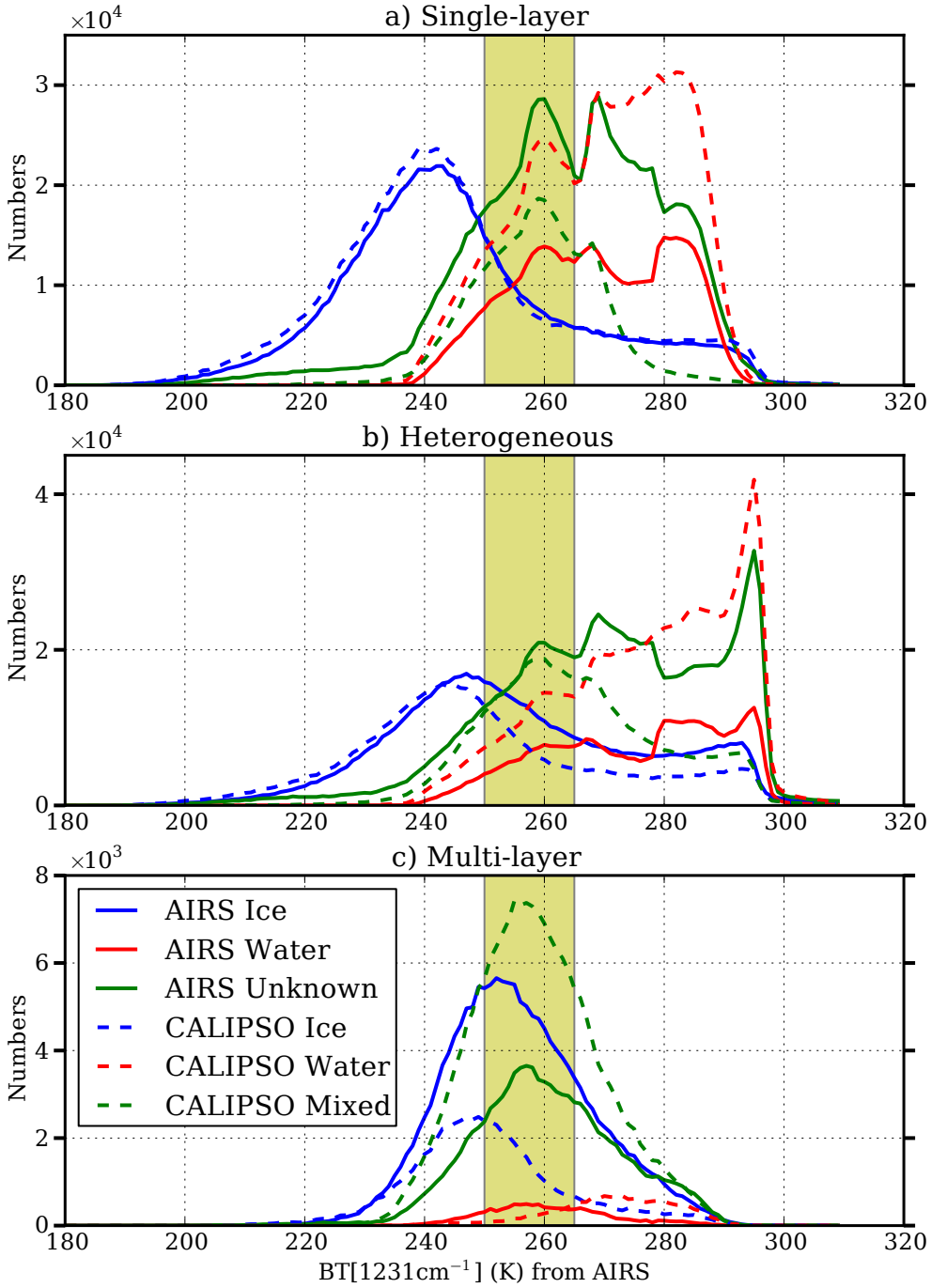

Figure 5.7 Distributions of AIRS (solid) and CALIOP (dashed) cloud phases as a function of BT at 1231 cm^{-1}. The yellow shaded area represents the BT between 250 and 265 K. a) single-layer; b) heterogeneous; c) multi-layer.

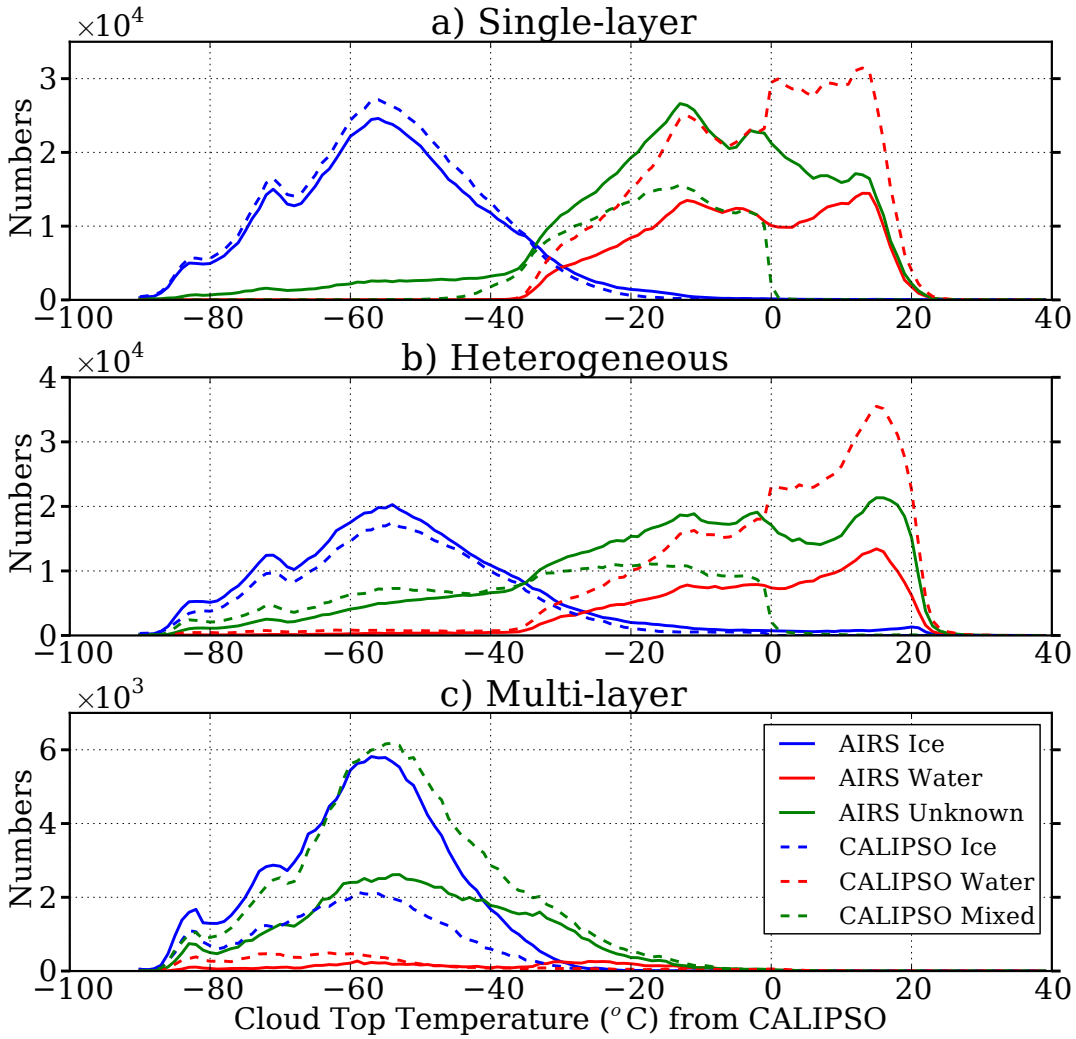

Figure 5.8 Similar to Figure 5.6, but as a function of cloud top temperature from CALIPSO.

5.3.1 Single-layer scene

First, we consider the scenes classified as single-layer clouds. As indicated in Table 5.2, AIRS and CALIPSO observe similar numbers of ice clouds, with AIRS lower than CALIPSO by about 3%. AIRS observes many fewer water clouds than CALIPSO, and approximately 50% of CALIPSO water cases fall into the AIRS unknown category. The phase sensitivity to liquid water is less than that to ice,

and this shows consistency with the radiative transfer model simulations in the last chapter.

The CALIPSO phase retrievals for each retrieved AIRS cloud phase are displayed in Fig. 5.4a. AIRS phase is shown on the x-axis, while the vertical bars represent the CALIPSO phases that fall within each category of AIRS phase. Of all the ice clouds detected by AIRS that are single-layered according to CALIPSO, CALIPSO classifies 93.18% as ice (either randomly or horizontally oriented ice crystals), 0.79% as water clouds, and 6% as mixed-phase clouds. Recall that our CALIPSO mixed-phase category is defined as an AIRS FOV containing CALIPSO retrievals of both ice and water. Therefore, when AIRS classifies pixels as ice clouds, up to 99% of single-layer cases are determined by CALIPSO as containing either some or all ice. For AIRS water, CALIPSO assigns a small portion (about 0.24%) as ice. Over 99% of the water clouds determined by AIRS contain either some or all water determined by CALIPSO. The false alarm rate for ice and water is negligible. However, the AIRS "unknown" category is a mixture of cloud types. CALIPSO categorizes about 10%, 60%, and 30% of all AIRS single-layer, unknown pixels as ice, water and mixed-phase, respectively.

Similar to Fig. 5.4a, the AIRS phase retrievals for each retrieved CALIPSO phase category are shown in Fig. 5.5a. AIRS identifies ice in 86% of all CALIPSO single-layer ice detections and a negligible number (0.15%) are called water. For CALIPSO water, only 0.58% are classified as ice by AIRS, and the remaining majority ($\sim$60%) are identified as unknown by AIRS. With regard to CALIPSO single-layer mixed-phase clouds, AIRS identifies approximately 65% of the pixels as unknown.

Fig. 5.6a shows the zonally averaged frequencies of AIRS and CALIPSO cloud phase for single-layer clouds. Ice clouds are the most frequent cloud type in the tropics according to both AIRS and CALIPSO, and the comparisons for all phase

categories are in the best agreement for low and mid-latitudes. CALIPSO reports slightly larger frequencies than AIRS from 10° N to 30° N where optically thin cirrus is prevalent. The largest ice cloud discrepancies are in the high latitudes of the southern hemisphere, likely due to the complexity of the polar atmosphere. In the ISCCP dataset, the polar cloud frequencies have the largest uncertainties (Rossow et al. 1993). The AIRS water frequencies generally track changes in the CALIPSO water zonal averages. Although the AIRS water frequency is on the order of a factor of two less than CALIPSO, this difference is somewhat higher (lower) in the SH (NH). Similarly, the AIRS unknown frequency is higher (lower) in the SH (NH).

Previous studies showed that the AIRS channel 1231cm^{-1} has good cloud phase sensitivity with minimum effects of absorption lines and channel noise (Nasiri and Kahn 2008; Kahn et al. 2011). Cloud top temperature is also closely related to the cloud phase. Figures 5.7a and 5.8a further break up the phase comparisons as a function of BT1231 and CTT. Good agreement between AIRS and CALIOP is found even in the difficult to characterize mid-temperature range (250-265K). Clearly, the AIRS IR algorithm is able to observe a preponderance of optically thin ice clouds ($BT_{1231} > 270K$), with similar frequencies of occurrence for CALIPSO. Slightly greater differences between AIRS and CALIPSO ice clouds are attributed to cold ice clouds in high latitudes. As shown before, AIRS classifies a much lower percentage of water clouds compared to CALIPSO, with bigger discrepancies in warm low-latitudes where AIRS is expected to be especially challenged due to the lack of thermal contrast in boundary layer clouds. These results show that when AIRS is not able to determine the correct phase, it tends to identify it as unknown, rather than misclassify it. This is entirely consistent with a lack of a strong spectral signature of thermodynamic phase.

5.3.2 Heterogeneous scenes

The spatial distributions of clouds within the AIRS FOV will contribute to the behavior of the cloud thermodynamic phase discrimination. Kahn et al. (2011) used AIRS and MODIS observations to show the impacts of subpixel cloud heterogeneity on IR thermodynamic phase assessment. They reported that the two-dimensional histograms of $BTD_{1231\text{-}960}$ and $BTD_{1231\text{-}1227}$, which are sensitive to cloud phase and column water vapor, show distinctly different signatures for homogeneous and heterogeneous clouds. Even though their study did not include AIRS and CALIPSO datasets, the results are probably transferable in these cases. AIRS and CALIPSO cloud phase for heterogeneous clouds are also shown in Table 5.2. The percentages listed for single-layer and heterogeneous scenes are comparable in the case of AIRS, although there is a slight reduction in liquid and ice, and a corresponding increase in unknown by 4.5%. The differences for CALIPSO for single-layer and heterogeneous cases are somewhat more striking. A large reduction in ice clouds is observed and an increase in mixed-phase clouds is observed compared to the single-layer clouds, with nearly zero change in water amount. This is unsurprising as more mixed-phase clouds are expected from CALIPSO in heterogeneous clouds compared to single-layered homogeneous clouds. However, the small changes in AIRS are dominated by water, and the larger changes in CALIPSO are dominated by ice.

The impacts of spatial heterogeneity on cloud phase are presented in the second panels in Figs. 5.4 through 5.8. The cloud layering and lack of spatial uniformity complicate the interpretation of heterogeneous scenes compared to single-layer cases. For instance, ice clouds observed by AIRS could be contaminated by mid- or low-level clouds that muddle the spectral signature of ice. In Fig. 5.4b, the frequency of pixels for which both AIRS and CALIPSO determine to be ice phase

decreases by about 30%. The detected CALIPSO mixed-phase increases from 6% in Fig. 5.4a to 31% in Fig. 5.4b. Since the CALIPSO mixed-phase clouds contain both ice and water, and the AIRS IR algorithm is most sensitive to ice, AIRS detects over 93% partial or total ice cloud by CALIPSO. For the remaining 6.15% of CALIPSO water pixels, this result may be consistent with the off-track presence of clouds within the AIRS FOV (Kahn et al., 2008). AIRS water and unknown categories similarly compare to CALIPSO as in the case of single-layer clouds. In Fig. 5.5b, 77.27% of the CALIPSO ice pixels are identified as AIRS ice, a decreases of 8.7% compared to single-layer scenes. It is advantageous that only 0.76% of CALIPSO ice is classified as AIRS water. Similar to Fig. 5.4a and Fig. 5.5a, the AIRS algorithm provides very few false alarms and generally classifies difficult to observe clouds as unknown phase, given a lack of a prominent spectral sensitivity to the cloud.

The zonal distributions for heterogeneous scenes in Fig. 5.6b show somewhat larger differences between AIRS and CALIPSO than in Fig. 5.6a for single-layer scenes. The dominant AIRS phase is unknown, and AIRS ice is about 5%$\sim$10% higher than water in the NH. These features highlight the difficulties of determining the phase of heterogeneous clouds (Kahn et al. 2011). AIRS ice detection peaks in the tropics and shows very good agreement with the sum of CALIPSO ice and mixed-phase at most low latitudes. For mid- and high-latitudes, a larger offset of AIRS ice is compensated by an increasingly larger portion of pixels falling into the unknown category. The BT and CTT peaks of ice clouds shift slightly in Fig. 5.7b and Fig. 5.8b when compared to single-layer cases. Furthermore, the mid-temperature between 250 and 265 K peaks in the unknown, water and mixed phase are greatly reduced in Figs. 5.7b and 5.8b, demonstrating that the heterogeneous clouds are more dominated by low-latitude, low altitude boundary layer clouds as described in Kahn et al. (2011). AIRS unknown is the most frequent phase across the entire

temperature range. The AIRS algorithm is capable of finding heterogeneous ice in the mid-temperature range and also optically thin ice, but the magnitude is lower compared to single-layered cloud due to the increased occurrence of unknown phase.

5.3.3 Multi-layer scenes

The assessment of cloud phase for multi-layer scenes is also very challenging. Most of the cloud phase signal originates from the top layer of a given multi-layer cloud regime. We use the CALIPSO cloud phase for the uppermost layer in this section. The statistics for multi-layer clouds are also shown in Table 5.1 and Table 5.2. The fraction of these clouds is similar to the single-layer in the three latitudinal regions with a significant reduction of over 85% of the total amount. AIRS observes more ice phase compared with single-layer and heterogeneous cases, increasing by over 25%. However, CALIPSO identifies that only 24% of the total amount of ice over water cloud systems is pure ice, which is much lower than AIRS. On the other hand, AIRS and CALIPSO classify a similar amount of water clouds, 4% and 6%, respectively.

The comparisons of CALIOP and AIRS phase retrievals for multi-layer clouds are presented in the third panels in Figs 5.4 through 5.8. The fraction of the pixels for which both AIRS and CALIPSO classify as ice is 31% in Fig 5.4c, decreasing by approximately 30% compared to heterogeneous scenes. The corresponding CALIPSO mixed-phase reaches as high as 65% of the total AIRS ice category. Again, AIRS is able to detect over 95% of the CALIPSO-detected ice phase. Compared to single-layer and heterogeneous clouds, AIRS observes relatively fewer water pixels than ice and unknown in the multi-layer cloud systems. A significant increase of CALIPSO mixed-phase is shown in the AIRS unknown category, implying the increase of complexity of clouds. When a low water cloud resides underneath optically thin cirrus or

within the AIRS FOV to the side of a cirrus cloud, the cloud will exhibit signatures more consistent with a mixed-phase cloud. In Fig 5.5c, AIRS determines a comparable amount of pure ice in the CALIPSO ice phase in comparison with heterogeneous scenes. About 55% of CALIPSO mixed-phase is classified as ice phase by AIRS. The percentage is 44% and 19% higher than single-layer and heterogeneous clouds.

The zonal frequencies in Fig. 5.6c show more differences between AIRS and CALIPSO than Figs. 5.6a and 5.6b. Overall, CALIPSO phases have larger variations than AIRS. Of all the cloud phases, CALIPSO mixed-phase and AIRS ice are the most frequent phases in all latitudes. The magnitude of frequency of CALIPSO ice is much lower than AIRS ice, due to a significant amount of these pixels being classified as CALIPSO mixed-phase. Both AIRS water and CALIPSO water show less than 20% of frequency of occurrence with CALIPSO higher than AIRS in the tropical regions.

A unique feature of the BT and CTT distributions of AIRS and CALIPSO cloud phases for multi-layer scenes is the "single mode" compared to single-layer and heterogeneous clouds in Figs 5.7c and 5.8c. More overlaps of AIRS and CALIPSO phases are found, implying the difficulties in cloud phase assessment when cloud systems become more complicated. The main peaks overlapping with the shaded mid-temperature in Fig. 5.7c results in a large amount of AIRS unknown and CALIPSO mixed-phase. In Fig 5.8c, the CTT for multi-layer clouds are shown less than about -15°C, with a majority of these pixels below -35°C. AIRS ice has a similar pattern as CALIPSO mixed-phase with lower magnitude between about -50°C and -20°C. Even though CALIPSO determines a significant amount of mixed-phase due to the contamination from the low water clouds, the low temperature indicates that ice occupies a tremendous portion of CALIPSO mixed-phase. AIRS determines a notable amount of pixels as water with temperatures as low as -30°C.

5.3.4 All cloudy scenes

The joint histograms of cloud top height and temperature for AIRS and CALIPSO cloud phase are presented in Figure 5.9. The frequency here refers to the ratio between the number of individual cloud phase to the total number of cloud phases in each bin. It important to note that the CALIPSO phase algorithm also includes cloud temperature as a second order input (Hu et al. 2009).

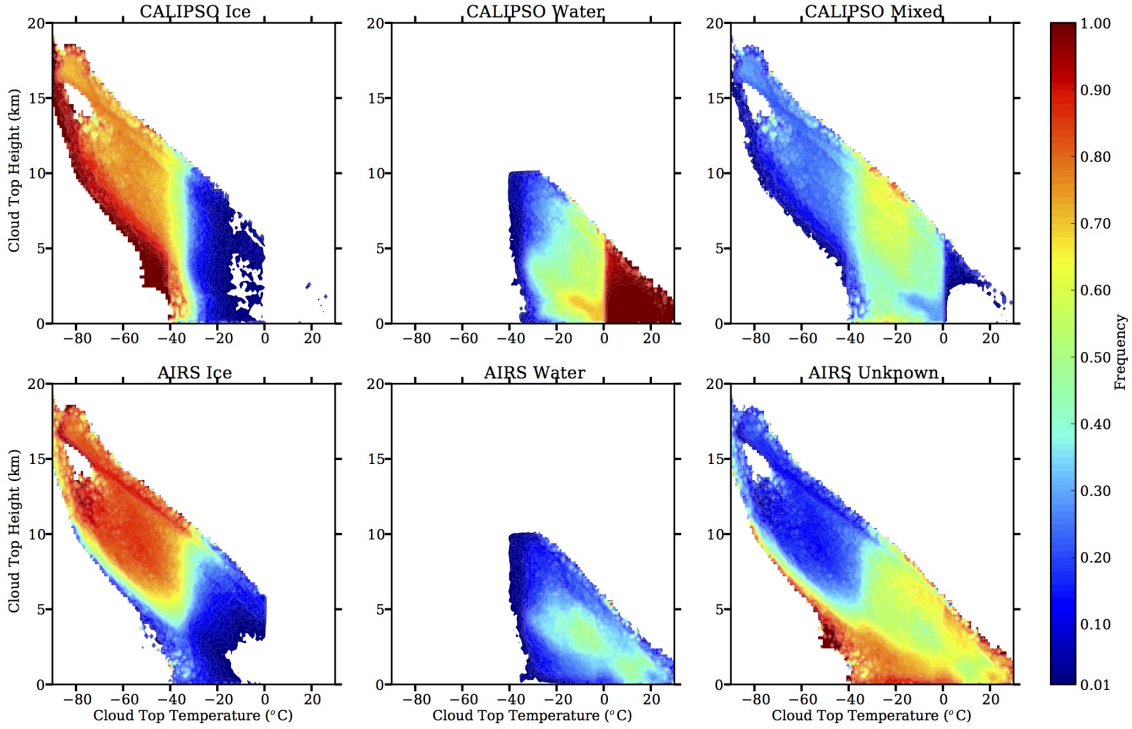

Figure 5.9 Joint histograms of AIRS and CALIPSO cloud phase frequencies as a function of cloud top height and cloud top temperature from CALIPSO.

The CALIPSO ice has similar frequencies with AIRS ice except below 5 km. These differences essentially exist in high-latitudes (not shown). Also, Shupe et al. (2011) found that at heights up to 11 km, cloud ice can occur 60%-70% of the time of a given year in the Arctic region. A large number of ice clouds occur at temperature below about -30°C and above 5 km in tropics and mid-latitudes (not shown). It is

clear that only a small fraction (< 1%) of the observed cloudiness is solely ice phase within the cloud top temperature range from -30°C to 0°C. Due to less sensitivity to liquid water, the frequency of AIRS water decreases dramatically compared to CALIPSO water with significant amounts falling into the AIRS unknown category.

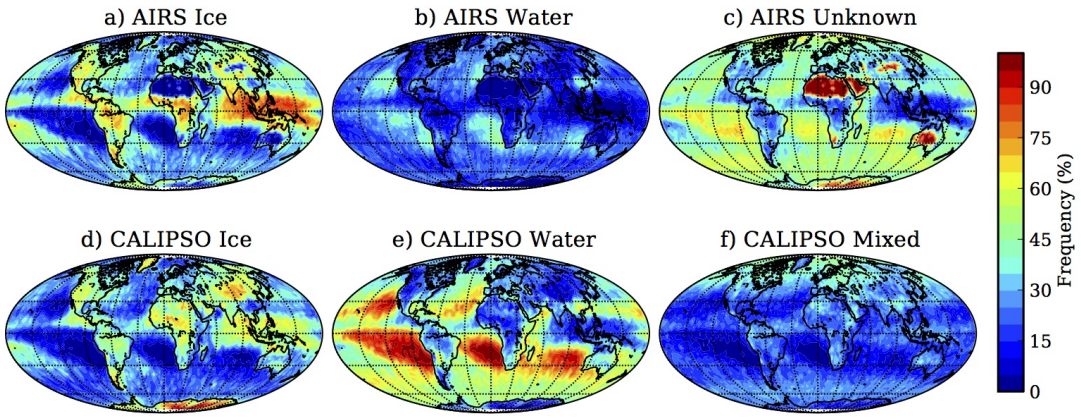

Figure 5.10 Global distributions of AIRS and CALIOP phases. a)-c): AIRS phase; d)-e): CALIOP phase. The frequency calculation is the same as Figure 5.2, but the size of grid box is 2.5°x2.5°. The frequency is not the real "frequency"; rather, it represents the fraction of each cloud phase within one grid box.

Global frequency maps of the AIRS and CALIOP phase retrievals are shown in Fig. 5.10. For the ice phase, AIRS and CALIOP show similar patterns, capturing ice clouds in the tropical region (particularly the Tropical Western Pacific) and storm tracks. AIRS shows a slightly higher frequency of ice than CALIOP due to the mixed-phase category. The major discrepancies are in high-latitudes. AIRS water generally follows the pattern of CALIOP water, however, the magnitude decreases by a factor of two. From Figs. 5.4 and 5.5, we know that approximately 10% and 60% of ice and water clouds are categorized as unknown phase. In Fig 5.10c, the high frequency in the Arctic region indicates potential mixed-phase or ice clouds, and over the oceans in the southern hemisphere, it shows potential stratocumulus cloud regimes.

5.4 Thermodynamic phase of mid-level clouds

AIRS and CALIPSO cloud phase frequencies for each of the ISCCP cloud levels are shown in Figure 5.11. The top panel shows the total of all of total cloudy scenes (single-layer+heterogeneous+multi-layer) for each of the three levels. At high-level, ice clouds are the major components, whereas only a small amount of AIRS water and CALIPSO water exists for about 5% and 2%. It is notable that AIRS unknown and CALIPSO mixed-phase occur about 20% and 27% of the time in the high-level. The current ISCCP climatology treats all high-level clouds above 440 hPa as ice (Rossow and Schiffer 1999). The fraction of non-ice phase suggests that the ISCCP threshold (440 hPa) to distinguish high- and mid-level clouds might need to be slightly adjusted. At the mid-level, ice, water, and mixed-phase clouds are approximately 20%, 40%, and 40%, respectively. The mixed-phase fraction is much lower than Zhang et al. (2010) found, when using CALIPSO and CloudSat to investigate mid-level liquid-layer topped stratiform clouds. They reported global mean mixed-phase to be about 61.8% within the mid-level liquid-layer topped stratiform clouds. Zhang et al. (2010) also found that approximately 12.4% of the mid-level liquid-layer topped stratiform clouds were super-cooled. The differences between our study and Zhang et al. (2010) are likely due to the different definitions used for mid-level clouds. Liquid water cloud is the most common cloud phase at low level, whereas both AIRS and CALIOP show infrequent pure ice phase (less than 2%). We also look at the cloud phase with height distribution for our single-layer, heterogeneous, and multi-layer categories. For the mid level, both ice and water phases decrease from Figs. 5.11b to 5.11d with obvious increases in the CALIPSO mixed-phase and AIRS unknown, which can lead to more uncertainties in the cloud property retrievals and cloud radiative effects.

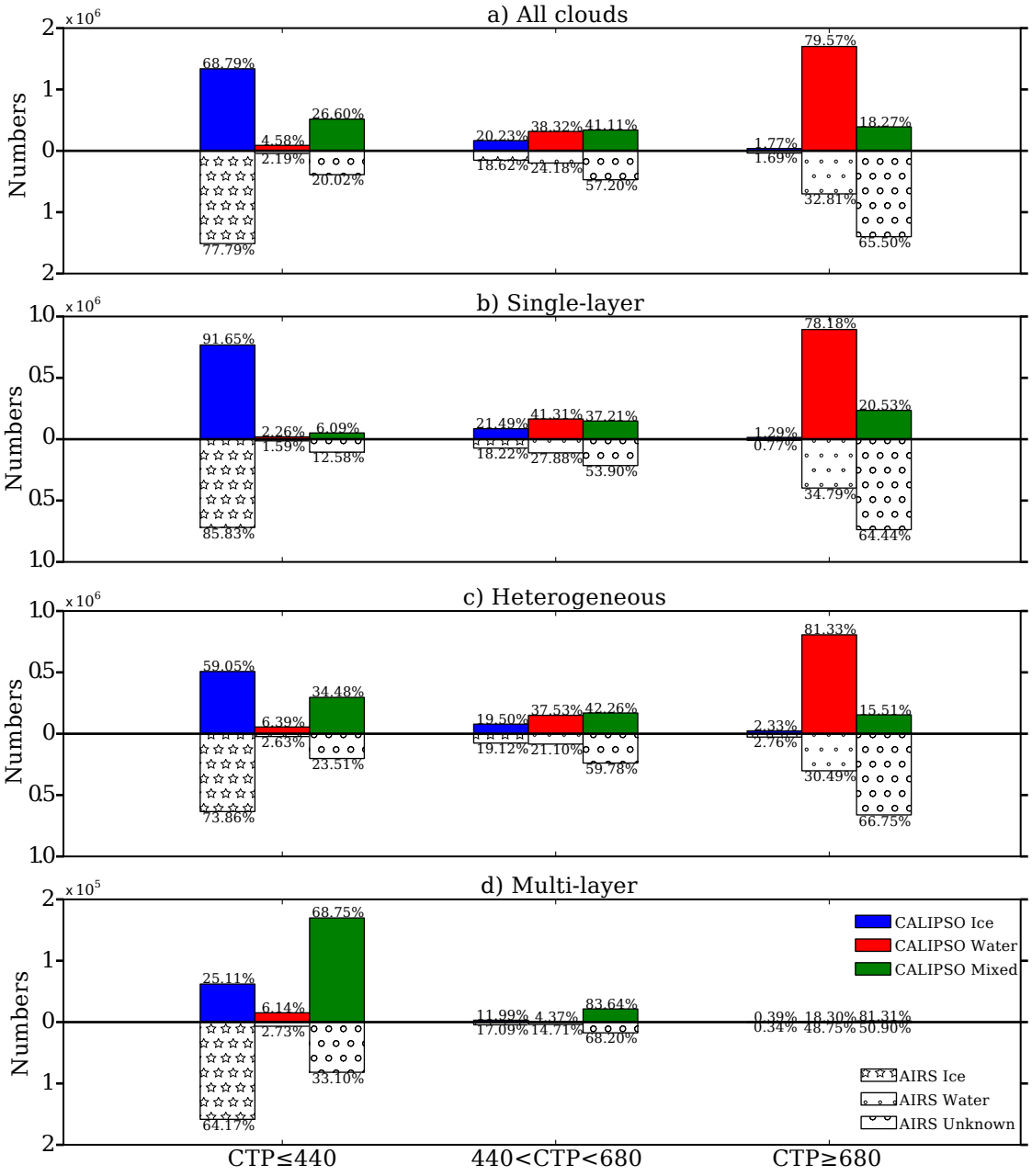

Figure 5.11 CALIPSO and AIRS cloud phase for clouds at different levels defined by the ISCCP definition.

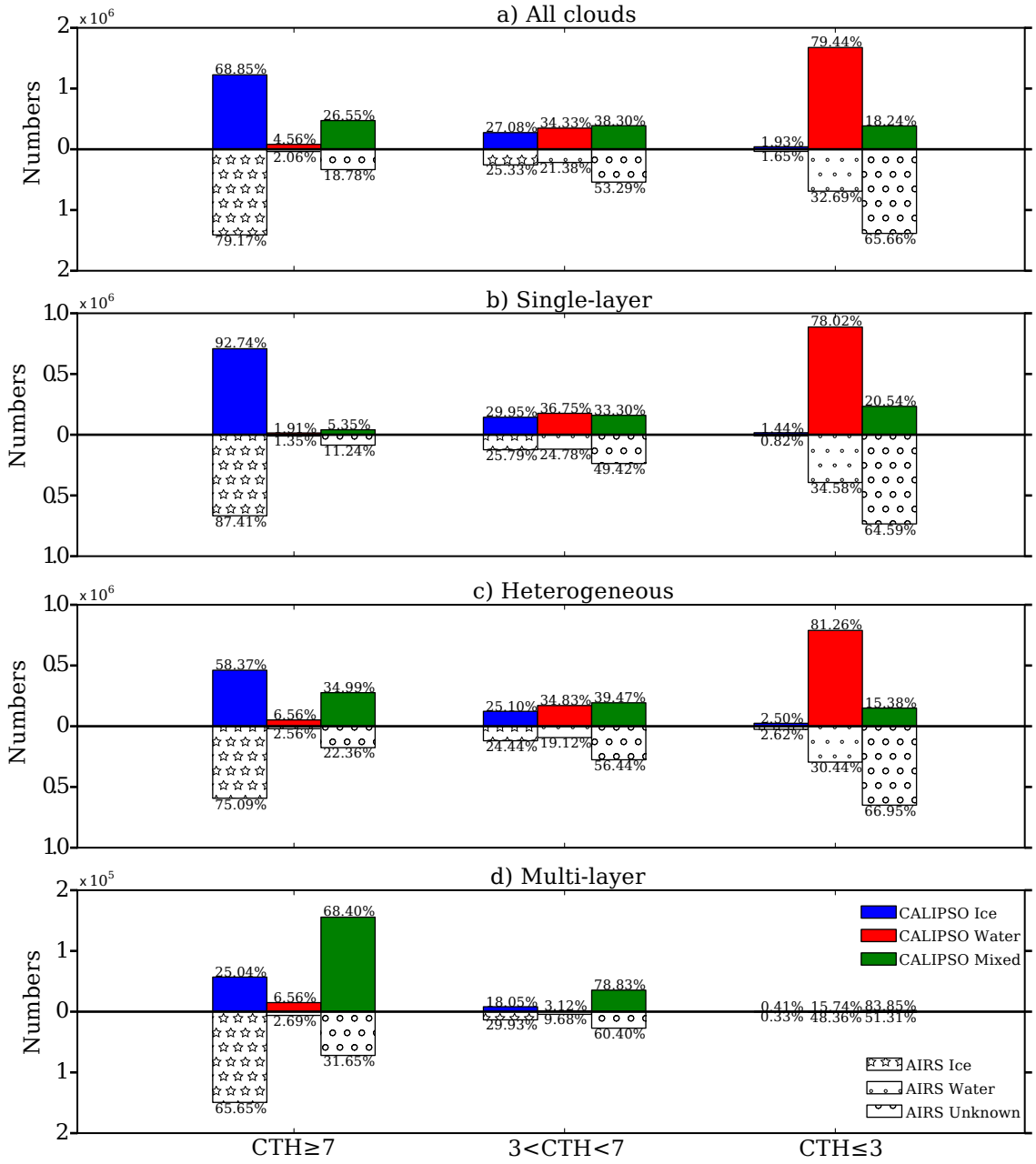

Figure 5.12 CALIPSO and AIRS cloud phase for clouds at different levels defined by the cloud-top definition.

The AIRS and CALIPSO cloud phase frequencies for high-, mid-, and low-level using the cloud-top height definition are shown in Figure 5.12. For the total cloud category, the phase distributions for high-level and low-level clouds are similar

to those see with the ISCCP cloud-top pressure definition in Figure 5.11. With respect to the mid-level, ice, water, and mixed-phase clouds account roughly for 27%, 34%, and 38%, respectively. The fraction of ice for both AIRS and CALIPSO increases by about 7%, while the fraction of liquid water phase decreases by roughly 4%. Regarding each investigation in the single-layer, homogeneous, and multi-layer cases, the ice and water phases also decrease from Figs 5.12b to 5.12d and have higher fractions than seen in Figs 5.11b-5.11d.

In Figure 5.11d and Figure 5.12d, only the topmost layer within the multi-layer cloud scenes are used. When the bottom layers are included, the number of mid-level clouds will increase significantly (Figure 3.1). In Figure 5.13, the independent dataset of CALIPSO 5-km cloud phase product for the same time period (December 2007-November 2008) is used to show information similar to that in Figs. 5.11d and 5.12d for multi-layer cloud scenes. The upper colored bars in each panel are for the top layer within the multi-layer clouds, and the lower bars with filled shapes are for the bottom layer. It is clear that the bottom layer contains a large amount of mid-level clouds, which also supports the statement that we have to include multi-layer clouds in the analysis of mid-level clouds. The fractions of ice and water increase significantly compared to Figures 5.11d and 5.12d.

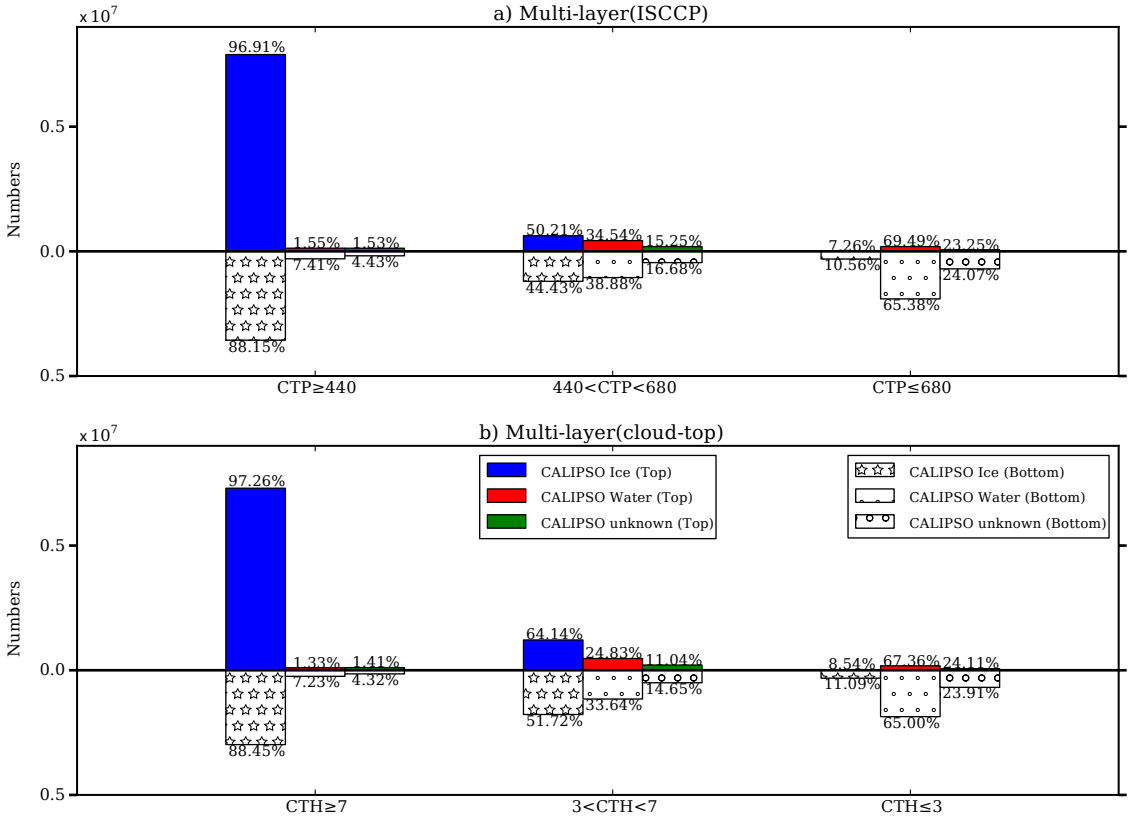

Figure 5.13 CALIPSO 5-km cloud phase (December 2007-Novermber 2008) for multi-layer clouds at different levels. a) uses the ISCCP cloud top pressure definition, and b) uses the cloud-top height definition. Upper colored bars: top layer; lower bars: bottom layer.

Table 5.3 Numbers of CALIPSO ice and AIRS ice phase in the adjusted thresholds of the ISCCP definition of mid-level clouds. The percentage shows the variation from values between 680 and 440 hPa.

	CALIPSO Ice				AIRS Ice			
CTP(hPa)	Global	Tropical (30°S-30°N)	Mid-latitude (30-60°S, 30-60°N)	High-latitude (60-90°S, 60-90°N)	Global	Tropical (30°S-30°N)	Mid-latitude (30-60°S, 30-60°N)	High-latitude (60-90°S, 60-90°N)
420−660	17.5%	22.5%	26.8%	15.0%	21.0%	9.4%	25.3%	20.9%
420−680	20.2%	24.2%	28.8%	18.0%	23.4%	15.0%	27.2%	22.8%
420−700	22.6%	25.7%	30.4%	20.6%	25.5%	20.9%	28.8%	24.5%
440−660	-2.7%	-1.7%	-2.0%	-2.9%	-2.3%	-5.6%	-1.9%	-1.9%
440−680	166,651	945	34,329	131,377	153,428	16,133	47,450	89,845
440−700	2.4%	1.5%	1.7%	2.6%	2.1%	5.9%	1.6%	1.7%
460−660	-20.3%	-13.8%	-25.1%	-19.1%	-22.4%	-19.1%	-24.7%	-21.8%
460−680	-17.6%	-12.1%	-23.1%	-16.2%	-20.1%	-13.5%	-29.1%	-18.7%
460−700	-15.2%	-10.6%	-21.6%	-1.0%	-18.0%	-7.6%	-21.1%	-18.2%

	CALIPSO Ice				AIRS Ice			
CTP(hPa)	Global	Tropical (30°S-30°N)	Mid-latitude (30-60°S, 30-60°N)	High-latitude (60-90°S, 60-90°N)	Global	Tropical (30°S-30°N)	Mid-latitude (30-60°S, 30-60°N)	High-latitude (60-90°S, 60-90°N)
420−660	195,818	1,158	43,520	151,140	185,701	17,645	59,436	108,620
420−680	200,366	1,174	44,201	154,991	189,257	18,555	60,352	110,350
420−700	204,344	1,188	44,778	158,378	192,500	19,511	61,124	111,865
440−660	162,103	929	33,648	127,526	149,872	15,223	46,534	88,115
440−680	166,651	945	34,329	131,377	153,428	16,133	47,450	89,845
440−700	170,629	959	34,906	134,764	156,671	17,089	48,222	91,360
460−660	132,765	815	25,711	106,239	119,063	13,046	35,734	70,283
460−680	137,313	831	26,392	110,090	122,619	13,956	36,650	72,013
460−700	141,291	845	26,926	113,477	125,862	14,912	37,422	73,528

Spatial distributions and frequencies of cloud phase can significantly impact the Earth's radiation budget (Ackerman et al. 1988, Hartmann et al. 1992; Yang et al. 2003; McFarquhar and Cober 2004). Tables 5.3 to 5.5 show the fractional cloud phase statistics of mid-level clouds for different latitudinal bands (tropics: 30° N−30° S; mid-latitude: 30°−60°N(S); high-latitude: 60°−90° N(S)) using AIRS and CALIPSO. In Table 5.3, the statistics clearly show that, if we keep the upper boundary (440 hPa), the numbers of ice phase change slightly by 2-5% globally of the mid-level ice clouds classified by the ISCCP definition of mid-level. Moreover, if we fix the bottom boundary (680 hPa), the numbers of mid-level ice change greatly by 10-30% globally with respect to the values between 680 and 440 hPa. Conversely, if the bottom boundary is fixed, the water clouds vary by 3-7% of the mid-level water between 680 and 440 hPa, whereas the variations are approximately 10-14% if the upper 440 hPa is kept. Correspondingly, the CALIPSO mixed-phase and AIRS unknown within the mid-level clouds changes approximately 2-15% globally. While not shown, the CALIPSO mixed-phase has the highest values (∼48%) in the mid-latitudes and lowest values (∼34%) in the tropics. Mid-level CALIPSO ice is approximately 1%, 13%, and 30% and mid-level CALIPSO water accounts for about 65%, 40%, 30% from tropics to polar regions. The results are somewhat different from the previous studies due to different focuses. Zhang et al. (2010) found that the mixed-phase fraction of mid-level cloud is about 35%-75% between the temperatures of -7°C and -16°C in the tropics. Choi et al. (2010) report that the clouds that contain liquid water ranges from 25% to 75% at -20°C throughout the tropics. While focusing on clouds in the Arctic regions, Shupe (2011) found that ice clouds occur 60%-70% and liquid water clouds occur 30%-60% of the time of a typical year.

Table 5.4 Similar to Table 5.3, but for CALIPSO water and AIRS water phase.

CTP(hPa)	CALIPSO Water				AIRS Water			
	Global	Tropical (30°S-30°N)	Mid-latitude (30-60°S, 30-60°N)	High-latitude (60-90°S, 60-90°N)	Global	Tropical (30°S-30°N)	Mid-latitude (30-60°S, 30-60°N)	High-latitude (60-90°S, 60-90°N)
420−660	-9.1%	-5.0%	-7.5%	-13.3%	-8.4%	-3.0%	-7.0%	-11.2%
420−680	3.7%	6.6%	4.4%	1.1%	3.3%	7.4%	4.1%	1.4%
420−700	17.8%	20.0%	17.4%	16.5%	15.6%	19.3%	15.7%	14.4%
440−660	-12.8%	-11.6%	-11.8%	-14.4%	-11.7%	-10.4%	-11.2%	-12.6%
440−680	315,766	85,597	106,423	123,746	199,239	31,316	73,552	94,371
440−700	14.1%	13.5%	13.0%	15.4%	12.3%	12.0%	11.6%	13.0%
460−660	-17.1%	-18.8%	-16.9%	-16.1%	-15.7%	-18.0%	-15.9%	-14.8%
460−680	-4.3%	-7.2%	-5.0%	-1.7%	-4.0%	-7.6%	-4.7%	-2.2%
460−700	9.7%	6.2%	8.0%	13.7%	8.4%	4.4%	6.9%	10.8%

CTP(hPa)	CALIPSO Water				AIRS Water			
	Global	Tropical (30°S-30°N)	Mid-latitude (30-60°S, 30-60°N)	High-latitude (60-90°S, 60-90°N)	Global	Tropical (30°S-30°N)	Mid-latitude (30-60°S, 30-60°N)	High-latitude (60-90°S, 60-90°N)
420−660	287,126	81,314	98,488	107,324	182,531	30,361	68,370	83,800
420−680	327,397	91,227	111,072	125,098	205,865	33,623	76,595	95,647
420−700	371,822	102,745	124,942	144,135	230,409	37,375	85,107	107,927
440−660	275,495	75,684	93,839	105,972	175,905	28,054	65,327	82,524
440−680	315,766	85,597	106,423	123,746	199,239	31,316	73,552	94,371
440−700	360,191	97,115	120,293	142,783	223,783	35,068	82,064	106,651
460−660	261,840	69,500	88,469	103,871	168,007	25,688	61,886	80,433
460−680	302,111	79,413	101,053	121,645	191,341	28,950	70,111	92,280
460−700	346,536	90,931	114,923	140,682	215,885	32,702	78,623	104,560

Table 5.5 Similar to Table 5.3, but for CALIPSO mixed-phase and AIRS unknown.

CTP(hPa)	CALIPSO Mixed-Phase				AIRS Unknown			
	Global	Tropical (30°S-30°N)	Mid-latitude (30-60°S, 30-60°N)	High-latitude (60-90°S, 60-90°N)	Global	Tropical (30°S-30°N)	Mid-latitude (30-60°S, 30-60°N)	High-latitude (60-90°S, 60-90°N)
420−660	1.0%	12.7%	2.0%	-3.0%	-2.5%	1.3%	-1.9%	-4.2%
420−680	8.8%	14.8%	9.8%	6.4%	7.0%	9.2%	7.5%	5.8%
420−700	16.6%	16.6%	17.6%	15.8%	17.0%	18.3%	17.8%	16.1%
440−660	-7.8%	-2.1%	-7.7%	-9.4%	-9.5%	-8.0%	-9.4%	-10.0%
440−680	338,687	44,162	132,422	162,103	471,261	84,118	153,016	234,127
440−700	7.8%	1.8%	7.9%	9.4%	10.0%	9.0%	10.3%	10.3%
460−660	-16.8%	-16.4%	-17.4%	-16.4%	-16.8%	-17.6%	-17.2%	-16.3%
460−680	-9.0%	-14.3%	-9.6%	-6.9%	-7.4%	-9.7%	-7.8%	-6.3%
460−700	-1.1%	-12.6%	-1.8%	2.5%	2.7%	-0.6%	2.5%	4.0%

CTP(hPa)	CALIPSO Mixed-Phase				AIRS Unknown			
	Global	Tropical (30°S-30°N)	Mid-latitude (30-60°S, 30-60°N)	High-latitude (60-90°S, 60-90°N)	Global	Tropical (30°S-30°N)	Mid-latitude (30-60°S, 30-60°N)	High-latitude (60-90°S, 60-90°N)
420−660	342,115	49,784	135,121	157,210	459,550	85,178	150,138	224,234
420−680	368,550	50,709	145,342	172,499	504,158	91,866	164,559	247,733
420−700	394,994	51,484	155,782	187,728	551,472	99,470	180,249	271,753
440−660	312,252	43,237	122,201	146,814	426,653	77,430	138,595	210,628
440−680	338,687	44,162	132,422	162,103	471,261	84,118	153,016	234,127
440−700	365,131	44,937	142,862	177,332	518,575	91,722	168,706	258,147
460−660	281,916	36,901	109,438	135,577	391,894	69,283	126,714	195,897
460−680	308,351	37,826	119,659	150,866	436,502	75,971	141,135	219,396
460−700	334,795	38,601	130,099	166,095	483,816	83,575	156,825	243,416

The global distributions of frequencies of AIRS and CALIPSO mid-level cloud phases are shown using the ISCCP and cloud-top definitions in Figures 5.14 and 5.15, respectively. The two figures have very similar distributional patterns with slight difference in magnitudes. The CALIPSO mid-level water clouds are mainly distributed in the low latitudes and over oceans in the Southern Hemisphere, and the CALIPSO mid-level mixed-phase clouds have high frequencies in mid- and high-latitudes in Northern Hemisphere. The mid-level ice clouds from CALIPSO have low frequencies in the tropics because a large amount are classified as the mixed-phase, and are found mainly in polar regions and in the Northern Hemisphere. Kanitz et al. (2011) using lidar observations also found high frequencies of ice in the NH. Approximately 60% of AIRS mid-level clouds are unknown phase (Tables 5.4 and 5.5) because AIRS has less sensitivity to lower clouds than to high-level clouds. The AIRS mid-level ice follows the distributional pattern in Figure 5.9a but is decreased in magnitude. The AIRS mid-level water shows relatively higher frequencies over the lands than oceans, which is different from the overall AIRS water classification in Figure 5.9b.

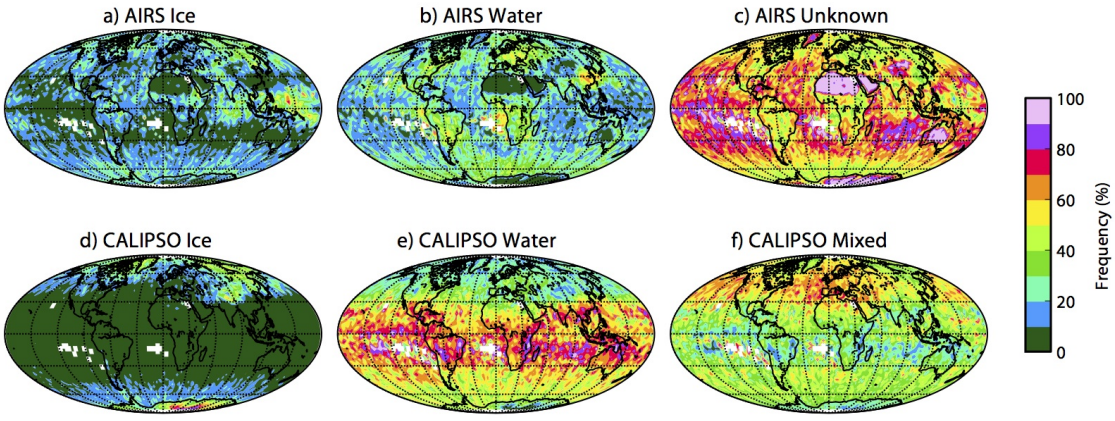

Figure 5.14 CALIPSO and AIRS cloud phase fractional frequencies for mid-level clouds defined by the ISCCP definition.

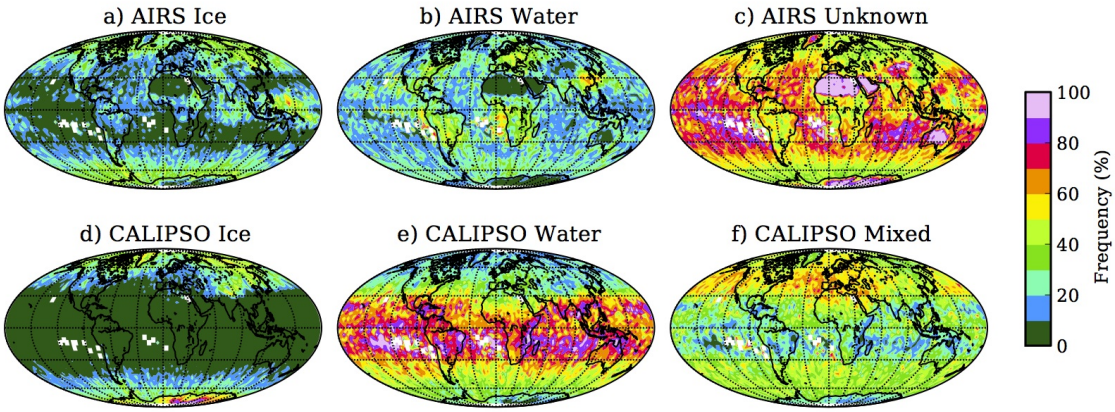

Figure 5.15 CALIPSO and AIRS cloud phase fractional frequencies for mid-level clouds defined by the cloud-top definition.

Cloud top temperature is also closely related to the cloud thermodynamic phase. Theoretical and laboratory studies find that the phase transition from liquid to ice occurs between 0°C and -40°C (Rogers and Yau 1989; Pruppacher and Klett 1997). The liquid cloud fraction decreases with decreasing cloud temperature and becomes negligible below -40°C due to homogeneous ice nucleation. Figure 5.16 shows the histograms for CALIPSO and AIRS cloud phases as a function of cloud top temperature for high-, mid-, and low-level clouds defined by the ISCCP definition. It is important to note that in the high-level, CALIPSO mixed-phase clouds are found below -40°C. This feature does not indicate that supercooled liquid water can still exist in very low temperature range. These CALIPSO mixed-phase clouds are mainly contributed by the heterogeneous and multi-layer scenes, which means high-level ice phase and low-level water are found simultaneously within AIRS footprint and considered as mixed-phase clouds.

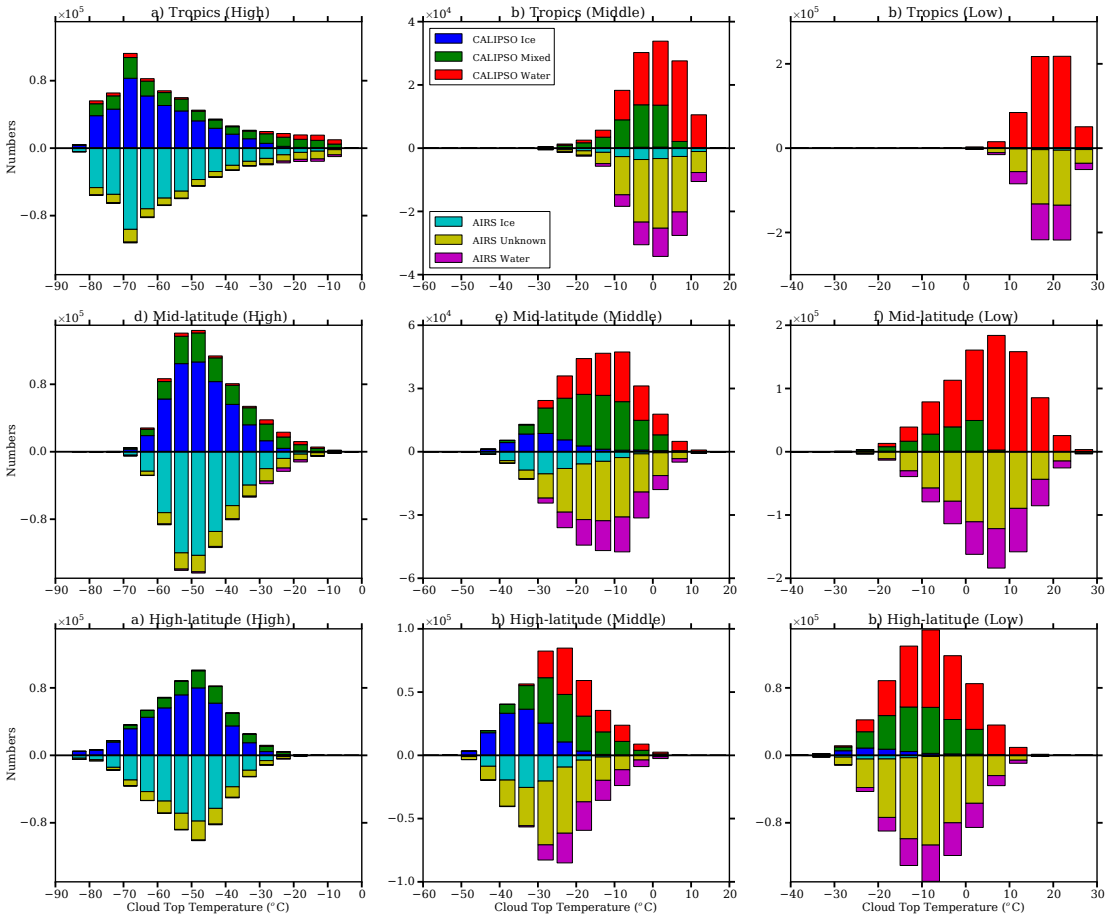

Figure 5.16 Histograms of CALIPSO and AIRS cloud phase as a function of cloud top temperature for mid-level clouds defined by the ISCCP definition.

Riihimaki et al. (2012) found that mid-level thin clouds have a high probability of containing supercooled liquid water at low temperatures at the ARM TWP site at Darwin in Australia. Using ground-based remote sensing measurements, they found that ∼20% of clouds at -30°C, ∼50% of clouds at -20°C, and ∼65% of clouds at -10°C contain supercooled liquid water. Their results are higher than our results in Figure 5.16b. Three possible reasons may cause the difference. First, we include both thin and thick mid-level clouds while they only consider thin clouds (less than 2 km thick with cloud tops between 0°C and -40°C). Second, the difference may be due to geographical variation. We select mid-level clouds in the tropics between 30°

N and 30° S while Riihimaki et al. (2012) focused on the ARM program TWP Darwin site in Australia. Ansmann et al. (2009), on the other hand, found that nearly all altocumulus clouds contain liquid water at all temperatures at the ARM TWP Darwin site. Third, we focused on the space-borne measurements while Riihimaki et al. (2012) used surface remote sensing.

In chapter 3, we demonstrated the cloud top temperature difference between mid-level and low-level clouds and between high-level and mid-level clouds. There are no distinct features between the middle clouds and low clouds, while the difference between high clouds and mid-level clouds show strong zonal signatures. We raised the issue of whether the cloud thermodynamic phase has impacts on the cloud top temperature difference between different levels. In Figure 5.16, it is clear that the mid-level clouds have different fractions of ice, liquid water, and mixed-phase clouds, and the cloud top temperatures also become colder when moving towards polar regions. The high-level clouds mainly consist of ice and mixed-phase with a peak around -70°C in the tropic. The high clouds and mid-level cloud top temperature distributions overlap more between -40°C and -10°C in mid- and high-latitudes than in the tropics.

6. SUMMARY AND FUTURE WORK

6.1 Summary

Mid-level clouds are an important component of the climate system, although the precise role of how they interact with solar and terrestrial radiation is still uncertain. Two major issues limit the understanding of mid-level clouds in climate studies. First, much of the uncertainty lies in the fact that mid-level clouds are rather poorly characterized. There is not even a standard definition of what constitutes the mid-level. Working definitions or classifications of mid-level clouds vary with observational technique, region, and purpose, which make the characterization of mid-level clouds challenging. Moreover, while multi-layer clouds are frequently observed globally, the impacts of overlapping clouds on satellite-based global statistics for clouds at different levels, in particular mid-level, are not yet fully understood.

Second, the thermodynamic phase of mid-level clouds is difficult to determine because the clouds have the potential for complex microphysics. This, in turn, can complicate the retrievals of cloud properties and the development of model parameterizations. Accurate estimates of cloud phase of mid-level clouds can improve our current understanding of mid-level cloud radiative effects and cloud feedbacks. Satellite remote sensing of cloud properties such as characteristics and thermodynamic phase has the potential for improving the representation of mid-level clouds in climate models as well as for monitoring their changes over time and space.

In chapter 2, the impacts of overlapping clouds on the satellite-based global statistics of clouds at different levels were discussed. The spatially collocated and merged CALIPSO and CloudSat measurements in the CCCM dataset for three and a half years (July 2006-December 2009) were used to determine the cloud layers. While

the CCCM dataset can provide information for up to six cloud layers, in the present study we screen the dataset and only consider single-layer clouds and multi-layer clouds with two layers. The global frequency map shows that multi-layer clouds can occur over the whole globe especially in the tropics. Moreover, the complete study of the impacts of multi-layer clouds on the statistics of clouds at different levels has not been done. Three traditional definitions of defining clouds as high-, mid-, and low-level were used:

1. the ISCCP definition (high: cloud top pressure (CTP) $\leq$ 440 hPa; mid: 440 hPa $<$ CTP $<$ 680 hPa; low: CTP $\geq$ 680 hPa);

2. the cloud-top height definition (high: cloud top height (CTH) $\geq$ 7 km; mid: 3 km $<$ CTH $<$ 7 km; low: CTH $\leq$ 3 km)

3. the cloud-base height definition (high: cloud base height (CBH) $\geq$ 5 km; mid: 2 km $<$ CBH $<$ 5 km; low: CBH $\leq$ 2 km)

Since some studies using the traditional satellite observations assume the clouds are single-layered, we compared the topmost-layer and all clouds (multi-layer top and bottom layers included) at different levels globally using each of the three definitions. The differences between topmost-layer and all clouds indicated that significant biases will be introduced if multi-layer clouds are not considered.

Because the ISCCP cloud climatology is widely used across the community through the comparisons with GCM simulations, we also compared our cloud amounts derived from the CCCM dataset to the ISCCP cloud amounts at three levels. The comparisons showed that ISCCP may underestimate high-level clouds except in a few areas over the oceans in low-latitudes. The ISCCP climatology also overestimates mid-level clouds globally and the discrepancy is larger than the results

in Rossow and Zhang (2010), which only found overestimation of mid-level clouds in polar regions. From the low-level clouds comparisons, the ISCCP climatology typically overestimates low-level clouds over the continents. We also found that there is an underestimation of low-level clouds by ISCCP over oceans between about 30^o N and 60^o S, whereas Rossow and Zhang (2010) only showed underestimation in southern mid-latitude oceans.

In chapter 3, we focused on three fundamental questions on the characteristics of mid-level clouds. These questions were: 1) what fraction of mid-level clouds occur in multi-layer cloud scenes? 2) What are the relationships between cloud frequency, cloud top and base height, cloud top pressure, geometrical thickness, and cloud top temperature for mid-level clouds? 3) In which cloud temperature regime do mid-level clouds tend to occur? We showed the characteristics of mid-level clouds using the three definitions of the mid-level, including cloud top pressure and height, cloud base height, cloud thickness, and cloud top temperature.

We first investigated the mid-level clouds in the multi-layer cloud regimes. In the tropics, less than 1% of the multi-layer cloud scenes are mid-level clouds over low clouds, and approximately 5% or 6% of the multi-layer cloud scenes were high clouds over mid-level clouds. In the mid- and high-latitudes, the mid-level over low clouds increase to around 4% and 5% of the total multi-layer cloud scenes, respectively. The high clouds over mid-level clouds also increase and are about 8% and 9% of the total multi-layer clouds in the mid-latitudes and polar regions.

Next, we found that the cloud top pressure-based definitions of the mid-level are more appropriate for global studies than cloud top height-based and cloud base height-based definitions. The statistics of testing the cloud boundaries to define mid-level clouds implied that changing the cloud top and base boundaries can lead to significant increase or decrease of the total number of mid-level clouds. Lastly, we

also found good correlations between cloud top temperature and cloud top height and pressure for mid-level clouds in the tropics. A strong zonal signature exists in the cloud top temperature difference between high clouds and mid-level clouds in the low-latitudes, which may be useful for improving the representation of mid-level clouds in GCMs.

In chapter 4, we introduced a new cloud thermodynamic phase algorithm using the AIRS radiance measurements. The AIRS cloud phase algorithm was based on radiative transfer simulations for a cloudy atmosphere. Observational support from CALIPSO cloud phase products is also shown. The AIRS phase algorithm includes four major parallel tests with different brightness temperature and/or brightness temperature difference combinations to distinguish ice and water clouds. The final phase output provides level of confidence, which is the summation of each individual test (ice or water) conducted simultaneously. Negative values, positive values, and 0 are considered to ice, liquid water, and unknown, respectively. There is also a warm scene flag included in the output, which can provide extra information for future analysis. The case studies indicate that the AIRS phase retrievals have good agreement with the CALIPSO cloud phase products along the CALIPSO surface track.

In chapter 5, we spatially collocated the AIRS and CALIPSO from December 2008 to November 2007. We then used the CALIPSO cloud phase products to evaluate the newly developed AIRS phase algorithm for single-layer, heterogeneous, and multi-layer cloud scenes. Single-layer clouds generally have larger phase signatures than heterogeneous and multi-layer cloud scenes. We found that the AIRS ice phase showed good agreement with the CALIPSO ice phase in over 90% of the cases, except for a large discrepancy in high-latitudes. AIRS demonstrates the ability to find ice phase clouds falling in the mid-temperature range (250-265 K) and also

optically thin ice clouds with window region brightness temperatures greater than 270 K. AIRS finds less water than ice in comparison with CALIPSO because AIRS spectral radiance have less sensitivity to water than ice. The ratio of "false alarm" of classifying ice and water, however, is fairly small, approximately 1∼2%. The AIRS algorithm was designed to call a case unknown if there is no strong spectral signature in any of the brightness temperature or brightness temperature difference tests.

The thermodynamic phase for mid-level clouds defined by the ISCCP and the cloud-top definitions of the mid-level were investigated. AIRS and CALIPSO cloud thermodynamic phases were shown at different levels for single-layer, heterogeneous, and multi-layered clouds. Overall, the statistics showed that ice, liquid water, and mixed-phase of the mid-level clouds are approximately 20%, 40%, and 40% globally, and the fractions of ice, liquid water, and mixed-phase changes with latitudes. Particularly, in the tropics, the ice clouds accounts for only about 1%, and liquid water and mixed-phase are roughly over 60% and 30%, respectively. As moving towards the polar regions, the ice phase increases to over 10% in the mid-latitudes and over 30% in the high-latitudes. The clouds containing liquid water decrease correspondingly. The highest mid-level mixed-phase clouds are approximately 50% in the mi-latitudes. The results are different from some of the previous studies, which are probably due to our main focus on mid-level clouds and the use of ISCCP and cloud-top definitions as well as our use of space-borne measurements.

The cloud phase variations were also tested when we adjusted the cloud boundary of the mid-level clouds using the ISCCP definition. The statistics showed that, if the upper boundary is kept (440 hPa) and change the bottom boundary for ±20 hPa, the mid-level ice clouds and liquid water clouds classified by the ISCCP cloud top pressure definition change by 2-5% and 10-14% globally. Moreover, if we fix the bottom boundary (680 hPa), the numbers of mid-level ice and water change

greatly by 10-30% and 3-7% globally with respect to the mid-level clouds between 680 and 440 hPa. The corresponding CALIPSO mixed-phase and AIRS unknown phase within the mid-level clouds changes approximately 2-15% globally.

The cloud phase distributions of ice, liquid water, and mixed-phase along the cloud top temperature are different from low latitudes towards polar regions. The high-level clouds and mid-level clouds have larger cloud temperature differences in the tropics than in the mid- and high-latitudes and have strong zonal signatures. It is indicated that the onset of glaciation cannot be faithfully represented by temperature only. The complex microphysical mechanisms also depend on subgrid-scale phase transitions, cloud particle size and shape, ambient humidity, aerosol composition and number concentration, and vertical velocity, among other factors.

Significant efforts have been made to improve the cloud radiative effects and cloud feedback studies. However, the clouds are still one of the major sources of uncertainties particularly for the mid-level clouds. This dissertation aims to address two major issues in the study of mid-level clouds: characteristics and thermodynamics. First, The investigation of overlapping clouds on the global satellite-based statics at different levels indicated that it is very important to involve multi-layer clouds in the statistical studies of clouds at vertical levels especially for mid-level clouds. For instance, a large amount of mid-level clouds exist in the high-level over mid-level cloud regimes in the tropics. Better understanding of the characteristics of mid-level clouds can bridge the statistical studies of mid-level clouds using different observational techniques. Second, improved knowledge of thermodynamic phase of mid-level clouds can facilitate the cloud property retrievals and model parameterizations, which can further advance the climate projections.

6.2 Future work

This dissertation is mainly focused on the global study of mid-level clouds. To better interpret our analysis, regional studies are necessary. Our global frequency map of mid-level clouds showed that there are a large amount of mid-level clouds are shown in the tropical western pacific (TWP). Although there exists studies in the ARM TWP surface site, a study with large coverage of TWP using satellite measurements can be done including the cloud statistics and thermodynamic phase and compared with the previous results to see whether the single surface site can represent the tropics.

REFERENCES

Ackerman, T. P., K.-N. Liou, F. P. J. Valero, and L. Pfister, 1988: Heating rates in tropical anvils. J. Atmos. Sci., 45, 1606−1623.

Aumann, H. H., et al., 2003: AIRS/AMSU/HSB on the Aqua mission: Design, science objectives, data products and processing systems. IEEE Trans. Geosci. Remote Sens., 41 (2), 253−264.

Ansmann, A., et al., 2009: Evolution of the ice phase in tropical altocumulus: SAMUM lidar observations over Cape Verde. J. Geophys. Res., 114, D17208, doi:10.1029/2008JD011659.

Barker, H. W., and Coauthors, 2003: Assessing 1D Atmospheric Solar Radiative Transfer Models: Interpretation and Handling of Unresolved Clouds. J. Climate, 16, 2676−2699.

Baum, B. A. and B. A. Wielicki, 1994: Cirrus cloud retrieval using infrared sounding data: Multilevel cloud errors. J. Appl. Meteor., 33, No. 1, 107-117.

Baum, B. A., P. F. Soulen, K. I. Strabala, M. D. King, S. A. Ackerman, W. P. Menzel, and P. Yang, 2000: Remote sensing of cloud properties using MODIS Airborne Simulator imagery during SUCCESS 2. Cloud thermodynamic phase. J. Geophys. Res., 105, 11 781− 11 792, doi:doi:10.1029/1999JD901090.

Baum, B. A., P. Yang, S. L. Nasiri, A. K. Heidinger, A. J. Heymsfield, and J. Li, 2007: Bulk scattering properties for the remote sensing of ice clouds. Part 3: High resolution spectral models from 100 to 3250 cm-1. J. Appl. Meteor. Clim., Vol. 46, 423-434.

Bodas−Salcedo, A., M. J. Webb, M. E. Brooks, M. A. Ringer, K. D. Williams, S. F. Milton, and D. R. Wilson, 2008: Evaluating cloud systems in the Met Ofce global forecast model using simulated CloudSat radar reßectivities. J. Geophys. Res., 113(D00A13), doi:10.1029/2007JD009620.

Cess, R. D., et al., 1990: Intercomparison and interpretation of climate feedback processes in 19 atmospheric general circulation models. J. Geophys. Res., 95, 16,601-−16,615, doi: 10.1029/JD095iD10p16601.

Chalon G, Cayla F, Diebel D, 2001. IASI: An Advanced Sounder for Operational Meteorology, Proceedings of the 52th Congress of IAF. Toulouse, France.

Chang, Fu-Lung, Zhanqing Li, 2005: A New Method for Detection of Cirrus Overlapping Water Clouds and Determination of Their Optical Properties. J. Atmos. Sci., 62, 3993−4009.

Chen B., J. Huang, P. Minnis, Y. Hu, Y. Yi, Z. Liu, D. Zhang, and X. Wang, 2010: Detection of dust aerosol by combining CALIPSO active lidar and passive IIR measurements, Atmos. Chem. Phys., 10, 4241-4251.

Chen, Ting, William B. Rossow, Yuanchong Zhang, 2000: Radiative Effects of Cloud-Type Variations. J. Climate, 13, 264−286.

Chepfer, H., S. Bony, D. Winker, M. Chiriaco, J.-L. Dufresne, and G. Sze, 2008: Use of CALIPSO lidar observations to evaluate the cloudiness simulated by a climate model, Geophys. Res. Lett., 35, L15704, doi:10.1029/2008GL034207.

Cho, H.-M., S. L. Nasiri, and P. Yang, 2009: Application of CALIOP measurements to the evaluation of cloud phase derived from MODIS infrared channels. J. Appl. Meteor. Climatol., 48, 2169−2180.

Chylek, P., S. Robinson, M. K. Dubey, M. D. King, Q. Fu, and W. B. Clodius, 2006: Comparison of near-infrared and thermal infrared cloud phase detections. J. Geophys. Res., 111 (D20203), doi:doi:10.1029/2006JD007140.

Curry, J. A., W. B. Rossow, D. Randall, and J. L. Schramm, 1996: Overview of arctic cloud and radiation characteristics. J. Climate, 9, 1731−1764.

Curry, J. A., P. V. Hobbs, M. D. King, D. A. Randall, P. Minnis, G. A. Isaac, J. O. Pinto, T. Uttal, A. Bucholtz, D. G. Cripe, H. Gerber, C. W. Fairall, T. J. Garrett, J. Hudson, J. M. Intrieri, C. Jakob, T. Jensen, P. Lawson, D. Marcotte, L. Nguyen, P. Pilewskie, A. Rangno, D. C. Rogers, K. B. Strawbridge, F. P. J. Valero, A. G. Williams, and D. Wylie, 2000: FIRE Arctic Clouds Experiment. Bull. Amer. Meteor. Soc., 81, 5−29.

Dessler, A. E., 2010: A determination of the cloud feedback from climate variations over the past decade. Science, 330, 1523−1527, doi:10.1126/science.1192546.

Dong, Xiquan, Gerald G. Mace, 2003: Arctic Stratus Cloud Properties and Radiative Forcing Derived from Ground-Based Data Collected at Barrow, Alaska. J. Climate, 16, 445−461.

Eldering, A., S. S. Kulawik, J. Worden, K. Bowman, and G. Osterman, 2008: Implementation of cloud retrievals for TES atmospheric retrievals: 2. Characterization of cloud top pressure and effective optical depth retrievals, J. Geophys. Res., 113, D16S37, doi:10.1029/2007JD008858.

Falk, M. J., and V. E. Larson, 2007: What causes partial cloudiness to form in multilayered midlevel clouds? A simulated case study, J. Geophys. Res., 112, D12206, doi:10.1029/2006JD007666.

Field, Paul R., 1999: Aircraft Observations of Ice Crystal Evolution in an Altostratus Cloud. J. Atmos. Sci., 56, 1925−1941.

Fleishauer, R. P., V. E. Larson, and T. H. Vonder Haar, 2002: Observed microphysical structure of midlevel, mixed-phase clouds. J. Atmos. Sci., 59(11), 1779−1804.

Fridlind, A. M., A. S. Ackerman, G. M. McFarquhar, G. Zhang, M. R. Poellot, P. J. DeMott, A. J. Prenni, and A. J. Heymsfield, 2007: Ice properties of single-layer stratocumulus during the Mixed-Phase Arctic Cloud Experiment (M-PACE): Part II, Model results. J. Geophys. Res., 112, D24202, doi: 10.1029/2007JD008646.

Garay, M. J., S. P. de Szoeke, and C. M. Moroney, 2008: Comparison of marine stratocumulus cloud top heights in the southeastern Pacific retrieved from satellites with coincident ship-based observations, J. Geophys. Res., 113, D18204, doi:10.1029/2008JD009975.

Garrett, Kevin J., Ping Yang, Shaima L. Nasiri, Christopher R. Yost, Bryan A. Baum, 2009: Influence of Cloud-Top Height and Geometric Thickness on a MODIS Infrared-Based Ice Cloud Retrieval. J. Appl. Meteor. Climatol., 48, 818−832.

Gayet, J.-F., S. Asano, A. Yamazaki, A. Uchiyama, A. Sinyuk, O. Jourdan, and F. Auriol, 2002: Two case studies of winter continental-type water and mixed-phase stratocumuli over the sea. 1. Microphysical and optical properties. J. Geophys. Res., 107, D21, 4569, doi: 10.1029/2001JD001106.

Girard, E., and J. Blanchet, 2001: Microphysical parameterization of arctic diamond dust, ice fog, and thin stratus for climate models. J. Atmos. Sci., 58, 1181-1198.

Goloub, P., M. Herman, H. Chepfer, J. Riedi, G. Brogniez, P. Couvert, and G. Sze, 2000: Cloud thermodynamical phase classification from the POLDER spaceborne instrument, J. Geophys. Res.,105(D11), 14,74714,759, doi:10.1029/1999JD901183.

Gregory, D. and D. Morris, 1996: The sensitivity of climate simulations to the specification of mixed phase clouds. Clim. Dyn., 12 (9), 641−651.

Hahn, C. J. and S. G. Warren, 1999: Extended edited synoptic cloud reports from ships and land stations over the globe, 1952-1996. ORNL/CDIAC-123 NDP026C, Carbon Dioxide Information Analysis Center, Oak Ridge National Laboratory, Oak Ridge, TN.

Hahn, C. J. and S. G. Warren, 2003: Cloud climatology for land stations worldwide, 1971-1996. Tech. Rep. NDP-026D, Carbon Dioxide Information Analysis Center, Oak Ridge National Laboratory, Oak Ridge, TN.

Hartmann, D. L., M. E. Ockert-Bell, and M. L. Michelsen, 1992: The effect of cloud type on EarthÕs energy balance: global analysis. J. Climate, 5, 1281−1304.

Haynes, J. M., and G. L. Stephens, 2007: Tropical oceanic cloudiness and the incidence of precipitation: Early results from CloudSat, Geophys. Res. Lett., 34, L09811, doi:10.1029/2007GL029335.

Heidinger, Andrew K., Michael J. Pavolonis, 2005: Global Daytime Distribution of Overlapping Cirrus Cloud from NOAA's Advanced Very High Resolution Radiometer. J. Climate, 18, 4772−4784.

Heymsfield, Andrew J., Larry M. Miloshevich, Anthony Slingo, Kenneth Sassen, David O'C. Starr, 1991: An Observational and Theoretical Study of Highly Supercooled Altocumulus. J. Atmos. Sci., 48, 923−945.

Hobbs, P.V., and A.L. Rangno, 1998: Microstructures of low and middle-level clouds over the Beaufort Sea, Quart. J. Roy. Meteor. Soc., 124, 2035-2071.

Hu, Y., 2007: Depolarization ratio−effective lidar ratio relation: Theoretical basis for space lidar cloud phase discrimination. Geophys. Res. Lett., 34 (L11812), doi:10.1029/ 2007GL029584.

Hu, Y., et al., 2009: CALIPSO/CALIOP cloud phase discrimination algorithm. J. Atmos. Oceanic Technol., 26, 2293−2309, doi:10.1175/2009JTECHA1280.1.

Hu, Y., S. Rodier, K. Xu, W. Sun, J. Huang, B. Lin, P. Zhai, and D. Josset, 2010: Occurrence, liquid water content, and fraction of supercooled water clouds from combined CALIOP/IIR/MODIS measurements. J. Geophys. Res., 115, D00H34, doi:10.1029/ 2009JD012384.

Huang, J., P. Minnis, B. Lin, Y. Yi, M. M. Khaiyer, R. F. Arduini, A. Fan, and G. G. Mace, 2005: Advanced retrievals of multilayered cloud properties using multispectral measurements, J. Geophys. Res., 110, D15S18, doi:10.1029/2004JD005101.

Jensen, E. J., Kinne, S., and Toon, O. B.: Tropical cirrus cloud radiative forcing: Sensitivity studies, Geophys. Res. Lett., 21, 2023−2026, 1994.

Jin, Menglin, Shunlin Liang, 2006: An Improved Land Surface Emissivity Parameter for Land Surface Models Using Global Remote Sensing Observations. J. Climate, 19, 2867−2881.

Jin, Yao, William B. Rossow, Don P. Wylie, 1996: Comparison of the Climatologies of High-Level Clouds from HIRS and ISCCP. J. Climate, 9, 2850−2879.

Johnson, Richard H., Thomas M. Rickenbach, Steven A. Rutledge, Paul E. Ciesielski, Wayne H. Schubert, 1999: Trimodal Characteristics of Tropical Convection. J. Climate, 12, 2397−2418.

Joiner, J., Vasilkov, A. P., Bhartia, P. K., Wind, G., Platnick, S., and Menzel, W. P.: Detection of multi-layer and vertically-extended clouds using A-train sensors, Atmos. Meas. Tech., 3, 233-247, doi:10.5194/amt-3-233-2010, 2010.

Kato, S., S. Sun-Mack, W. F. Miller, F. G. Rose, Y. Chen, P. Minnis, and B. A. Wielicki, 2010: Relationships among cloud occurrence frequency, overlap, and effective thickness derived from CALIPSO and CloudSat merged cloud vertical profiles, J. Geophys. Res., 115, D00H28, doi:10.1029/2009JD012277.

Kahn, B. H., K. N. Liou, S.-Y. Lee, E. F. Fishbein, S. DeSouza-Machado, A. Eldering, E. J. Fetzer, S. E. Hannon, and L. L. Strow, 2005: Nighttime cirrus detection using Atmospheric Infrared Sounder window channels and total column water vapor, J. Geophys. Res., 110, D07203, doi:10.1029/2004JD005430.

Kahn, B. H., K. N. Liou, S.-Y. Lee, E. F. Fishbein, S. DeSouza-Machado, A. Eldering, E. J. Fetzer, S. E. Hannon, and L. L. Strow (2005), Nighttime cirrus detection using Atmospheric Infrared Sounder window channels and total column water vapor, J. Geophys. Res., 110, D07203, doi:10.1029/2004JD005430.

Kahn, B. H., M. T. Chahine, G. L. Stephens, G. G. Mace, R. Marchand, Z. Wang, C. D. Barnet, A. Eldering, R. E. Holz, R. E. Kuehn, and D. G. Vane, 2008: Cloud-type comparisons of AIRS, CloudSat, and CALIPSO cloud height and amount, Atmos. Chem. Phys., 8, 1231-1248.

Kahn, B. H., S. L. Nasiri, M. M. Schreier, and B. A. Baum, 2011: Impacts of subpixel cloud heterogeneity on infrared thermodynamic phase assessment. J. Geophys. Res., 116 (D20), doi:10.1029/2011JD015774.

Key, J. and J. Intrieri, 2000: Cloud particle phase determination with the avhrr. J. Appl. Meteorol., 39, 1797−1805.

Klein, S., et al., 2009: Intercomparison of model simulations of mixed-phase clouds observed during the ARM Mixed-Phase Arctic Cloud Experiment. I: single-layer cloud. Quart. J. Roy. Meteor. Soc., 135 (641), 979−1002.

Knap, W. H., P. Stammes, and R. B. A. Koelemeijer, 2002: Cloud thermodynamic phase determination from near-infrared spectra of reflected sunlight. J. Atmos. Sci., 59, 83−96.

Koelemeijer, R. B. A., P. Stammes, J. W. Hovenier, and J. F. de Haan, 2002: Global distributions of effective cloud fraction and cloud top pressure derived from oxygen

A band spectra measured by the Global Ozone Monitoring Experiment: Comparison to ISCCP data, J. Geophys. Res., 107(D12), 4151, doi:10.1029/2001JD000840.

Kokhanovsky, A. A., O. Jourdan, and J. P. Burrows, 2006: The cloud phase discrimination from a satellite. IEEE Trans. Geosci. Remote Sens., 3, 103−106.

Korolev, A. V., and Co-authors, 2003: Microphysical characterization of mixed?phase clouds, Q. J. R. Meteorol. Soc., 129(587), 39−65, doi:10.1256/qj.01.204.

Li, J. M., Y. H. Yi, P. Minnis, J. P. Huang, H. R. Yan, Y. J. Ma, W. C. Wang, and J. K. Ayers, 2011: Radiative effect differences between multi-layered and single-layer clouds derived from ceres, calipso, and cloudsat data. J. Quant. Spectrosc. Radiat. Transfer, 112, 361−375, doi:10.1016/j.jqsrt.2010.10.006.

Liu, X, S. Xie, and S. J. Ghan, 2007: Evaluation of a New Mixed-Phase Cloud Microphysics Parameterization with CAM3 Single-Column Model and M-PACE Observations. Geophys. Res. Lett., 34, L23712. doi: 10.1029/2007GL031446.

Luo, Y., K. M. Xu, H. Morrison, and G. McFarquhar, 2008: Arctic Mixed-Phase Clouds Simulated by a Cloud-Resolving Model: Comparison with ARM Observations and Sensitivity to Microphysics Parameterizations. J. Atmos. Sci., 65, 1285−1303.

Mace, G. G., S. Benson-Troth, 2002: Cloud-Layer Overlap Characteristics Derived from Long-Term Cloud Radar Data. J. Climate, 15, 25052515.

Mace, G. G., S. Benson, and S. Kato, 2006: Cloud radiative forcing at the Atmospheric Radiation Measurement Program Climate Research Facility: 2. Vertical redistribution of radiant energy by clouds. J. Geophys. Res., 111(D11S91), doi:10.1029/2005JD005922.

Mace, G., 2007, "Level 2 GEOPROF Product Process Description and Interface Control Document Algorithm version". 5.3, http.//www.cloudsat.cira.colostate.edu/.

Mace, G. G., Q. Zhang, M. Vaughan, R. Marchand, G. Stephens, C. Trepte, and D. Winker, 2009, A description of hydrometer layer occurrence statistics derived from the first year of merged CloudSat and CALIPSO data, J. Geophys. Res., 114, D00A26, doi:10.1029/2007JD009755.

McClatchey RA, Fenn RW, Selby JEA, Volz FE, Garing JS, 1972: Optical Properties of the Atmosphere, 3rd edn. Air Force Cambridge Research Laboratories, Report No. AFCRL-72-0497, L.G. Hanscom Field, Bedford MA.

McFarlane, S. A., R. T. Marchand, and T. P. Ackerman, 2005: Retrieval of cloud phase and crystal habit from multiangle imaging spectroradiometer (misr) and moderate resolution imaging spectroradiometer (modis) data. J. Geophys. Res., 110 (D14201), doi:10.1029/ 2004JD004831.

McFarquhar, G.M., A.J. Heymsfield, J. Spinhirne, and W. Hart, 2000: Subvisible tropopause tropical cirrus: Observations and radiative impacts. J. Atmos. Sci., 57, 1841-1853.

McFarquhar, G.M., P. Yang, A. Macke, and A.J. Baran, 2002: A new parameterization of single-scattering solar radiative properties for tropical ice clouds using observed ice crystal size and shape distributions. J. Atmos. Sci., 59, 2458-2478.

McFarquhar, G. M. and S. G. Cober, 2004: Single-scattering properties of mixed-phase arctic clouds at solar wavelengths: Impacts on radiative transfer. J. Climate, 17, 3799−3813.

Menzel, W. Paul, and Coauthors, 2008: MODIS Global Cloud-Top Pressure and Amount Estimation: Algorithm Description and Results. J. Appl. Meteor. Climatol., 47, 11751198.

Minnis, Patrick, Patrick W. Heck, David F. Young, 1993: Inference of Cirrus Cloud Properties Using Satellite-observed Visible and Infrared Radiances. Part II: Verification of Theoretical Cirrus Radiative Properties. J. Atmos. Sci., 50, 1305−1322.

Minnis, P., J. Huang, B. Lin, Y. Yi, R. F. Arduini, T.-F. Fan, J. K. Ayers, and G. G. Mace, 2007: Ice cloud properties in ice-over-water cloud systems using Tropical Rainfall Measuring Mission (TRMM) visible and infrared scanner and TRMM Microwave Imager data, J. Geophys. Res., 112, D06206, doi:10.1029/2006JD007626.

Mishchenko, M. I., W. B. Rossow, A. Macke, and A. A. Lacis, 1996: Sensitivity of cirrus cloud albedo, bidirectional reflectance and optical thickness retrieval accuracy to ice particle shape, J. Geophys. Res., 101(D12), 16,97316,985, doi:10.1029/96JD01155.

Morrison, H. J. A. Curry, M. Shupe, P. Zuidema, 2005: A new double-moment microphysics parameterization for application in cloud and climate models. Part II: Single-column modeling of arctic clouds. J. Atmos. Sci., 62, 1678-1693.

Nasiri, Shaima L., Bryan A. Baum, 2004: Daytime Multilayered Cloud Detection Using Multispectral Imager Data. J. Atmos. Oceanic Technol., 21, 11451155.

Nasiri, S. L. and B. H. Kahn, 2008: Limitations of bi-spectral infrared cloud phase determination and potential for improvement. J. Appl. Meteor. Climatol., 47 (11), 2895−2910.

Nasiri, S. L., H. C. Jin, C. X. Wang and B. H. Kahn: Cloud thermodynamic phase determination using AIRS: Part I: Algorithm development. To be submitted to Journal of Atmospheric and Oceanic Technology.

Naud, C., A. D. Del Genio, and M. Bauer, 2006: Observational constraints on cloud thermodynamic phase in midlatitude storms. J. Climate, 19, 5273−5288.

Naud, C. M., B. A. Baum, M. Pavolonis, A. Heidinger, R. Frey, and H. Zhang, 2007: Comparison of MISR and MODIS cloud top heights in the presence of cloud overlap. Remote Sensing of the Environment, Vol. 107, 200−210.

Norris, Joel R., Christopher P. Weaver, 2001: Improved Techniques for Evaluating GCM Cloudiness Applied to the NCAR CCM3. J. Climate, 14, 2540−2550.

Pagano, T. S., H. H. Aumann, D. E. Hagan, and K. Overoye, 2003: Prelaunch and in-flight radiometric calibration of the atmospheric infrared sounder (airs). IEEE Trans. Geosci. Remote Sens., 41, 265−273.

Pilewskie, P. and S. Twomey, 1987: Cloud phase discrimination by reflectance measurements near 1.6 and 2.2 μm. J. Atmos. Sci., 44, 3419−3420.

Pinto, J. O., 1998: Autumnal mixed-phase cloudy boundary layers in the Arctic. J. Atmos. Sci., 55, 2016−2038.

Platnick, S., M. D. King, S. A. Ackerman, W. P. Menzel, B. A. Baum, and R. A. Frey, 2003: The MODIS cloud products: Algorithms and examples from Terra. IEEE Trans. Geosci. Remote Sens., 41, 459−473.

Poetzsch-Heffter, C., Q. Liu, E. Ruperecht, and C. Simmer, 1995: Effect of cloud types on the earth radiation budget calculated with the ISCCP Cl dataset: Methodology and initial results. J. Climate, 8, 829−843.

Poore, K., J. H. Wang, and W. B. Rossow, 1995: Cloud layer thicknesses from a combination of surface and upper-air observations. J. Climate, 8, 550−568.

Randall, David A., Harshvardhan, Donald A. Dazlich, Thomas G. Corsetti, 1989: Interactions among Radiation, Convection, and Large-Scale Dynamics in a General Circulation Model. J. Atmos. Sci., 46, 1943−1970.

Rauber, R., and A. Tokay, 1991: An explanation for the existence of supercooled water at the top of cold clouds. J. Atmos. Sci., 48, 1005−1023.

Riedi, J., M. Doutriaux-Boucher, P. Goloub, and P. Couvert, 2000: Global distribution of cloud top phase from POLDER/ADEOS I. Geophys. Res. Lett., 27, 1707−1710.

Riedi, J., et al., 2010: Cloud thermodynamic phase inferred from merged polder and modis data. Atmos. Chem. Phys., 10, 11 851−11 865, doi:10.5194/acp-10-11851-2010.

Riihimaki, L., S. McFarlane, and J. Comstock, 2012: Climatology and Formation of Tropical Mid-level Clouds at the Darwin ARM Site. J. Climate. doi:10.1175/JCLI-D-11-00599.1, in press.

Riley, E. M. and B. E. Mapes, 2009: Unexpected peak near ?15¡C in CloudSat echo top climatology, Geophys. Res. Lett., 36, L09819, doi:10.1029/2009GL037558.

Riley J. T, 1998: Mixed-phase icing conditions: a review. Technical Report of Federal Aviation Administration, DOT/FAA/AR-98/76, Washington DC.

Rossow, William B., Andrew A. Lacis, 1990: Global, Seasonal Cloud Variations from Satellite Radiance Measurements. Part II. Cloud Properties and Radiative Effects. J. Climate, 3, 1204−1253.

Rossow, William B., Leonid C. Garder, 1993: Cloud Detection Using Satellite Measurements of Infrared and Visible Radiances for ISCCP. J. Climate, 6, 23412369.

Rossow, W. B. and Schiffer, R. A., 1999: Advances in understanding clouds from ISCCP. Bulletin of the American Meteorological Society, 80, pp. 2261−2287.

Rossow, William B., Yuanchong Zhang, 2010: Evaluation of a Statistical Model of Cloud Vertical Structure Using Combined CloudSat and CALIPSO Cloud Layer Profiles. J. Climate, 23, 6641−6653.

Rotstayn, L., B. Ryan, and J. Katzfey, 2000: A scheme for calculation of the liquid fraction in mixed-phase stratiform clouds in large-scale models. Mon. Wea. Rev., 128 (4), 1070−1088.

Sassen, Kenneth, 1991: The Polarization Lidar Technique for Cloud Research: A Review and Current Assessment. Bull. Amer. Meteor. Soc., 72, 1848−1866.

Schreier, M. M., B. H. Kahn, A. Eldering, D. A. Elliott, E. Fishbein, F. W. Irion, and T. S. Pagano, 2010: Radiance comparisons of modis and airs using spatial response information. J. Atmos. Oceanic Technol., 27, 1331−1342.

Seemann, S. W., E. E. Borbas, R. O. Knuteson, G. R. Stephenson, and H. L. Huang, 2008: Development of a global infrared land surface emissivity database for application to clear sky sounding retrievals from multispectral satellite radiance measurements. J. Appl. Meteor. Climatol., 47, 108−123, doi:http://dx.doi.org/10.1175/2007JAMC1590.1.

Seifert, P., et al., 2010: Saharan dust and heterogeneous ice formation: Eleven years of cloud observations at a central European EARLINET site. J. Geophys. Res., 115, D20201, doi: 10.1029/2009JD013222.

Shupe, M., et al., 2008: A focus on mixed-phase clouds. Bull. Am. Meteorol. Soc., 89, 1549−1562.

Shupe, M. D., 2011, Clouds at Arctic atmospheric observatories. Part II: Thermodynamic phase characteristics, J. Appl .Meteor. Climatol., 50, 645−661.

Slingo, A. and Slingo, J. M., 1988: The response of a general circulation model to cloud longwave radiative forcing. I: Introduction and initial experiments. Q.J.R. Meteorol. Soc., 114: 1027−1062. doi: 10.1002/qj.49711448209

Slingo, J. M. and Slingo, A., 1991: The response of a general circulation model to cloud longwave radiative forcing. II: Further studies. Q.J.R. Meteorol. Soc., 117: 333−364. doi: 10.1002/qj.49711749805

Smith, A. J., V. E. Larson, J. Niu, J. A. Kankiewicz, and L. D. Carey, 2009: Processes that generate and deplete liquid water and snow in thin midlevel mixed-phase clouds, J. Geophys. Res., 114, D12203, doi:10.1029/2008JD011531.

Soden, B. J., and I. M. Held, 2006: An assessment of climate feedbacks in coupled ocean−atmosphere models. J. Climate, 19, 3354−3360.

Stephens, G. L., and Co-authors, 2002: THE CLOUDSAT MISSION AND THE A-TRAIN. Bull. Amer. Meteor. Soc., 83, 1771−1790.

Stephens, Graeme L., 2005: Cloud Feedbacks in the Climate System: A Critical Review. J. Climate, 18, 237−273.

Stephens, G. L., et al., 2008: CloudSat mission: Performance and early science after the first year of operation, J. Geophys. Res., 113, D00A18, doi:10.1029/2008JD009982.

Strabala, K. I., S. A. Ackerman, and W. P. Menzel, 1994: Cloud properties inferred from 8-12 μm data. J. Appl. Meteorol., 33, 212−229.

Stubenrauch, C. J., A. Chedin, G. Radel, N. Scott, and S. Serrar, 2006: Cloud properties and their seasonal and diurnal variability from TOVS Path-B. J. Climate, 19, 5531−5553.

Subrahmanyam, K.V. and Karanam Kishore Kumar, 2011: "CloudSat Observations of the Multi Layered Clouds across the Globe: Implications to General Circulation", TROPMET. pp. 198-199, December 14-16, Hyderabad, India.

Sun Z, Shine KP, 1994: Studies of radiative of ice and mixed-phase clouds. Q J R Meteorol Soc. 120:111−37.

Sun Z, Shine KP, 1995: Parameterization of ice clouds radiative properties and its application to potential climatic importance of mixed-phase clouds. J. Climate 9:1874−88.

Susskind, J., C. D. Barnet, and J. M. Blaisdell, 2003: Retrieval of atmospheric and surface parameters from AIRS/AMSU/HSB data in the presence of clouds. IEEE Trans. Geosci. Remote Sens., 41, 390−409.

Tian, Baijun, Duane E. Waliser, Eric J. Fetzer, Bjorn H. Lambrigtsen, Yuk L. Yung, Bin Wang, 2006: Vertical Moist Thermodynamic Structure and Spatial−Temporal Evolution of the MJO in AIRS Observations. J. Atmos. Sci., 63, 2462−2485.

Tian, L., and J. A. Curry, 1989: Cloud Overlap Statistics, J. Geophys. Res., 94(D7), 9925−9935, doi:10.1029/JD094iD07p09925.

Treut HL, Li ZX, Forichon M., 1994: Sensitivity of the LMD general circulation model to greenhouse forcing associated with two differerent cloud water parameterizations. J Climate 7:1827−41.

Uttal, Taneil, Janet M. Intrieri, Wynn L. Eberhard, Eugene E. Clothiaux, Thomas P. Ackerman, 1995: Cloud Boundary Statistics during FIRE II. J. Atmos. Sci., 52, 4276−4284.

Verlinde, J., and Coauthors, 2007: The Mixed-Phase Arctic Cloud Experiment. Bull. Amer. Meteor. Soc., 88, 205−221.

Wang, C., P. Yang, S. Platnick, A. K. Heidinger, B. A. Baum, T. Greenwald, Z. Zhang, and R. E. Holz: Retrieval of ice cloud properties from AIRS observations based on a fast high-spectral resolution radiative transfer model. Submitted to J. Appl. Meteor. Clim.

Wang, L. and A. E. Dessler, 2006: Instantaneous cloud overlap statistics in the tropical area revealed by ICESat/GLAS data, Geophys. Res. Lett., 33, L15804, doi:10.1029/2005GL024350.

Wang, Junhong, William B. Rossow, 1998: Effects of Cloud Vertical Structure on Atmospheric Circulation in the GISS GCM. J. Climate, 11, 3010−3029.

Wang, Junhong, William B. Rossow, Taneil Uttal, Margaret Rozendaal, 1999: Variability of Cloud Vertical Structure during ASTEX Observed from a Combination of Rawinsonde, Radar, Ceilometer, and Satellite. Mon. Wea. Rev., 127, 2484−2502.

Wang, J. H., W. B. Rossow, and Y. Zhang, 2000: Cloud vertical structure and its variations from a 20-yr global rawinsonde dataset. J. Climate, 13, 3041−3056.

Wang, Z. and K. Sassen, 2007: Level 2 cloud scenario classification product process description and interface control document: Version 5.0. Cooperative Institute for Research in the Atmosphere, Colorado State University.

Wang, W., J. Huang, P. Minnis, Y. Hu, J. Li, Z. Huang, J. K. Ayers, and T. Wang, 2010: Dusty cloud properties and radiative forcing over dust source and downwind regions derived from A-Train data during the Pacific Dust Experiment, J. Geophys. Res., 115, D00H35, doi:10.1029/2010JD014109.

Weare, B.C., 2001: Effects of cloud overlap on radiative feedbacks. Clim. Dyn., 17, 143-150.

Wielicki, Bruce A., Edwin F. Harrison, Robert D. Cess, Michael D. King, David A. Randall, 1995: Mission to Planet Earth: Role of Clouds and Radiation in Climate. Bull. Amer. Meteor. Soc., 76, 2125−2153.

Winker, D. M. and C. R. Trepte, 1998: Laminar cirrus observed near the tropical tropopause by LITE, Geophys. Res. Lett., 25(17), 33513354, doi:10.1029/98GL01292.

Winker, D. M., J. Pelon, and M. P. McCormick, 2003: The Calipso Mission: Spaceborne Lidar for Observation of Aerosols and Clouds. Proc. SPIE, 4893, 1-11.

Winker, D. M., M. A. Vaughan, A. Omar, Y. Hu, Z. L. K. A. Powell, W. H. Hunt, and S. A. Young, 2009: Overview of the calipso mission and caliop data processing algorithms. J. Atmos. Oceanic Technol., 26, 2310−2323.

Wu, D. L., et al., 2009: Vertical distributions and relationships of cloud occurrence frequency as observed by MISR, AIRS, MODIS, OMI, CALIPSO, and CloudSat, Geophys. Res. Lett., 36, L09821, doi:10.1029/2009GL037464.

Wyant M. C., and co-authors, 2006: A comparison of low-latitude cloud properties and their response to climate change in three AGCMs sorted into regimes using mid-tropospheric vertical velocity. Climate Dynamics, 27(2-3), 261-279.

Wylie, D. P., W. P. Menzel, 1989: Two Years of Cloud Cover Statistics Using VAS. J. Climate, 2, 380−392.

Wylie, Donald P., W. Paul Menzel, Harold M. Woolf, Kathleen I. Strabala, 1994: Four Years of Global Cirrus Cloud Statistics Using HIRS. J. Climate, 7, 1972−1986.

Wylie, Donald P., W. Paul Menzel, 1999: Eight Years of High Cloud Statistics Using HIRS. J. Climate, 12, 170−184.

Wylie, Donald, Darren L. Jackson, W. Paul Menzel, John J. Bates, 2005: Trends in Global Cloud Cover in Two Decades of HIRS Observations. J. Climate, 18, 3021−3031.

Yang, P., H.-L. Wei, B. A. Baum, H.-L. Huang, A. J. Heymsfield, Y. X. Hu, B.-C. Gao, and D. D. Turner, 2003: The spectral signature of mixed-phase clouds composed of nonspherical ice crystals and spherical liquid droplets in the terrestrial window region. J. Quant. Spectrosc. Radiat. Transfer, 79-80, 1171−1188.

Yasunaga, K., K. Yoneyama, H. Kubota, H. Okamoto, A. Shimizu, H. Kumagai, M. Katsumata, N. Sugimoto, and I. Matsui, 2006: Melting layer cloud observed during R/V Mirai cruise MR01-K05. J. Atmos. Sci, 63, 3020−3032.

Zelinka, Mark D., Stephen A. Klein, Dennis L. Hartmann, 2012: Computing and Partitioning Cloud Feedbacks Using Cloud Property Histograms. Part I: Cloud Radiative Kernels. J. Climate, 25, 3715−3735.

Zhang, D., Z. Wang, and D. Liu, 2010: A global view of midlevel liquid-layer topped stratiform cloud distribution and phase partition from CALIPSO and CloudSat measurements. J. Geophys. Res., 115, D00H13, doi:10.1029/2009JD012143.

Zhang, M. H. et al., 2005: Comparing clouds and their seasonal variations in 10 atmospheric general circulation models with satellite measurements. J. Geophys. Res., 110(D15S02), doi:10.1